Chemical Technology Division
Chemical Technology Division
Chemical Technology Division
Chemical Technology Division
Chemical Technology Division
Chemical Technology Division
Chemical Technology Division
Chemical Technology Division
Chemical Technology Division
Chemical Technology Division
Chemical Technology Division
Chemical Technology Division
Chemical Technology Division
Chemical Technology Division
Chemical Technology Division
Chemical Technology Division
Chemical Technology Division
Chemical Technology Division
Chemical Technology Division

ANL-98/12

Yucca Mountain Project – Argonne National Laboratory, Annual Progress Report, FY 1997

for Activity WP 1221

Unsaturated Drip Condition Testing of Spent Fuel and Unsaturated Dissolution Tests of Glass

by P. A. Finn, D. J. Wronkiewicz, R. J. Finch, J. C. Hoh, C. Mertz, J. W. Emery, E. C. Buck, J. Fortner, S. F. Wolf, L. A. Neimark, and J. K. Bates

Argonne National Laboratory, Argonne, Illinois 60439
operated by The University of Chicago
for the United States Department of Energy under Contract W-31-109-Eng-38

Chemical Technology Division
Chemical Technology Division
Chemical Technology Division
Chemical Technology Division

Argonne National Laboratory, with facilities in the states of Illinois and Idaho, is owned by the United States government, and operated by The University of Chicago under the provisions of a contract with the Department of Energy.

DISCLAIMER

This report was prepared as an account of work sponsored by an agency of the United States Government. Neither the United States Government nor any agency thereof, nor any of their employees, makes any warranty, express or implied, or assumes any legal liability or responsibility for the accuracy, completeness, or usefulness of any information, apparatus, product, or process disclosed, or represents that its use would not infringe privately owned rights. Reference herein to any specific commercial product, process, or service by trade name, trademark, manufacturer, or otherwise, does not necessarily constitute or imply its endorsement, recommendation, or favoring by the United States Government or any agency thereof. The views and opinions of authors expressed herein do not necessarily state or reflect those of the United States Government or any agency thereof.

Reproduced from the best available copy.

Available to DOE and DOE contractors from the
Office of Scientific and Technical Information
P.O. Box 62
Oak Ridge, TN 37831
Prices available from (423) 576-8401

Available to the public from the
National Technical Information Service
U.S. Department of Commerce
5285 Port Royal Road
Springfield, VA 22161

DISCLAIMER

Portions of this document may be illegible in electronic image products. Images are produced from the best available original document.

ANL-98/12

ARGONNE NATIONAL LABORATORY
9700 South Cass Avenue
Argonne, Illinois 60439

YUCCA MOUNTAIN PROJECT — ARGONNE NATIONAL LABORATORY, ANNUAL PROGRESS REPORT, FY 1997

for

Activity WP 1221

UNSATURATED DRIP CONDITION TESTING OF SPENT FUEL and UNSATURATED DISSOLUTION TESTS OF GLASS

by

P. A. Finn, D. J. Wronkiewicz, R. J. Finch, J. C. Hoh, C. Mertz
J. W. Emery, E. C. Buck, J. Fortner, S. F. Wolf, L. A. Neimark, and J. K. Bates

Chemical Technology Division

June 1998

TABLE OF CONTENTS

Page

ABSTRACT 1

EXECUTIVE SUMMARY 2

I. UNSATURATED TESTS WITH IRRADIATED SPENT FUEL 7
- A. Introduction 7
- B Objective 7
- C. Background and Experimental Approach 7
- D. Results and Discussion 8
  - 1. Reaction of the ε–Phase and the Release of ^{99}Tc to the Leachate 8
  - 2. Radionuclide Releases Compared to the ^{99}Tc Release 15
  - 3. Spent Fuel and Its Alteration Products 19
  - 4. Reaction Pathways 21
  - 5. Potential Mechanism in the Spent Fuel Reaction 22
  - 6. Radionuclide Release in the ATM-106 Low-Drip-Rate Test after 10 Minute Immersion in EJ-13 23
- E. Conclusions 24
- F. Ongoing Studies 24

II. OPTICAL, SEM, AND XRD RESULTS FOR REACTED SPENT FUEL SAMPLES 25
- A. Results for High-Drip-Rate Tests 25
  - 1. ATM 103 Fuel - 3.7 Years Reaction 25
  - 2. XRD Results for ATM-106 Fuel Sample from the Zircaloy Retainer after 0.8 Years 27
  - 3. Analysis of Sample from ATM-106 Fuel after 3.7 Years Reaction 29
  - 4. Analysis of Sample from ATM-106 Fuel after 4.1 Years Reaction 30
  - 5. Discussion of the High-Drip-Rate Tests 32
- B. Results for Low-Drip-Rate Tests 36
  - 1. Analysis of Sample from ATM-103 Fuel after 4.1 Years Reaction 36
  - 2. Discussion of Low-Drip-Rate Tests 36
- C. Vapor-Hydration Tests 39
  - 1. Analysis of Sample from ATM-103 Fuel after 4.1 Years Reaction 39
  - 2. Analysis of Sample from ATM-106 Fuel after 4.1 Years Reaction 40
  - 3. Discussion of Vapor-Hydration Tests 41
- D. Summary 42

III. EXAMINATION OF SPENT NUCLEAR FUEL WITH ANALYTICAL TRANSMISSION ELECTRON MICROSCOPY 45
- A. Introduction and Background 45
- B. Objectives 45
- C. Technical Approach 45
- D. Results and Discussion 45
  - 1. Incorporation of Neptunium into Secondary Phases 46
  - 2. Evidence for the Dissolution of ε-Particles in Vapor and High-Drip-Rate Tests with ATM-103 49
  - 3. Plutonium Enrichment During the Corrosion of Spent Nuclear Fuel 51
- E. Future Studies 54

TABLE OF CONTENTS (contd.)

Page

IV. PETRI-DISH TESTS 55
- A. Background 55
- B. Experimental Setup 55
- C. Analyses 61
  - 1. Analytical Methodology 61
  - 2. Results 64
- D. Discussion of UO_2 Dissolution and Alteration-Phase Formation 83
- E. Thermodynamic and Kinetic Considerations 91
- F. Effect of H_2O_2 95
- G. Steel Corrosion and Rust Formation 96
- H. Summary and Conclusions 101

V. DEVELOPMENT OF METHODS TO TEST CLAD FUEL 103
- A. Introduction 103
- B. Objectives 103
- C. Technical Approach 103
- D. Results 103
- E. Ongoing Work 103

VI. PROCUREMENT OF A NEW APPROVED TESTING MATERIAL 105
- A. Introduction 105
- B. Objective 105
- C. Technical Approach 105
  - 1. Procurement 105
  - 2. Shipping 106
- D. Results 106
- E. Ongoing Work 106

VII. UNSATURATED DRIP TESTS WITH UO_2 107
- A. Introduction 107
- B. UO_2 Reactions 107
- C. Summary 108
- D. Ongoing Work 108

VIII. UNSATURATED DISSOLUTION TESTS IN GLASS 111
- A. Introduction 111
- B. Objective 111
- C. Technical Approach 111
- D. Results 112
  - 1. Solution Cation Analyses 112
  - 2. Colloidal Particle Analyses 122
- E. Summary 124
- F. Ongoing Work 124

IX. VAPOR HYDRATION TESTING OF GLASS 125
- A. Introduction 125
- B. Objective 125
- C. Technical Approach 126
- D. Results and Ongoing Effort 129

TABLE OF CONTENTS (contd.)

Page

X. DEVELOPMENT OF METHODS TO STUDY WASTE FORM COLLOIDS 131
- A. Introduction 131
- B. Objective 131
- C. Technical Approach 131
  - 1. Instrumentation 131
  - 2. Service and Maintenance 131
  - 3. Calibration 132
  - 4. DLS Measurements on Waste Form Solutions 132
  - 5. Data Analysis 132
- D. Results 133
  - 1. Calibration Using Polystyrene Standards 133
  - 2. Leachate from Long-Term, Intermittent, Flow Test on Radioactive Glass 134
  - 3. Leachate from Long-Term, Static Test on Radioactive Glass 137
  - 4. Spent Fuel Leachate 138
- E. Conclusions 138
- F. Ongoing Work 139

XI. ACKNOWLEDGMENTS 141

XII. REFERENCES 143

LIST OF FIGURES

		Page
1.	Image of Corroded Pit in Altered Fuel Grain with Reacted ε-Phase Particles at Fuel Surface	13
2.	ATM-103 High-Drip-Rate Test after 3.7 Years of Reaction: Concentration of Pu (Pu-M_5 peak) in Unreacted Fuel (minor peak) and in Reacted Fuel (large peak)	14
3.	Electron Energy Loss Spectrum of β-uranophane on the ATM-103 Fragment	14
4.	ATM-103 High-Drip-Rate Test: ^{99}Tc, ^{238}U, and ^{239}Pu Interval Release Fractions	16
5.	ATM-106 High-Drip-Rate Test: ^{99}Tc, ^{238}U, and ^{239}Pu Interval Release Fractions	16
6.	Cross Section through a Reacted Fragment of ATM-103 after 3.7 Years of Reaction	20
7.	Linear Time Dependence of ^{99}Tc Cumulative Release Fractions in the ATM-103 High-Drip-Rate Test	23
8.	ATM-103 Sample: SEM Micrographs of Polished Sections through the Contact between Fuel Grains and Corrosion Rind	26
9.	ATM-106 Sample: SEM Micrographs of Na-boltwoodite	31
10.	ATM-103 Sample: Fuel Grains Covered by Mixed U_{6+} Alteration Phases, Mounted on C-Tape	37
11.	ATM-103 Sample: Red-Orange Particle Mounted on C-Tape	37
12.	ATM-103 Sample: Uranyl Oxy-Hydroxides from Surface of Sample, Mounted on C-Tape	40
13.	Electron Energy-Loss Spectrum of Dehydrated Schoepite Showing the Presence of Np in the Phase	47
14.	X-ray EDS of an Alteration Phase from a High-Drip-Rate Test Reacted for 44 Months	48
15.	Transmission Electron Microscopy Image of ε-Ruthenium Particle within a Spent Fuel Grain	51
16.	Evidence of Pu-Rich Regions in a Vapor Test	53
17.	Schematic Diagram of the Test Vessel and Hanger with Screen	57
18.	SEM Micrographs of Polished Cross Sections through the UO_2 Starting Material	58

LIST OF FIGURES (contd.)

Page

19. SEM Micrograph of a Polished Cross Section through the UO_2 Starting Material Showing Unidentified Fe-Silicate Impurity 58

20. SEM Micrograph of a Polished Cross Section through Reacted Solids from PDT-3 Showing Metal-Alloy Impurity from PDT-3 59

21. SEM Micrograph of Glass Shard Found in Reacted Solids of PDT-3 60

22. Reported Na and Si Concentrations in EJ-13 Waters Prepared by Reacting J-13 with Tuff at 90°C for 80 Days..... 62

23. Total Recovery Rate of Test Solutions..... 66

24. PDT-1: SEM Micrograph of a Polished Section through Reacted UO_2 (BSE image) Showing UO_2 Particle and Internal Grain Boundaries 67

25. PDT-1: SEM Micrograph of a Polished Section through Reacted UO_2 (BSE image) Showing Heterogeneous Fe-Silicate that has Formed a Stringer which Appears to Mimic the Square Grid of the Mesh Screen..... 68

26. PDT-3: SEM Micrograph of Polished Section through Reacted UO_2 Particles Showing Grain-Boundary-Enhanced Dissolution Near the Surface..... 69

27. PDT-3: SEM Micrograph of the Fine-Grained Mixture of Ferric Oxy-Hydroxides and Fe-Silicate on UO_2 Particles 70

28. PDT-3: SEM Micrograph of Ferric Oxy-Hydroxide Precipitated on UO_2 Particles 70

29. PDT-5: SEM Micrograph of Metaschoepite Crystals Precipitated among UO_2 Particles..... 72

30. PDT-5: SEM Micrograph of Metaschoepite Crystals with Fine-Grained Coating..... 72

31. PDT-3: SEM Micrograph of Polished Section through Reacted UO_2 Showing Metaschoepite Crystals between UO_2 Particles 72

32. PDT-5: SEM Micrograph of Unidentified Polycrystalline Particle..... 73

33. PDT-7: SEM Micrograph of UO_2 Particle with a Surface Covered by Small Acicular Crystals that May Be Uranophane..... 74

34. PDT-7: SEM Micrograph of Cluster of UO_2 Particles with Fe-Oxide and Fe-Silicate 75

35. PDT-7: SEM Micrograph of Unidentified Greenish Material..... 75

LIST OF FIGURES (contd.)

		Page
36.	PDT-4: SEM Micrograph of Dehydrated Schoepite Crystals on the Surface of UO_2 Particle	76
37.	PDT-4: SEM Micrograph of Polished Section through Reacted UO_2 Showing Dissolution of UO_2 Particle and Replacement by Dehydrated Schoepite	77
38.	PDT-4: SEM Micrograph of Polished Section through Reacted UO_2 Showing Particle Displaying Little Reaction Texture	77
39.	PDT-4: SEM Micrograph of Ferric Oxy-Hydroxide Precipitated on a UO_2 Particle	78
40.	PDT-6: SEM Micrograph of UO_2 Particle Coated by Thick Layer of Mixed U^{6+} Alteration Phases	79
41.	PDT-6: SEM Micrograph of Sub-Micron-Sized Soddyite Crystals Coating Dehydrated Schoepite Crystals	79
42.	PDT-6: SEM Micrograph of Polished Section through Reacted UO_2 Showing a UO_2 Particle Covered by Dehydrated Schoepite	80
43.	PDT-6: SEM Micrograph of Fe-Oxy-Hydroxide Precipitated on UO_2 Grains	81
44.	PDT-6: SEM Micrograph of Polished Section through Reacted UO_2 Showing Mixed Fe-Oxide and Fe-Silicate Impurity with a Coating of Dehydrated Schoepite	81
45.	PDT-8: SEM Micrograph of Surface of a Reacted UO_2 Particle Covered by Crystals that May Be Dehydrated Schoepite or Another Unidentified Uranyl Oxy-Hydroxide	82
46.	PDT-8: SEM Micrograph of Crystals on the Surface of a Reacted UO_2 Particle Covered by Crystals that May Be Dehydrated Schoepite or Another Unidentified Uranyl Oxy-Hydroxide	83
47.	Variation of U with Reaction Progress	84
48.	Variation of Solution pH with Reaction Progress	85
49.	Variation of U with pH	85
50.	Variation of EJ-13 Components in Test Solutions as Reaction Proceeds	86
51.	Variation of EJ-13(ox) Components in Test Solutions as Reaction Proceeds	86
52.	Variation of Dissolved U with Dissolved Si	87
53.	Variation of Dissolved U with Dissolved Na	88
54.	Variation of Dissolved U with Dissolved Ca	88

LIST OF FIGURES (contd.)

Page

55. Variation of Dissolved U with Dissolved Mg 89

56. Variation of Dissolved U with Dissolved K 89

57. Variation of Dissolved U with Dissolved Li 90

58. Variation of Dissolved U with Dissolved Al 90

59. Variation of Dissolved U with Dissolved B 91

60. Predicted Stability of U Species in EJ-13 Water as a Function of fO_2 and pH for $\{U\}_T = 10^{-5}$ M (25°C) 92

61. Predicted Stability of U Species in EJ-13 Water in Air $\log pO_2 = -0.7$ at 25°C. 94

62. Concentrations of Stainless Steel Components from Tests with Unmodified EJ-13 Water as Reaction Proceeds 97

63. Concentrations of Stainless Steel Components from Tests with EJ-13(ox) Water as Reaction Proceeds 97

64. Variation of Dissolved U with Dissolved Fe 98

65. Variation of Dissolved U with Dissolved Mn 99

66. Variation of Dissolved U with Dissolved Ni 99

67. Variation of Dissolved U with Dissolved Cr 100

68. Variation of Dissolved U with Dissolved Mo 100

69. Cumulative Release of Uranium over Time for Tests 5 and 6 107

70. Cumulative Release of Boron and Lithium from the N2 Tests as a Function of Elapsed Time 115

71. Normalized Cumulative Release of Boron and Lithium from the N2 Tests as a Function of Elapsed Time 115

72. Cumulative Uranium Release from the N2 Tests as a Function of Time 116

73. Cumulative Mass Releases for the Transuranic Elements Np, Pu, and Am from the N2 Tests 117

74. Normalized Actinide Release from the N2 Tests 117

75. Normalized Release of Np, B, Am, and Pu from a Single Test Series, N2-10, which Displayed Evidence of Excessive Clay Spallation 119

LIST OF FIGURES (contd.)

Page

76. Cumulative Release of Boron and Lithium from the N3 Tests as a Function of Elapsed Time 120

77. Normalized Cumulative Release of Boron and Lithium from the N3 Tests as a Function of Elapsed Time 120

78. Cumulative Mass Releases for the Transuranic Elements Np, Pu, and Am from the N3 Tests 121

79. Normalized Actinide Release from the N3 Tests 121

80. Correlation between Count Rate and Concentration for 74 and 304 nm PS Standards 134

81. Intensity Autocorrelation Function Data as a Function of Channel Number for N4-2 Leachate Sample 135

82. Particle Size Distribution for Leachate Sample N4-2 135

83. Intensity Autocorrelation Function Data as a Function of Channel Number for Leachate Sample N4-2 136

84. Particle Size Distribution for Leachate Sample N4-2 136

85. Intensity Autocorrelation Function Data for Leachate Solution from Reaction of SRL 131A Glass with EJ-13 Groundwater at 2000 m^{-1} for 70 Days 137

86. Particle Size Distribution for Leachate Solution from Reaction of SRL 131A Glass with EJ-13 Groundwater at 2000 m^{-1} for 70 Days 138

LIST OF TABLES

Page

1. Disposition of Elements in ε-Phase for Selected Reactive Intervals - ATM-103 High-Drip-Rate Test 10
2. Disposition of Elements in ε-Phase for Selected Reactive Intervals - ATM-106 High-Drip-Rate Test 11
3. Composition of Reacted ε-Phase Particles in ATM-103 Tests 12
4. Cumulative Release Fractions for the High-Drip-Rate Tests 18
5. High-Drip-Rate Tests - Alteration Products after 3.1 Years of Reaction 18
6. Release Fractions for the ATM-106 Low-Drip-Rate Test after 3.1 Years of Reaction and Immersion for Ten Minutes in EJ-13 24
7. X-ray Diffraction d-Spacings for Sample from ATM-103 Reacted for 3.7 Years 28
8. X-ray Diffraction d-Spacings Measured for Specimen Scraped from Zircaloy Retainer from ATM-106 Reacted for 0.8 Years 29
9. X-ray Diffraction d-Spacings for Sample from ATM-106 Fuel Reacted for 4.1 Years 33
10. Alteration Phases Identified by SEM or XRD from ATM Test Samples 43
11. Analyses of Dehydrated Schoepite 47
12. Composition of ε-phase from the Results of the ATM-103 Vapor Hydration Tests 52
13. Composition of ε-phase from the Results of the ATM-103 High-Drip-Rate Tests . 52
14. Test Matrix 56
15. Listing of Several Ferric Oxides, Ferric-Oxy-Hydroxides and Ferric-Silicates 59
16. Compositions of the Two Batches of EJ-13 Water Used in PDTs 61
17. Mass and Recovery Rate of Solution Aliquots at Test Termination 62
18. Concentrations of Components of EJ-13 Water and U at Test Termination 64
19. Concentrations of Stainless Steel Components in Leachant at Test Termination 65
20. Solid Alteration Products Identified or Suggested in PDTs 65

LIST OF TABLES

Page

21. Compositions, in Oxide Weight Percent, of Glasses Used in the N2 and N3 Tests 113

22. Typical Composition of the EJ-13 Water Used in the N2 and N3 Tests 114

23. Composition of the Unfiltered Test Solution Collected from N2-10 on June 17, 1996 115

24. Normalized Release Rates over the Latest 2.5-year Period for Selected Elements from the N2 Test Series 116

25. Comparison of Transuranic Content in Unfiltered and Ultracentrifuge-Filtered Solutions from the N2-12 Test Sampled December 18, 1995 119

26. Alteration Phases Identified on N2 Solid Components 120

27. Normalized Release Rates over the Latest 2.5-year Period for Selected Elements from the N3 Tests Series 122

28. Summary of Alteration Phases Noted on the N3 Test Components Surfaces 123

29. Release Rates over the Latest 2.5-year Period for Technetium from the N2 and N3 Tests Series 124

30. Initial Test Matrix for 200S Glass 126

31. Test Matrix for 200S, 202U, and 165U Glasses 127

32. Proposed Test Matrix for 202R Glass 128

33. Compositions of Glass to be Used in the Vapor Hydration Tests 129

34. Particle Size of Polystyrene Standards Measured by DLS System 133

NOMENCLATURE

AEM	analytical transmission electron microscopy
AGHCF	Alpha-Gamma Hot Cell Facility (at ANL)
ANL	Argonne National Laboratory
AR	autoradiography
ATM	Approved Test Material
BWR	boiling water reactor
CCD	charge coupled device
CONTIN	computer modeling program
DLS	dynamic light scattering
DOE	U.S. Department of Energy
DWPF	Defense Waste Processing Facility
ED	electron diffraction
EDS	energy dispersive spectroscopy
EELS	electron energy loss spectroscopy
ELS	electrophoretic light scattering
EM	U.S. Department of Energy's Office of Environmental Restoration and Waste Management
FY	fiscal year
GENE	General Electric Nuclear Energy
HLW	high-level waste
LLNL	Lawrence Livermore National Laboratory
LLW	low-level waste
M&O	U.S. Department of Energy's Management and Operating Contractor
MCC	Materials Characterization Center
PNNL	Pacific Northwest National Laboratory
PCT	product consistency test
PDF	Powder Diffraction File
PMT	photomultiplier tube
R/T	ratio of mass of radionuclide collected to mass of radionuclide calculated
RH	relative humidity
S	surface area
SEM	scanning electron microscopy
SNM	Special Nuclear Material Division (at ANL)
SOW	Statement of Work
SRL	Savannah River Laboratory
TEM	transmission electron microscopy
ICP-MS	inductively coupled-plasma mass spectroscopy
V	volume
VHT	vapor hydration test
WPA	waste package assemblage
WVDP	West Valley Demonstration Project
XRD	X-ray diffraction
YMP	Yucca Mountain Project

YUCCA MOUNTAIN PROJECT — ARGONNE NATIONAL LABORATORY, ANNUAL PROGRESS REPORT, FY 1997

for

Activity WP 1221

UNSATURATED DRIP CONDITION TESTING OF SPENT FUEL and UNSATURATED DISSOLUTION TESTS OF GLASS

by

P. A. Finn, D. J. Wronkiewicz, R. J. Finch, J. C. Hoh, C. Mertz
J. W. Emery, E. C. Buck, J. Fortner, S. F. Wolf, L. A. Neimark, and J. K. Bates

ABSTRACT

This document reports on the work done by the Nuclear Waste Management Section of the Chemical Technology Division of Argonne National Laboratory in the period of October 1996 through September 1997. Studies have been performed to evaluate the behavior of nuclear waste glass and spent fuel samples under the unsaturated conditions (low-volume water contact) that are likely to exist in the Yucca Mountain environment being considered as a potential site for a high-level waste repository. Tests with actinide-doped waste glasses, in progress for over 11 years, indicate that the transuranic element release is dominated by colloids that continuously form and spall from the glass surface. The nature of the colloids that form in the glass and spent fuel testing programs is being investigated by dynamic light scattering to determine the size distribution, by autoradiography to determine the chemistry, and by zeta potential to measure the electrical properties of the colloids.

Tests with UO_2 have been ongoing for 12 years. They show that the oxidation of UO_2 occurs rapidly, and the resulting paragenetic sequence of secondary phases forming on the sample surface is similar to that observed for uranium found in natural oxidizing environments. The reaction of spent fuel samples in conditions similar to those used with UO_2 have been in progress for over six years, and the results suggest that spent fuel forms many of the same alteration products as UO_2. With spent fuel, the bulk of the reaction occurs via a through-grain reaction process, although grain boundary attack is sufficient to have reacted all of the grain boundary regions in the samples. New test methods are under development to evaluate the behavior of spent fuel samples with intact cladding: the rate at which alteration and radionuclide release occurs when water penetrates fuel sections and whether the reaction causes the cladding to split. Alteration phases have been formed on fine grains of UO_2 in contact with small volumes of water within a several month period when the radiolysis product H_2O_2 is added to the groundwater solution. The test setup has been mocked up for operation with spent fuel in the hot-cell.

EXECUTIVE SUMMARY

Work is ongoing at Argonne National Laboratory -East in support of the Yucca Mountain Project (YMP). This work consists of studies that evaluate the behavior of commercial spent nuclear fuel samples and defense high-level waste (HLW) glass under conditions likely to occur in the potential repository at Yucca Mountain. This report consists of a general overview of drip tests that have been in progress for over five years, with the data tabulated through 3.7 years. Additionally, there are detailed discussions of analyses that have been done on the samples taken from the drip tests. Two new sets of tests that have been developed for use with spent fuel samples are discussed. These are batch tests and drip and vapor tests with clad fuel. Also, drip and vapor hydration tests (VHTs) performed with HLW glass are described.

The drip tests on spent fuel are being done with Approved Test Materials (ATMs) 103 and 106. Considerable information has been presented regarding these tests, and in this report, selected aspects of the data are discussed. Our conclusions for the high-drip-rate tests are as follows.

1. The ^{99}Tc interval release fractions provide a lower limit for the spent fuel reaction in the high-drip-rate tests. In the ATM-103 fuel, 3 wt% of the total inventory of ^{99}Tc is released in 3.7 years.
2. Oxidation of the ε-phase suggests that the oxidizing potential at the fuel surface may be as high as 0.6 V. The oxidant may be H_2O_2, a product of alpha radiolysis of water.
3. The constancy of the ^{99}Tc release fractions over 3.1 years of reaction indicates that a surface reaction is the rate-controlling mechanism for fuel reaction under unsaturated conditions and that the oxidant is possibly H_2O_2, a product of alpha radiolysis of water.
4. Two reaction pathways have been identified from scanning electron microscopy (SEM) examination of through-grain dissolution, seen at the fragment scale, with subsequent formation of uranyl alteration products and dissolution along grain boundaries. The latter pathway results in friability of a spent fuel fragment.
5. The major alteration product identified by X-ray diffraction (XRD) and SEM is Na-boltwoodite, $Na[(UO_2)(SiO_3OH)]\cdot H_2O$, which is formed from sodium and silicon in the water leachant.
6. Elements other than uranium, including Ru, Mo, Cs, and Ba, are incorporated into the U^{6+} alteration products examined so far.
7. Plutonium appears to be concentrated in the spent fuel. It is not found in the leachate nor the alteration products.

The high-drip-rate tests appear to have sufficient liquid to transport dissolved material from the spent fuel to the test vessel. For the low-drip-rate tests, water was sufficient for fuel reaction, but due to water evaporation because of decay heat, the amount of water was reduced too much for radionuclide transport.

Combined optical, SEM, XRD, and energy-dispersive spectroscopy (EDS) examinations of samples taken from tests being performed on the two ATM fuel samples provided detailed information regarding the reaction progress. These examinations indicate that the rate at which groundwater contacts the fuel samples may be the most important single factor determining which alteration phases form as spent UO_2 fuel corrodes in a humid oxidizing environment. Results of the three tests (high-drip-rate, low-drip-rate, and vapor) show several similarities, including corroded grain boundaries, dissolution of fuel grains, and precipitation of U^{6+} phases. The vapor tests display the simplest assemblage of alteration products: only U and the radionuclides in the fuel dissolve into the thin film of water in contact with the fuel surfaces. The most abundant phase

identified in the vapor tests is probably dehydrated schoepite, $(UO_2)O_{0.25-x}(OH)_{1.5+2x}$ ($0 \leq x \leq 0.15$).

The drip tests display more chemically complex alteration phases due to interaction of the fuel with EJ-13 water (rather than only water vapor). The most abundant elements in EJ-13 water are Na and Si, and not surprisingly, the most abundant alteration products in the drip tests are Na- and Si-bearing U^{6+} phases. Other U^{6+} phases are also present, including metaschoepite and β-uranophane, indicating the importance of additional minor phases and elements to the overall corrosion process.

An important observation at this stage is that the time-dependent evolution of the alteration-phase assemblage appears to be strongly dependent on the rate at which the EJ-13 water contacts the spent fuel. Fuel samples exposed to the higher drip rates (nominally 10-times higher than the low-drip rates) display a comparatively simple phase assemblage, consisting of two uranophane-group silicates, β-uranophane and Na-boltwoodite. In contrast, the sample from the low-drip-rate test displays a more complex alteration-phase assemblage, with four or five phases identified. We believe that the simpler phase assemblage in the high-drip-rate tests reflects higher reaction rates for the spent fuel in these tests. Also, samples were not taken from the first sampling periods, and it is possible that the first phases in the paragenetic sequence actually formed but were simply not detected.

Another important observation concerns the identification of uranyl oxy-hydroxides in the VHTs. The precipitation of dehydrated schoepite and metaschoepite in these tests indicates that the film of water that forms on the fuel surface is sufficiently corrosive to dissolve the fuel and form a thin corrosion rind of alteration products. Such a water film is likely present in the drip tests as well, during those intervals when EJ-13 water is not being dripped onto the fuel. It seems likely that the corrosion processes important in the vapor tests are also important in the drip tests. Dehydrated schoepite and/or metaschoepite may continue to form in the drip tests between water injections. If these phases are present when contacted by EJ-13 water, they may be at least as susceptible to dissolution and/or replacement as the unoxidized fuel. The degree to which this phenomenon may be important is unknown.

The mechanism by which the fuel reacted during these tests is important, although we have only limited information available at this time. Most striking is that the fuel in the high-drip-rate test on sample ATM-103 has dissolved along a uniform front that has penetrated from the outer surface into the spent fuel fragments. This "through-grain" dissolution has proceeded without regard to existing grain boundaries. The replacement of the fuel by Na-boltwoodite at the fuel surface may also be self-accelerating. Through-grain dissolution appears to be an important mechanism by which the fuel is reacting in the high-drip-rate tests. Of course, the dissolution of the fuel along grain boundaries is also important in the high-drip-rate tests. This dissolution is especially evident from the extent to which the grain boundaries in one fragment of ATM-103 had been opened, resulting in a friable fragment that decomposed during sample handling.

These data are still preliminary. We must examine additional grains and fragments of reacted fuel to understand more fully the corrosion and alteration processes, including grain-boundary penetration by water, changes in the reactive surface area, and the distribution of radionuclides between the alteration phases and the EJ-13 water.

The drip tests currently being performed on UO_2 and spent UO_2 fuel have demonstrated that these tests are effective methods for examining the alteration of UO_2 and spent fuel in an unsaturated environment, such as may be expected in the proposed repository at Yucca Mountain. Previous drip-test results demonstrated that UO_2 and spent fuel both react with a thin film of water to form a suite of U^{6+} alteration phases. With current experimental designs, the suite of U^{6+} phases

takes two to five years to fully develop. A new type of test termed a "petri-dish" test is intended to accelerate alteration reactions observed in drip tests, so that relevant observations might be made in six months or less, allowing more rapid evaluation of alteration phases. In addition, the composition of the film of water in contact with UO_2 or fuel is not well-known for the drip tests. In the current drip-test methodology, a solution of known composition (EJ-13) is injected into a test vessel, where the water reacts with UO_2 or fuel. This solution eventually drips down through the UO_2 or fuel and accumulates at the bottom of the reaction vessel, where it is periodically sampled. The analysis gives an indication of chemical changes that the solution undergoes between injection and sampling; however, detailed knowledge of the composition of the thin film of water that is actually reacting with the UO_2 or fuel remains elusive. By providing just enough water to maintain a constant film on a small quantity of fuel in a batch test, we plan to monitor the compositional evolution of the water as it reacts to form U^{6+} alteration phases. Note, however, that in drip tests, cations consumed during reaction are replenished, while in the petri-dish tests, the cations are not replenished.

A set of batch tests performed at a high ratio of the UO_2 surface area (S) to the volume of leachant (V) were run as trial experiments for setting up similar tests on spent UO_2 fuel. At this stage, test components and procedures have been examined, with the goal of understanding what factors are most important for the tests on spent fuel. No systematic study of all the experimental conditions has been made yet. Nevertheless, the information gained from these few experiments on UO_2 provides insight into the corrosion of UO_2 at high S/V ratios. We have also gained additional understanding of the potential importance of H_2O_2 (and by implication, radiolytic products) in enhancing fuel dissolution and possibly changing the mechanisms by which fuel corrodes, including the alteration phases that may precipitate. The ease of implementation and relatively rapid results makes these batch tests useful for increasing our understanding of fuel corrosion in an unsaturated environment. These tests are response tests and, thus, provide specific data related to the test conditions. Some information may not be readily available from these tests (e.g., sorption of elements by the screens and vessel walls). However, with proper planning and sample analysis, a great deal can be learned from these experiments.

While the ongoing drip tests simulate the reaction that takes place between a breached fuel rod and dripping water or saturated water vapor, it is likely that the initial contact between water and spent nuclear fuel will be occur when cladding is nearly intact, with only minor perforations existing for water ingress. Under this limited liquid water or water vapor contact, the extent, nature, and rate of spent fuel reaction is of interest. In particular, if the cladding stays mainly intact, even during alteration of the fuel, the release of radionuclides may be reduced. Two sets of tests are being developed to address the reaction of spent nuclear fuel under conditions of intact cladding: (1) water dripping slowly through a defected rod and (2) water vapor reacting with fuel in a defected rod.

The objectives of these dripping-water tests are the same as those for the ongoing drip tests. In addition, the effect of fuel reaction on cladding integrity will be observed. It is possible that alteration products may not form due to stress within the spent fuel section or, if they do form, they may obstruct the throughflow of water. The tests with vapor will be done to determine whether reaction with vapor, which will occur prior to contact by liquid water, will cause failure of the cladding. These tests have been mocked-up and are ready to be started with spent fuel samples.

Ongoing tests with spent nuclear fuel are being performed with Approved Testing Materials (ATMs) that were procured and characterized by the Materials Characterization Center in support of the YMP. Through a review process that included the YMP, the M&O, Lawrence Livermore National Laboratory (LLNL), Pacific Northwest National Laboratory (PNNL), and Argonne, it was determined that additional ATMs are required to complete the suite of spent fuel types that may

be placed in the repository. This year it was determined to procure a high burnup spent fuel, characterize it, and distribute it for testing.

The fuel chosen is a high burnup (60-80 MWd/kU) boiling water reactor (BWR) fuel that satisfies the YMP need for testing the highest burnup BWR fuel currently available. Four of the segments procured contain UO_2 fuel with an original U-235 enrichment of 3.0 or 3.8 wt%. The current enrichments are estimated to be 0.05 and 0.15 wt%, respectively. The other two segments contain $(U,Gd)O_2$ fuel with original enrichments of 3.0 wt% U-235 and 2.0 wt% Gd; the current U-235 enrichment is estimated to be 0.12 wt%. The samples have been received at ANL and are undergoing characterization.

Drip tests designed to replicate the synergistic interactions between waste glass, repository groundwater, water vapor, and sensitized 304L stainless steel in the proposed Yucca Mountain Repository have been in progress for over 10 years with actinide-doped glasses. The N2 Test Series on Defense Waste Processing Facility (DWPF)-type glass has clearly demonstrated the importance of alteration phases in controlling actinide release from the corroding waste glass. These alteration phases may be spalled from the glass surface, releasing the actinides as solution-borne colloids and particulates. The N3 Tests on West Valley Demonstration Project (WVDP)-type glass has formed unusual actinide-containing phases, several of which have been identified. As in the N2 Tests, the N3 Tests initially retain actinides in alteration phases, later releasing them by layer spallation as glass corrosion progresses. This alteration/spallation process effectively results in near-congruent release of elements from the glass, regardless of their solubilities.

Prior to contact with liquid water, HLW glass will contact water vapor (vapor hydration), which will corrode the glass and alter its properties such that the glass initially contacted by dripping water likely will not be as-cast fresh glass. To predict the amount of vapor hydration that will occur under disposal conditions, it is necessary to establish the rate of reaction between water vapor and glass in a water-vapor-saturated air atmosphere as a function of glass composition and temperature. On the basis of on these measurements, it is possible to calculate an activation energy and rate constant for each glass and, from this information, to extrapolate the reaction of glass in saturated water vapor to different temperatures as required by repository performance assessment calculations. As part of this work, a procedure will be developed and documented that can be used to perform the VHT to provide quantitative rate information. As part of the VHT, the alteration phases that form on the surface of the glass will be identified. Although we recognize that radiation may affect the rate of vapor hydration of glass, the bulk of the tests will be performed using glasses containing no fission products. The glasses may contain U or Th. Some tests will be done using a sludge-based radioactive glass to confirm the results generated with the nonradioactive glass.

Development of colloid characterization techniques will provide essential information on colloids generated from waste-form reaction in tests that simulate the expected conditions for the repository. Dynamic light scattering (DLS) has been demonstrated as a technique to examine and monitor waste-form colloids. This task shows that DLS measurements can provide useful information on the particle size distribution and concentration of colloidal species that form during the corrosion of waste forms. Test solutions from ongoing glass and spent fuel tests have been examined by the DLS method. *In situ* DLS measurements have shown that waste-form colloids exist as stable species (for 10 days in two of the cases examined in this study). Dynamic light scattering is a technique that can minimize disadvantages in studying colloids due to poor statistical representation of the leachate colloids, and possible sample preparation artifacts with analytical electron microscopy, and interactions with filter membranes is sequential filtration techniques.

I. UNSATURATED TESTS WITH IRRADIATED SPENT FUEL

A. Introduction

A potential site for the U.S. high-level waste repository is in the volcanic tuff beds at Yucca Mountain, Nevada, a hydrologically unsaturated zone. To qualify this site for licensing, performance assessment calculations are needed to evaluate the impact of potential radionuclide releases. Information and data feed for a source term in these calculations is provided from laboratory information on the reaction behavior of spent fuel under unsaturated and oxidizing conditions. Testing under unsaturated, i.e., limited water, and oxidizing conditions are in progress to evaluate the long-term behavior of commercial spent nuclear oxide fuel at 90°C. In the tests, a thin film of water continuously contacts and reacts with the fuel. All tests are performed in a saturated water vapor environment to evaluate the reactivity of fuel under that condition. In some tests, water is dripped on the fuel to provide additional liquid for transport of reacted material. All tests are done at 90°C. The nominal drip rate is 0.75 mL every 3.5 days in the high-drip-rate test and 0.075 mL every 3.5 days in the low-drip-rate-test.

The purpose of the experiments is to determine the relationship between the rate of fuel alteration and the release rate of radionuclides under unsaturated conditions. Therefore, the extent of spent fuel alteration, e.g., dissolution, under unsaturated conditions is assessed, as is the effect of fuel alteration on radionuclide release. In all tests, a film of water, maintained by the saturated water vapor atmosphere environment, continuously contacts the fuel fragments and provides a potential pathway for material transport. In the high-drip-rate tests, excess water is available to enhance transport of reacted material. The low-drip-rate tests have less water available, thus reducing the amount of radionuclides transported. In the vapor tests, minimum water is available for transport, and the absence of added cations and anions limits the type of alteration products that may form.

B. Objective

The objective of this report is to provide an update on the behavior of commercial oxide spent fuel after 4.1 years of reaction under oxidizing and unsaturated conditions. We report several sets of results: (1) corrosion of ε-phase intermetallic particles composed of Ru-Mo-Tc-Rh-Pd as measured by leachate results and transmission electron microscopy (TEM) examination of the fuel, (2) radionuclide release into the leachate, and (3) reaction of the UO_2 matrix as noted from scanning electron microscopy (SEM) examination. The three sets of results provide a picture of extensive corrosion of the spent fuel. The four areas to be examined are (1) evidence from leachate and TEM data that supports reaction of the ε-phase particles and the use of ^{99}Tc as a marker for fuel reaction, (2) data on the release of radionuclides other than ^{99}Tc, (3) evidence from SEM data that provides information on the types of predominant reaction pathways, and (4) insight into the reaction kinetics based on the ^{99}Tc release behavior. The leachate data for the high-drip-rate tests cover the first 3.7 years of reaction. Scanning electron microscopy and TEM data are available for a few samples at the later test intervals. Detailed discussions of these latter data are found in other sections of this report, while this section provides a general overview.

C. Background and Experimental Approach

Samples of two pressurized-water-reactor fuels, ATM-103, [GUENTHER-1988a] and ATM-106 [GUENTHER-1988b], with burnups of 30 and 45 MW·d/kg U, respectively, are used in the tests. The grain sizes are 17-20 μm and 6-16 μm, respectively. The fuel samples, 7 - 8.5 g each, are fragments with masses in the range of 0.3-1.2 g. The average geometric surface area of the fragments is 2.1×10^{-4} m^2/g. The measured percent distribution of ^{99}Tc [GRAY-1992] for both fuels in the gap, grain-boundary, and fuel matrix is <0.1, <0.1, and >99.8%, respectively. The reported distribution [THOMAS-1989] of ^{99}Tc in ε-phase particles in ATM-103 is as follows.

Most ε-phase particles are within the grains and their diameters vary as a function of radial position, being 20 nm diameter at the pellet edge and 50-100 nm diameter in the pellet mid- and center sections. Particles at (or along) grain boundaries are ≤1 μm diameter and are located in the mid- and center sections. For ATM-106 fuel [THOMAS-1992], the ε-phase particles within the grains are 20-100 nm diameter in the mid-section. Near the pellet center, 3-10 μm diameter particles were found along grain boundaries. These particles also contained gas bubbles and secondary precipitates.

The experimental configuration, the test procedures, and the composition of the leachant, EJ-13, have been described previously [FINN-1994]. Solution compositions were analyzed with inductively-coupled plasma mass spectroscopy (ICP-MS) in the single standard scan mode with an indium internal standard. For samples after 2.5 years of reaction, bismuth is used as the internal standard for actinides. This technique has a precision of ±15% for the isotopes in the middle mass range (80-160 atomic mass units), but for the actinides and the light elements, the precision may be ±50%. The uncertainties in the ICP-MS data are a maximum of ±50%, depending on radionuclide concentration. The assignment of a mass unit to a particular isotope is done by comparison with the isotopic distribution given in results from ORIGEN code calculations [GUENTHER-1988a]. The term "interval" for the leachate data refers to the time between sequential samplings of the leachate. The "interval release fraction" for a given radionuclide is defined as the ratio (R/T) where R is the mass of radionuclide collected in a given interval, i.e., the total mass in the leachate and the acid strip, and T is the mass of radionuclide calculated to be in the fuel [GUENTHER-1988a]. Since material incorporated into alteration products, adsorbed on the Zircaloy sample holder or adsorbed on the spent fuel, is not included in solution, the release rate of the radionuclide with the largest interval release fraction provides a minimum estimate of the spent fuel reaction rate. The interval release fractions are used to compare releases of different radionuclides for the same reaction interval and of the same radionuclide for different reaction intervals. A "cumulative release fraction" is the sum of the individual interval release fractions over total reaction time.

Sampling took place twice in the last year. The physical appearance of the spent fuel in each test was recorded on videotape by using a macro lens with 10-19X magnification. A fragment of fuel was removed from each test at the 4.1-year test interval for characterization using SEM and TEM. Tape was rolled over the removed fragment to collect alteration products and small pieces of fuel with alteration products attached. This process resulted in the removal of some of the porous alteration products.

The results to date of these characterizations are reported here and in other sections of this report. When appropriate, electron diffraction (ED) data are compared to X-ray diffraction (XRD) data to assist in identification of alteration phases found on the fuel.

D. Results and Discussion

We report results for (1) corrosion of ε-phase intermetallic particles composed of Ru-Mo-Tc-Rh-Pd as interpreted from leachate results and TEM examinations of reacted fuel, (2) radionuclide release into the leachate, and (3) reaction of the UO_2 matrix as noted from SEM and TEM examinations that provide information on reaction pathways.

1. Reaction of the ε-Phase and the Release of ^{99}Tc to the Leachate

This section examines the reaction of the ε-phase in high-drip-rate tests in the leachate for the first 3.1 years of reaction and in some TEM samples from high-drip-rate and vapor tests.

a. Leachate Results

Table 1 provides a summary of the release behavior of the five elements in the ε-phase (Tc, Mo, Ru, Rh, Pd) for tests with ATM-103 for successive reaction intervals. Similar information for the ATM-106 test is shown in Table 2. The information includes (1) the released mass (μg) for the isotope of each element with minimal interference from other elements; (2) the total released mass of each element calculated on the basis of the isotope measured and the element's isotopic distribution; (3) the calculated mass of elements from the ε-phases that reacted, based on the ^{99}Tc release and the distribution of each element in the ε-phase; and (4) the amount of each element that was not released, based on the difference between the material released (column 2) and that calculated to have reacted (column 3). The isotope ^{99}Tc was the dominant element released from ATM-103 and ATM-106 at each reaction interval. Ten per cent of the Mo and only trace amounts of Rh, Ru, Pd were detected in the leachate.

b. TEM Results

Microtomed samples of reacted fuel were examined to determine if ε-phase particles (Ru-Mo-Tc-Rh-Pd) were being oxidized as proposed [FINN-1997]. Table 3 shows the distribution of the five elements in unreacted fuel and the ratio Mo/(Ru+Pd), which can range from 0.9 to 1.5, depending on fission yield [GUENTHER-1988a] or the distribution found in unreacted fuel [GUENTHER-1988a]. To determine if the ε-phase particles had reacted in both the ATM-103 high-drip-rate and the vapor tests, the Mo/(Ru+Pd) mass ratio also was measured in reacted particles, as was the change in the relative masses of the five elements in the ε-phase particles.

Reaction of the ε-phase particles as fuel grains dissolve is evident in Fig. 1, in which individual ε-phase particles <10 nm diameter are shown. Three locations in the TEM sample were examined to find ε-phase particles from the high-drip-rate test that had not totally reacted. The regions are designated edge, dissolution pit, and Pu-rich region. The edge region refers to a location on a reacted fuel grain. The dissolution pit is an area in which only reacted ε-phase particles are found. The Pu-rich region is one in which the Pu concentration is 20 times greater than that expected from the fuel burnup. In Fig. 2, the TEM/electron energy loss spectrum (EELS) spectrum at the U-M absorption edge shows the Pu increase in an area in which spent fuel has reacted. A similar buildup in Pu concentration for reacted fuel has been found in the ATM-103 vapor test. In all three regions in the fuel from the high-drip-rate test (see Table 3), the ε-phase particles have reacted in a similar fashion, i.e., the proportional Ru and Rh content is greater than that of the unreacted ε-phase, and the particles have a new composition in which the Mo/(Ru+Pd) mass ratio is 0.2-0.3. In both the edge region and the Pu-rich region, there is a significant decrease in the Tc and Mo concentrations, but an increase in the Pd concentration. Thus, ε-phase particles that are not totally reacted (i.e., disappeared from the fuel) are depleted in Tc and Mo.

In the ATM-103 vapor test after 4.1 years of reaction, several reacted ε-phase particles were examined (see Table 3). All had a Mo/(Ru+Pd) mass ratio that was lower than that for the unreacted particle, i.e., 0.4-0.5 versus 0.9, and had also retained more Mo than had those in the high-drip-rate test, i.e., about 80% more based on the Mo/Ru mass ratio.

Reaction and dissolution of the ε-phase particles with later incorporation of Mo, Rh, Ru, Pd in alteration products is indicated by two additional pieces of data. First, Mo is found in $(Cs_{0.9}Ba_{0.55})[(UO_2)_5(MoO_2)O_4(OH)_6] \cdot 6H_2O$, a compound found attached to a reacted fuel grain [BUCK-1997]. Second, 1-2 wt% of Ru and Mo are incorporated into β-uranophane, a uranyl silicate, whereas only parts per million of Tc are found in β-uranophane (See Fig. 3).

Table 1. Disposition of Elements in ε-Phase for Selected Reactive Intervals — ATM-103 High-Drip-Rate Test

Isotope	Measured[a] Released Element[b] (μg)	Calculated Released Element[c] (μg)	Calculated Amount Reacted (μg)	Element Retained[d] (mass %)
		0.3 Years Reaction		
^{99}Tc	20	20	20	—
^{97}Mo	0.9	4	50	93
^{101}Ru	0.02	0.07	50	100
^{103}Rh	0.6	0.6	7	92
^{105}Pd	0.04	0.1	0.5	75
		0.8 Years Reaction		
^{99}Tc	10	10	10	—
^{97}Mo	0.05	2	30	94
^{101}Ru	6E-5	2E-4	40	100
^{103}Rh	0.06	0.06	5	99
^{105}Pd	ND[e]	ND	0.3	100
		1.6 Years Reaction		
^{99}Tc	40	40	40	—
^{97}Mo	8	30	100	77
^{101}Ru	2E-3	7E-3	200	100
^{103}Rh	0.02	0.02	20	100
^{105}Pd	2E-3	9E-3	1	100
		2.1 Years Reaction		
^{99}Tc	5	5	5	—
^{97}Mo	2	10	20	44
^{101}Ru	8E-5	2E-4	20	100
^{103}Rh	7E-3	7E-3	3	100
^{105}Pd	8E-3	0.03	0.2	83
		2.5 Years Reaction		
^{99}Tc	10	10	10	—
^{97}Mo	1	6	30	82
^{101}Ru	6E-4	2E-3	30	100
^{103}Rh	0.02	0.02	5	100
^{105}Pd	5E-3	0.02	0.3	94

[a]Measured mass in leachate. Values were rounded to one significant figure.
[b]The isotopic distribution for each element and the mass of the measured isotope were used to determine the total mass released.
[c]For ATM-103, the wt% in the ε-phase are: Tc(11.8); Mo(39.9); Ru(42.3); Rh(5.6); Pd(0.4) [GUENTHER-1998a]. The released ^{99}Tc was the basis for the reacted amount of a given element.
[d]This is the minimum amount retained and is based on ^{99}Tc and its wt% in the ε-phase.
[e]ND = not detected.

Table 2. Disposition of Elements in ε-Phase for Selected Reactive Intervals – ATM-106 High-Drip-Rate Test

Isotope	Measured[a] Released Element[b] (μg)	Calculated Released Element[c] (μg)	Calculated Amount Reacted (μg)	Element Retained[d] (mass %)
		0.3 Years Reactions		
^{99}Tc	0.07	0.07	0.07	---
^{97}Mo	0.05	0.2	0.2	4
^{101}Ru	0.03	0.1	0.2	50
^{103}Rh	0.1	0.1	0.04	XS[e]
^{105}Pd	0.04	0.2	0.1	XS
		0.8 Years Reaction		
^{99}Tc	0.9	0.9	0.9	—
^{97}Mo	4	20	3	XS
^{101}Ru	0.02	0.05	3	83
^{103}Rh	0.02	0.02	0.4	50
^{105}Pd	ND[f]	ND	2	100
		1.3 Years Reaction		
^{99}Tc	0.4	0.4	0.4	---
^{97}Mo	0.08	0.3	1	70
^{101}Ru	8E-3	0.03	1	97
^{103}Rh	0.03	0.03	0.2	85
^{105}Pd	0.03	0.1	0.8	87
		1.6 Years Reaction		
^{99}Tc	10	10	10	—
^{97}Mo	2	9	40	77
^{101}Ru	6E-4	2E-3	30	100
^{103}Rh	4E-3	4E-3	5	100
^{105}Pd	ND	ND	20	100
		2.1 Years Reaction		
^{99}Tc	30	30	30	—
^{97}Mo	0.07	3	105	97
^{101}Ru	1E-3	3E-3	90	100
^{103}Rh	6E-3	6E-3	15	100
^{105}Pd	3E-3	0.01	60	100
		2.5 Years Reaction		
^{99}Tc	30	30	30	—
^{97}Mo	0.07	3	105	100
^{101}Ru	1E-4	3E-4	90	100
^{103}Rh	0.01	0.01	15	100
^{105}Pd	5E-3	0.02	60	100

[a]Measured mass in leachate. Values were rounded to one significant figure.
[b]The isotopic distribution for each element and the mass of the isotope that was measured were used to determine the total mass released.
[c]The wt% for ATM-106 for the ε-phase were: Tc(10); Mo(35); Ru(30); Rh(5); Pd(20) [THOMAS-1992]. The released ^{99}Tc mass was the basis for the amount of a given element that reacted.
[d]This is the minimum amount retained and is based on ^{99}Tc and its wt% in the ε-phase.
[e]XS = excess measured.
[f]ND = not detected.

Table 3. Composition of Reacted ε-Phase Particles in ATM-103 Tests (elements in wt%)

Unreacted Particles

Element	Fission Yield[a]	Grains[b] Boundary	Grains[b]
Mo	40	39.9	52
Tc	10	11.8	8
Ru	30	42.3	23
Rh	5	5.6	6
Pd	15	0.4	12
Mo/(Ru+Pd)	0.9	0.9	1.5

High-Drip-Rate Test after 3.7 Years of Reaction

Element	Edge Region	Pit Region	Pu-Rich[c] Region
Mo	12	17	15
Tc	5	10	4
Ru	42	45	45
Rh	8	8	10
Pd	33	11	26
Mo/(Ru+Pd)	0.2	0.3	0.2

Vapor Test after 4.1 Years

Element	Sample #1	Sample #2	Sample #3	Sample #4	Sample #5
Mo	29	30	30	29	26
Tc	9	12	11	17	15
Ru	40	30	30	33	42
Rh	—	—	—	—	—
Pd	22	28	28	22	17
Mo/(Ru+Pd)	0.5	0.5	0.5	0.5	0.4

[a]This is the average distribution in the fuel.
[b]Guenther-1988a
[c]Quantification of the electron energy loss spectrum was done using a 100-eV window and the oscillator strength values calculated from a Dirac-Foch model.

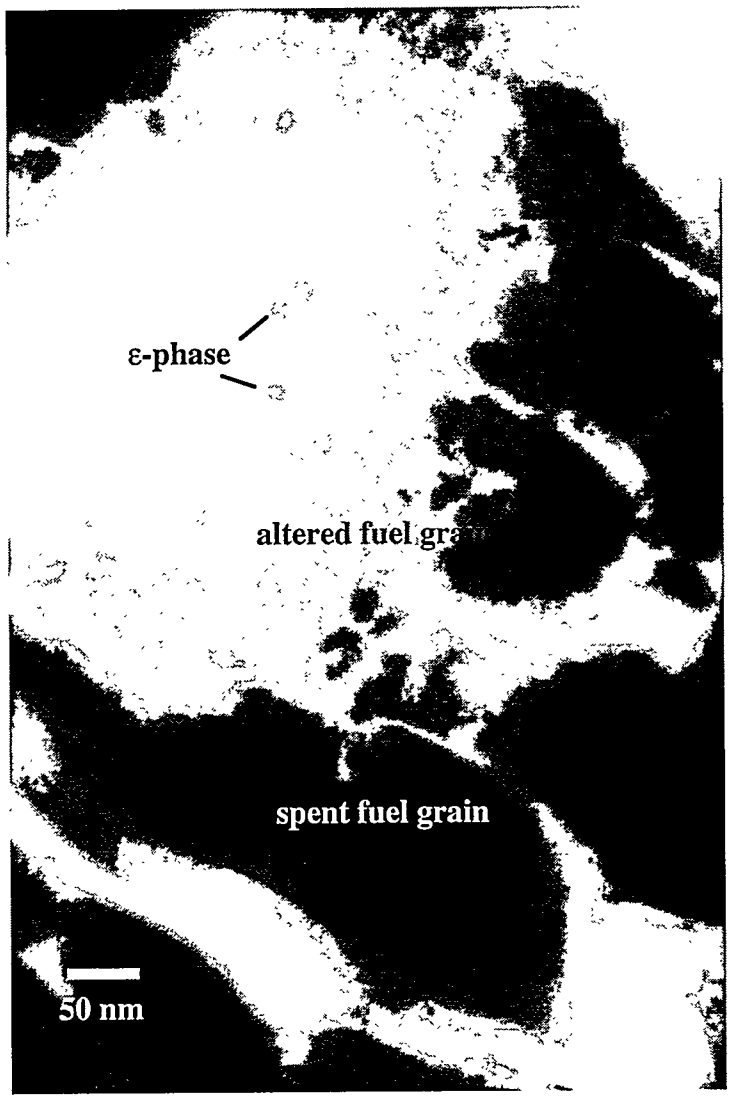

Fig. 1. Image of Corroded Pit in Altered Fuel Grain with Reacted ε-Phase Particles at Fuel Surface

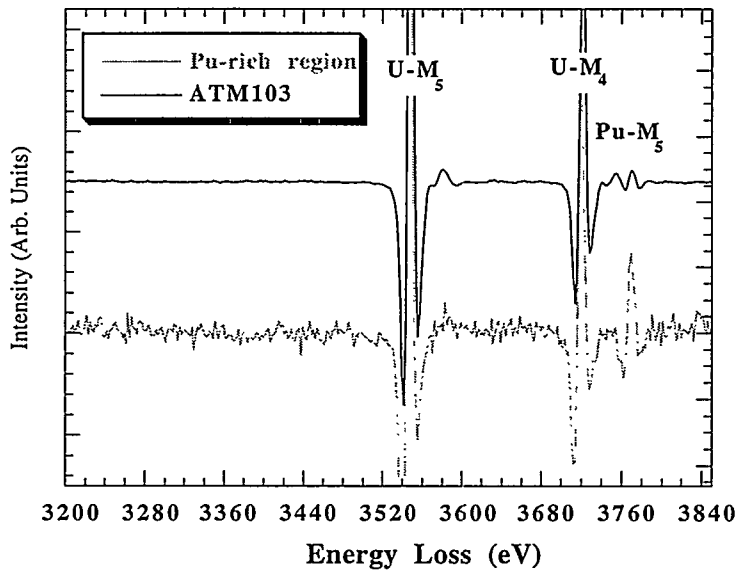

Fig. 2. ATM-103 High-Drip-Rate Test after 3.7 Years of Reaction: Concentration of Pu (Pu-M_5 peak) in Unreacted Fuel (minor peak) and in Reacted Fuel (large peak)

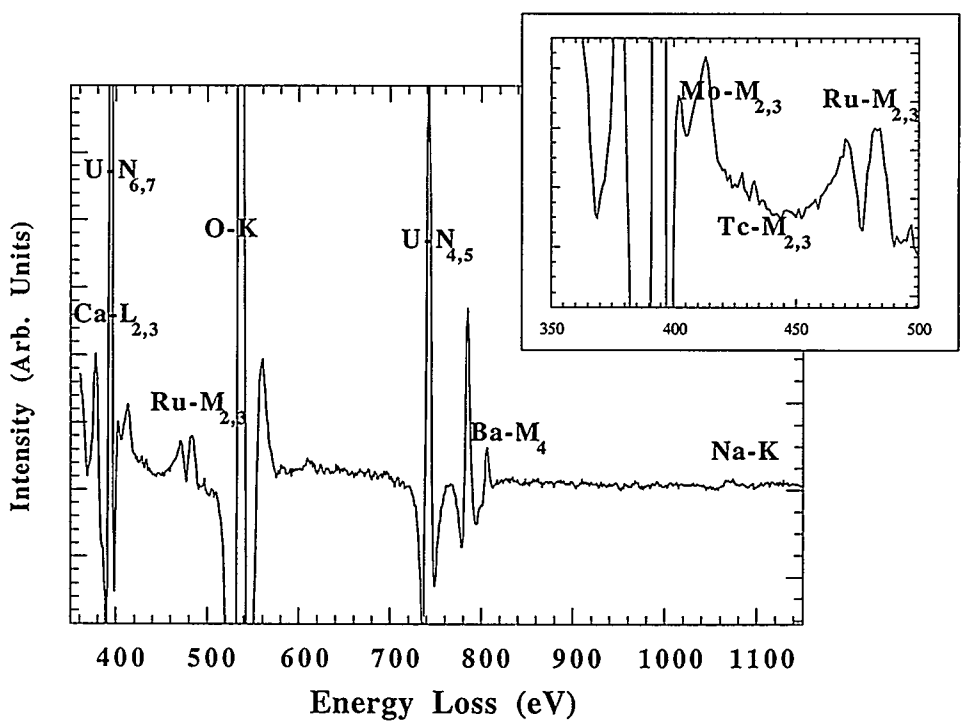

Fig. 3. Electron Energy Loss Spectrum of β-uranophane on the ATM-103 Fragment. (Uranophane has incorporated at least 1-2 wt% Ru [also seen in the energy dispersive spectrum], and Mo and 100 times less Tc [See insert]).

c. Oxidation Potential

The presence of soluble forms of ^{99}Tc and ^{97}Mo in the leachate (pH 7 at room temperature) indicates that the fuel matrix surrounding the ε-phase particles dissolves, exposing the particles to an oxidizing environment. For comparison, Kleykamp [KLEYKAMP-1985] notes that complete dissolution of ε-phase particles 0.15-1.5 μm in diameter requires eight hours for complete dissolution in boiling nitric acid.

In our "unsaturated" tests, water vapor at 90°C supplies a continuous thin film of water on each spent fuel surface, a film that may be <10 nm thick [HAGYMASSY-1969]. Allen noted that the primary yield of H_2O_2 from alpha radiolysis of water is 1.2 times that from gamma radiolysis of water [ALLEN-1961]. The unique nature of alpha radiolysis is that the H_2O_2 is produced in dense tracks within the first 30 μm (the alpha particle range) of the fuel surface, thus ensuring that the relative concentration of the H_2O_2 is very high at the surface of the spent fuel.

We estimate how high an oxidation potential exists at the fuel surface in two ways. Shoesmith et al. [SHOESMITH-1985] note that for reaction of unirradiated UO_2 at pH 9.5 with an alpha source 30 μm away, the redox potential is 0.11 V (versus a saturated calomel electrode), a value similar to that in an equivalent H_2O_2 solution or in a saturated O_2-containing solution. (The corresponding corrosion potential would be -0.14 V.)

Since we note dissolution of Ru, Mo, and Tc in the unsaturated tests, we estimate the corrosion potential in the unsaturated tests by considering the Eh required to form soluble ions of Tc, Mo, Ru, Rh, and Pd based on Eh/pH diagrams [BROOKINS-1988] for 10^{-8} M concentrations. For Mo and Tc at pH 7, a minimum Eh of 0 and 0.3 V, respectively, is needed to stabilize TcO_4^- and $HMoO_4^{2-}$, whereas for PdO_2 and RuO_4^-, a minimum Eh of 0.5 and 0.6 V, respectively, is needed. For Rh, a soluble form is noted only at pH 4 and an Eh of 0.65 V. Recognizing that these diagrams are applicable for 25°C, we applied them to the test conditions; thus, the oxidation potential at the fuel surface may be as high as 0.6 V since Ru dissolved and is incorporated into β-uranophane. Thus, ε-phase particles (<1-100 nm diameter) could react and release ^{99}Tc in each 0.5 year reaction interval, but larger particles (1 μm) might not completely react (see Fig. 1).

Since the ε-phase particles are homogeneously dispersed in the ATM-103 fuel matrix [GUENTHER-1988a] and both fuels have similar ^{99}Tc release behavior, we propose the use of ^{99}Tc release fraction as an indicator of the minimum extent of the reaction of the fuel matrix under unsaturated and oxidizing conditions. Support for this proposal can be found in comments of earlier workers. Forsyth and Werme [FORSYTH-1991] found that after 2.7 years of reaction under oxidizing conditions, ^{99}Tc was the only radionuclide whose release fraction had remained constant in batch tests with spent oxide fuels. They suggested that ^{99}Tc was oxidized and released as the matrix around the ε-phase particles reacted. Wilson [WILSON-1990] also suggested that Tc was oxidized prior to release in "semi-static" tests. Curtis and Gancarz [CURTIS-1983] proposed that oxidative dissolution of the uraninite at the Oklo natural reactor site in Gabon, Africa, was caused by water radiolysis in the reactor zones, which led to production of species that oxidized uraninite, dissolved the ε-phase, and permitted transport of soluble species from the reactor zone.

2. Radionuclide Releases Compared to the ^{99}Tc Release

The use of the ^{99}Tc release fraction as a marker for the minimum extent of the spent fuel reaction (minimum since there may be some Tc holdup in alteration products - see below) has been proposed [FINN-1997]. The ^{99}Tc interval release fraction has been relatively constant over 3.7 years of reaction for the high-drip-rate tests for ATM-103 fuel (Fig. 4) and from 1.3 to 3.7 years of reaction for ATM-106 fuel (Fig. 5). Also shown in Fig. 4 and Fig. 5 are the interval

release fractions for ^{238}U and ^{239}Pu. The decrease in the U and Pu release fractions after 1.6 years of reaction is apparent in both figures.

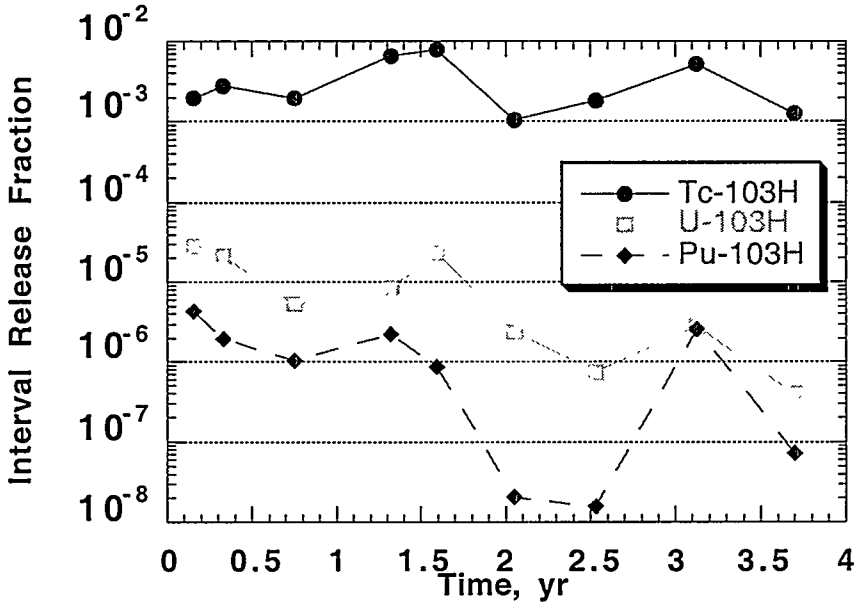

Fig. 4. ATM-103 High-Drip-Rate Test: ^{99}Tc, ^{238}U, and ^{239}Pu Interval Release Fractions

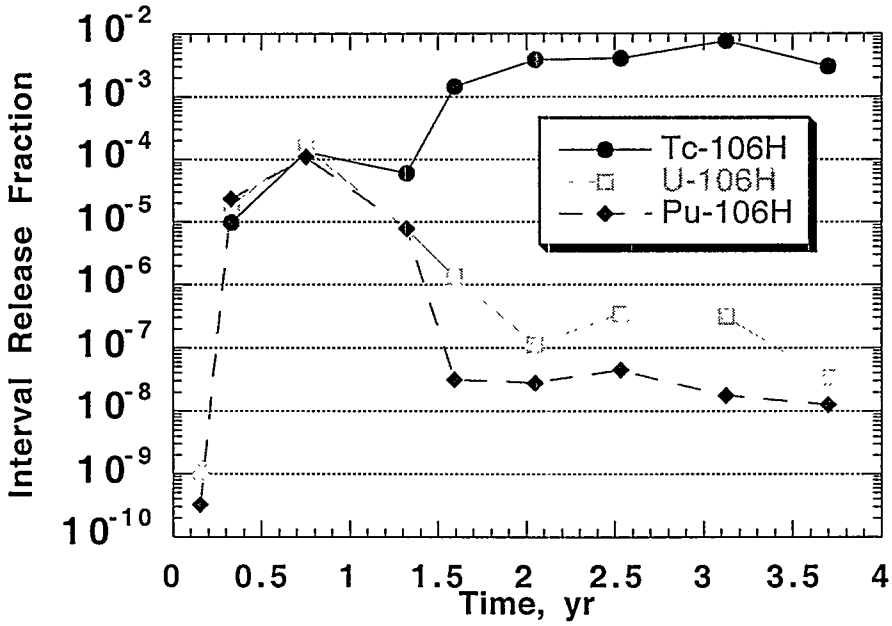

Fig. 5. ATM-106 High-Drip-Rate Test: ^{99}Tc, ^{238}U, and ^{239}Pu Interval Release Fractions

Our estimate of the mass of fuel dissolved at the time is based on the Tc results. The estimate will be improved with additional analyses of the reacted samples. However, the small amount of Tc held in β-uranophane, combined with the close structural similarity of Na-boltwoodite to β-uranophane, makes the following calculation a reasonable first approximation. Based on our Tc release data, three percent of the spent fuel has been dissolved as of 3.7 years. The fuel initially contained approximately 95% or greater UO_2, and since each test contains approximately 8 g of fuel approximately 0.23 grams of UO_2 was in the fuel that dissolved. As a first approximation, we assume that Na-boltwoodite incorporated all the dissolved UO_2 (99.9% actually) and that Na-boltwoodite is the only alteration product formed. Ideally, Na-boltwoodite contains 66.8 wt% UO_2, which implies the formation of approximately 0.34 g of Na-boltwoodite. We can assume further that the concentration of Tc found in β-uranophane is the same as in Na-boltwoodite, i.e., a few ppm Tc (say, 2.5 ppm). This means alteration products (modeled as Na-boltwoodite) contain approximately 8.5×10^{-7} g Tc. The concentration of Tc in the original fuel was approximately 10^{-5} Ci gram of UO_2, meaning that 2.3×10^{-6} Ci of Tc have been dissolved from the fuel. The specific activity of Tc is 1.69×10^{-2} Ci g^{-1}, so that a total 1.36×10^{-4} g of Tc was dissolved along with the 0.23 g of UO_2. This simple approach indicates that alteration products have retained approximately 0.6% of the Tc dissolved from the fuel. We have made some simplifying assumptions, implying a fairly high degree of uncertainty. Nevertheless, the actual amount is almost certainly within a fractor of 10.

In Table 4, the cumulative release fractions for ^{99}Tc, ^{238}U, and ^{239}Pu, as well as for ^{137}Cs and ^{97}Mo, are shown for several cumulative reaction times. Table 4 illustrates the following points. First, after 3.7 years of reaction, the cumulative ^{99}Tc release fractions for the two fuels are similar, 3% of the total inventory for ATM-103 and 2% for ATM-106. Second, for the ATM-103 fuel, the ^{97}Mo cumulative release fraction after 3.7 years of reaction is similar to the ^{99}Tc cumulative release fraction; however, for the ATM-106 fuel, the ^{97}Mo release fraction is only 10% of the ^{99}Tc release fraction. Thus, some of the ^{97}Mo appears to be held up in the ATM-106 test. However, at 4.1 years of reaction, the ^{97}Mo and ^{99}Tc release fractions appear comparable (data analysis is still in progress). Third, the ^{137}Cs cumulative release fractions for the two fuels are similar but are only 10-20% of the cumulative ^{99}Tc release fraction. It appears that most ^{137}Cs is held up. An alteration product that can incorporate both Cs and Mo is $(Cs_{0.9}Ba_{0.55})[(UO_2)_5(MoO_2)O_4(OH)_6] \cdot 6H_2O$ [BUCK-1997]. The formation of this alteration product could account for the hold up of ^{137}Cs and ^{97}Mo relative to ^{99}Tc, especially in the ATM-106 test prior to 4.1 years of reaction. Fourth, prior to the first 1.6 years of reaction, both fuels had a large ^{238}U release fraction (Figs. 4 and 5), but thereafter, most (99.9%) of the reacted uranium remained on the fuel surface in alteration products. This point is based on the difference in release fractions between ^{99}Tc and U, the visual appearance of the fuel, and the weight gain measured. Fifth, prior to the first 1.6 years of reaction, both fuels had a ^{239}Pu release fraction that was equivalent to 10-40% of the U release fraction. At longer reaction times, most of the Pu was held up. (See Figs. 4 and 5).

The reaction suggested by the leachate data for both fuels is one in which there is a continuous release of ^{99}Tc over four years of reaction, consisting of at least 0.3% of the total inventory in each six-month interval. The U release effectively ceases after about a year, but uranium is incorporated into alteration products that form on the surface of the fuel. Alteration phase formation increases after 1.6 years of reaction, but the ^{99}Tc release does not increase. The ^{99}Tc release fraction can be used to calculate the fraction and thus the mass of uranium that has reacted. This value can be compared to the amount of sodium and silicon removed from the dripped EJ-13 water. In addition, the mass gain for the reacted spent fuel can be compared to the expected increase in mass due to the formation of alteration products. These data are summarized in Table 5 for the two fuels after 3.1 years of reaction. (Units of moles are used for simplicity in comparing the different elements.)

Table 4. Cumulative Release Fractions[a] for the High-Drip-Rate Tests

ATM No.	^{99}Tc	^{97}Mo	^{137}Cs	^{238}U	^{239}Pu
		1.6 Years of Reaction			
ATM-103	2.1E-2[b]	1.9E-3	1.8E-3	8.6E-5	9.8E-6
ATM-106	1.6E-3	8.5E-4	3.0E-3	1.8E-4	1.4E-4
		2.5 Years of Reaction			
ATM-103	2.4E-2	2.6E-3	2.0E-3	9.0E-5	9.9E-6
ATM-106	9.6E-3	1.0E-3	3.4E-3	1.8E-4	1.4E-4
		3.1 Years of Reaction			
ATM-103	2.9E-2	1.4E-2	3.7E-3	9.2E-5	1.0E-5
ATM-106	1.7E-2	0.8E-3	4.0E-3	1.8E-4	1.4E-4
		3.7 Years of Reaction			
ATM-103	3.0E-2	1.6E-2	4.7E-3	9.3E-5	1.0E-5
ATM-106	2.0E-2	2.1E-3	5.0E-3	1.8E-4	1.4E-4

[a]Cumulative release fractions have been rounded to two significant figures.
[b]Exponential notation is used. The number following the E refers to the exponent of 10 by which to multiply the number before the E; e.g., 2.1E-2 means 2.1×10^{-2}.

Table 5. High-Drip-Rate Tests - Alteration Products after 3.1 Years of Reaction

Species	Na-Boltwoodite[a] (mol)	Dehydrated Schoepite[b] (mol)	Excess[c] (mol)	Total (mol)	Calculated Weight[d]-UO_2 (g)	Measured Weight Gain[e] (g)
ATM-106					0.07	0.06
U	2.9E-4	6E-5	1E-4	4.5E-4		
Si	2.9E-4	—	—	2.9E-4		
Na	2.9E-4	—	6E-4	8.9E-4		
ATM-103					0.07	0.05
U	2.7E-4	2E-4	2.9E-4	8E-4		
Si	2.7E-4	—	—	2.7E-4		
Na	2.7E-4	—	5E-5	3.2E-4		

[a] Formula: $Na[(UO_2)(SiO_3OH)] \cdot H_2O$. This was the major alteration product based on XRD analysis; the silicon was assumed to be primarily in this product. The total moles of uranium are based on the ^{99}Tc release fraction.
[b] Formula: $UO_3 \cdot 0.8\ H_2O$. This was identified in the vapor test.
[c] The moles listed are the difference between the measured and the total moles. The excess may result from uncertainty in the analyses of Na and U in solution and U unaccounted for during solids analysis.
[d] Difference between sum of masses of alteration products and the original fuel's UO_2.
[e] Difference between original fuel weight and that after 3.1 years of reaction. The weight gain for the interval between 2.5 and 3.1 years was estimated as the average over the previous 2.5 years: 0.01 g/0.5 yr for ATM-106 and 0.007 g/0.5 yr for ATM-103. Weights when water was retained were not used.

The major alteration product in the high-drip-rate tests is Na-boltwoodite on the basis of SEM and XRD analyses. Some uranium is also incorporated into dehydrated schoepite on the basis of its identification in the vapor test [BUCK-1998]. Other alteration products present include the Cs-bearing uranyl molybdenum-oxy-hydroxide.

3. Spent Fuel and Its Alteration Products

As spent fuel reacts, there is the potential for incorporation of radionuclides from the reacted spent fuel into alteration products. This incorporation could reduce or delay the release of radionuclides from the waste package. For example, using TEM, Np was detected in dehydrated schoepite that formed in a vapor test. See later sections of this report for details.

Bright-yellow alteration products are first clearly observed on the fuel surface in the high-drip-rate tests after 2.5 years of reaction [FINN-1995]. Examination of the fuel fragments from these tests after 3.7 years of reaction indicate two layers of light-yellow alteration products. The outer layer is easily manipulated with a fine tungsten needle, but a thinner inner layer immediately adjacent to the fuel is denser and adheres tenaciously to the surface.

As a fuel fragment in the ATM-103 high-drip-rate test was examined after 3.7 years of reaction, it disintegrated into individual grains and clumps of grains. This suggests that reaction occurs along the grain boundaries throughout the fuel fragment. A piece of this friable fragment was polished and examined with SEM. Based on crystal morphology, chemical composition (energy dispersive spectroscopy [EDS]), and XRD, the most abundant (~80 vol%) alteration product is Na-boltwoodite, $Na[(UO_2)(SiO_3OH)] \cdot H_2O$. Additional minor phases are detected by TEM and XRD analyses, including β-uranophane, $Ca[(UO_2)_2(SiO_3OH)_2] \cdot 5H_2O$ (~10-20 vol%). (From TEM/EELS analysis, both Mo and Ru are found at levels of 1-3 wt% in the β-uranophane.)

In Fig. 6, a cross section through one piece of the reacted ATM-103 fragment is shown. Gaps of ≤ 0.5 μm between the fuel grains are visible in the brightest region in the image. No alteration phases are detected between the grain boundaries, nor is Si evident in the grain boundaries from EDS. TEM examination of the edges of the fuel grains found no evidence for oxidation of UO_2 to $UO_{2.25}$, although evidence for additional reaction appears in some preliminary SEM micrographs.

Surrounding the fuel is an alteration layer (~20-40 μm thick) consisting predominantly of Na-boltwoodite. This layer consists of two regions: a dense inner layer, 5-10 μm thick, closest to the fuel surface, and a porous outer layer, 10-30 μm thick. No difference in composition is evident between the two layers from EDS. Near the outer edge of the dense inner layer is an interface defined by a gap (dark band) that lies approximately 10 μm above the fuel surface and 2-3 μm below the outer edge of the dense layer. Below the gap, crystals of Na-boltwoodite have formed more or less perpendicular to the fuel surface, whereas above the gap, Na-boltwoodite forms a dense mat of crystals sub-parallel to the fuel surface. Above these flat-lying crystals is the porous outer layer. As the fuel dissolves, Na-boltwoodite replaces the fuel at the surface uniformly inward from the original outer surface in a fairly uniform fashion, thus forming the inner dense layer.

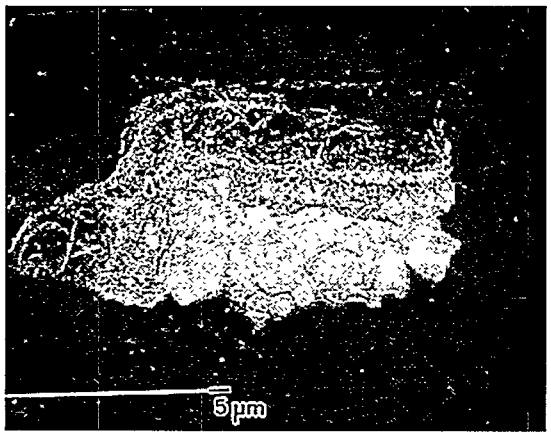

a)

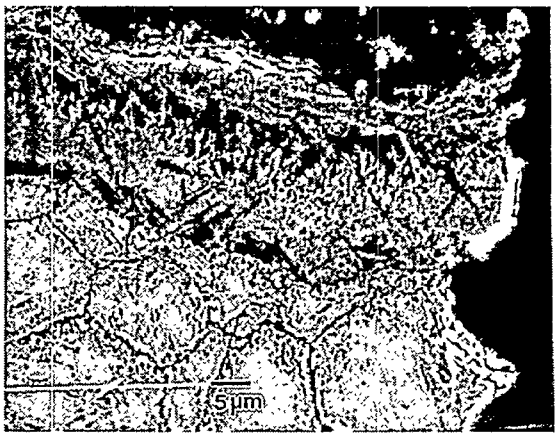

b)

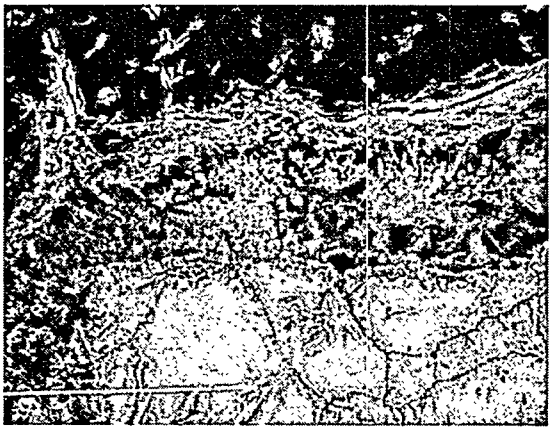

c)

Fig. 6. (a) Cross Section through a Reacted Fragment of ATM-103 after 3.7 Years of Reaction. (Brightest area is fuel grains with grain boundary gaps. Medium contrast is Na-boltwoodite. Darkest contrast is epoxy.) (b) A Magnified View of the Right Side of the Cross Section Showing the Grain Boundary in the Fuel and the Two Layers of Na-boltwoodite. (c) A Magnified View of the Left Side of the Cross Section Showing a Thinner Reaction Layer of Na-boltwoodite.

A large volume of alteration products is forming on the surface of the spent fuel fragments. The presence of these alteration products does not appear to reduce the rate of spent fuel reaction in the high-drip-rate tests, as shown by the continued release of ^{99}Tc and the friable nature of the ATM-103 fuel fragment after 3.7 years of reaction. The disintegration of the ATM-103 fragment is similar to fuel behavior in oxidation tests done at 200°C [WASYWICH-1993] in the presence of water vapor. In those tests, schoepite formed along grain boundaries but did not impede further reaction progress throughout the grain-boundary network. Since our tests use a silicate-groundwater, yellow uranyl silicates form on the fuel surface. These products and their control over access of reactants to the fuel surface will be carefully examined in future evaluation of the test results.

4. Reaction Pathways

We have [FINN-1997] suggested that the dissolution of spent fuel is controlled by the oxidizing effect of the products of alpha radiolysis of the thin film (<10 nm [HAGYMASSY-1969]) of water at the fuel surface [SHOESMITH-1985]. The oxidants also facilitate oxidation and dissolution of the ε-phase particles. Since the ε-phase particles are homogeneously dispersed in the ATM-103 fuel matrix [GUENTHER-1988a], the rate of matrix dissolution should govern their rate of exposure to the oxidizing environment, and, consequently, the ^{99}Tc release fraction should reflect the minimum matrix dissolution rate.

In the ATM-103 high-drip-rate test, 3% of the ^{99}Tc inventory is released after 3.7 years of reaction. This release occurs in steady increments, which suggests either that the reaction pathways have been constant during this time or that the contribution from multiple reaction pathways has not varied over time. From mass balance considerations, i.e., the depletion of sodium and silicate from the EJ-13 leachant, the fraction of uranium that reacts to form Na-boltwoodite is comparable to the fraction of ^{99}Tc released. The change in composition of partially reacted ε-phase particles is consistent with the leachate data, i.e., that the ε-phase particles are reacting as the spent fuel dissolves, leaving behind insoluble Rh and Pd.

The SEM data for the ATM-103 high-drip-rate sample provides insight into the possible reaction pathways that contribute to matrix dissolution. The two pathways seen in Fig. 6 are through-grain dissolution and grain-boundary dissolution. The configuration of the alteration products leads us to believe that the dense inner layer represents a region in which the spent fuel has been replaced by Na-boltwoodite. The gap, which is ~10 μm above the fuel surface, is interpreted as corresponding to the position of the original surface of the unreacted fuel.

In Fig. 6c, the thickness of the dense layer is ≤ 5 μm at the extreme left corner, which may suggest that replacement is not isovolumetric. However, to obtain an estimate of the maximum amount of spent fuel that reacts by through-grain dissolution, one can use the average thickness of the reacted layer (10 μm) and assume that replacement is 100% isovolumetric. The maximum amount of reacted fuel is then 2.3 wt% of the total mass of uranium in the test, assuming a geometric surface area of 2.1×10^{-4} m^2/g and an ~8-g sample. However, because there is about a four-fold volume increase from cubic UO_2 (molar volume = 0.041 nm^3) to monoclinic Na-boltwoodite (molar volume = 0.157 nm^3), a maximum of 25% of the uranium in the replaced fuel layer is incorporated by the Na-boltwoodite within the dense inner layer. The remaining 75% of the uranium is transported out of this layer. Of this latter amount, perhaps up to half can be accounted for by the outer porous layer of Na-boltwoodite. The other half may be accounted for by (1) the portion of the alteration layer that is lost in preparing the SEM sample, (2) the nonuniform thickness of the alteration layer noted in visual examinations, (3) the amount of alteration phases remaining in the base of the Zircaloy fuel holder (noted but not measured), and (4) the uranium released to solution.

Dissolution also occurs along grain boundaries, as is evident from the friable nature of the fuel fragment and the gaps found between grains (Fig. 6). The minimum extent of the grain-boundary reaction can be estimated by subtracting the maximum extent of through-grain reaction (2.3 wt%) from the cumulative ^{99}Tc release fraction (3 wt%); this minimum is 0.7 wt% of the total mass. Through-grain dissolution of the UO_2 fuel matrix seems to predominate over grain boundary dissolution, since the surface area of fuel reacted along grain boundaries is quite large compared to a uniform ~10-μm-thick surface replacement layer. Thus, as the grain boundaries open, the ^{99}Tc release fractions should increase if grain boundary dissolution predominates.

The formation of Na-boltwoodite at the fuel surface suggests that subsequent to matrix dissolution, uranium ions in solution coprecipitate with the sodium (Na^+) and the silicon (H_4SiO_4) from the groundwater. An equation that accounts for the net oxidative dissolution of the

UO_2 fuel by an oxidizing source (represented by O_2), and the subsequent formation of Na-boltwoodite is:

$$UO_2 + H_4SiO_4 + Na^+ + 1/2\ O_2 \Rightarrow Na[(UO_2)(SiO_3OH)]\cdot H_2O + H^+ \qquad (1)$$

As Na- and Si-rich EJ-13 water is added to an unsaturated system with an oxidizing source, the net replacement reaction proceeds to the right provided H^+ is removed. The effects of other reactions are considered in Section IV.

5. Potential Mechanism in the Spent Fuel Reaction

Grambow et al. [GRAMBOW-1996] found that for unirradiated UO_2 the reaction rate depends only on the concentration of the oxidant and concludes that even under initially anoxic conditions, the spent fuel dissolution process is oxidative. Therefore, the local steady-state concentration of oxidants at the surface is of key importance for the extent of the fuel reaction and may provide an upper limit to the total amount of reaction.

In the unsaturated tests, there is a steady-state concentration of H_2O_2, as well as other radiolysis products, in the thin film of water at the fuel surface. Reaction with the oxidants occurs at the surface and proceeds along grain boundaries as shown by the friable nature of the ATM-103 fragment. The alteration products do not form a protective layer that decreases fuel dissolution since the ^{99}Tc interval release fractions are constant over 3.1 years of reaction. Since ppm of ^{99}Tc are present in the alteration phases, the fuel reaction rate is slightly higher than that estimated from ^{99}Tc interval release fractions.

If one accepts ^{99}Tc release as a measure of fuel reaction rate, then it can be used to examine five suggested reaction processes [GRAMBOW-1990]. These are: (1) solubility-limited dissolution of alteration products, (2) transport of oxygen to the UO_2 surface, (3) growth of alteration products, (4) the rate of formation of oxidants by radiolysis, and (5) surface reaction.

For solubility-limited dissolution to control rate, radionuclide release rates have to decrease significantly as a function of time. This might control ^{238}U release but not the reaction of the fuel, since the ^{99}Tc release fractions do not decrease as a function of time.

For oxygen transport to control the rate, a diffusion process has to be established. Diffusion does not appear to control the rate since the best fit of ^{99}Tc cumulative release was found to have a linear dependence on time (see Fig. 7).

For the growth of alteration products to control the rate, release should be constant or should increase as the surface area increases, i.e., as grain boundaries open. For both unsaturated tests, no increase was noted in the ^{99}Tc release rate as a function of time, although the surface area increased. Instead, the ^{99}Tc release fractions for ATM-103 are the same order of magnitude during 3.1 years of reaction. Thus, this mechanism does not appear to control the rate.

The rate of formation of oxidants by radiolysis also does not appear to control the fuel reaction rate since Grambow et al. noted [GRAMBOW-1996] that, even in a reducing environment, radiolysis supplied sufficient oxidants to oxidize spent fuel. However, if the rate of a surface reaction is faster than the rate of oxidant formation, the rate of oxidant formation could be rate controlling since it determines the oxidant concentration that is available for the surface reaction.

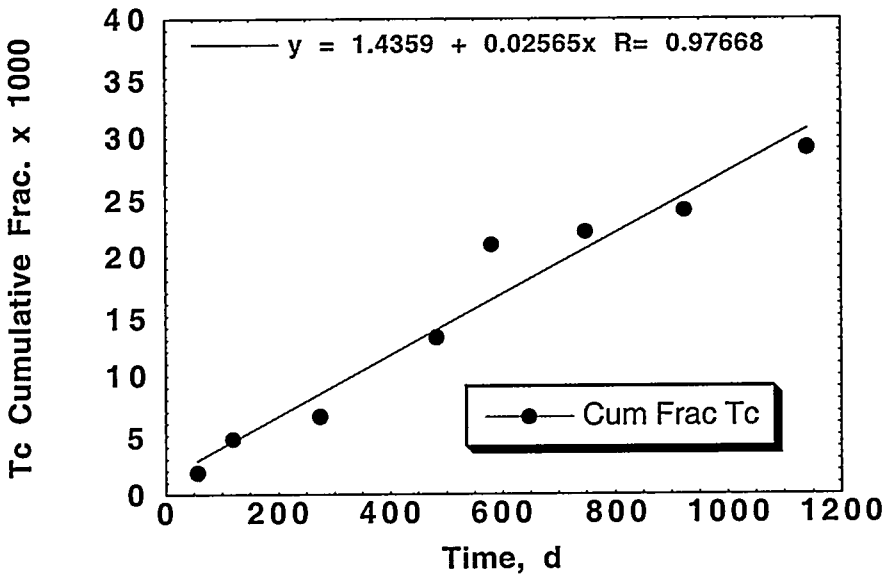

Fig. 7. Linear Time Dependence of ^{99}Tc Cumulative Release Fractions in the ATM-103 High-Drip-Rate Test (Equation is for linear least squares fit.)

Since the reaction rate defined by the ^{99}Tc interval release fractions remains constant with time, a surface reaction appears to be the rate-controlling mechanism. Support for control of the rate by a surface reaction is provided by Eriksen et al who observed in tests [ERIKSEN-1995] with spent fuel that nearly 100% of the oxidants from radiolysis are taken up by the fuel surface.

6. Radionuclide Release in the ATM-106 Low-Drip-Rate Test after 10 Minute Immersion in EJ-13

In Table 6, the cumulative release fractions for ^{99}Tc, ^{97}Mo, ^{137}Cs, ^{238}U, and ^{239}Pu for the ATM-106 low-drip-rate test after 2.5 years and 3.1 years of reaction are compared. At the longer time period, the fuel fragments were immersed in EJ-13 for 10 minutes to determine if reaction had occurred but that insufficient liquid had been present for transport of the released radionuclides. After immersion, the ^{99}Tc release fraction increased two orders of magnitude, yielding a total release of ~1%, which is comparable to the cumulative release of 3% in the high-drip-rate test after 3.7 years. Nearly all of the ^{99}Tc released after immersion (93%) was in the leachate, as was most of the ^{97}Mo release. From 90-100% of the ^{137}Cs, ^{238}U, and ^{239}Pu release in the 3.1 year interval is sorbed on the stainless steel. The sorption behavior on stainless steel is not surprising for the actinides but is not expected for cesium.

Table 6. Release Fractions for the ATM-106 Low-Drip-Rate Test after 3.1 Years of Reaction and Immersion for Ten Minutes in EJ-13

	Cumulative		Sampling Interval
Radionuclide	2.5 yr	3.1 yr	3.1 yr
^{99}Tc	1.0E-4	9.4E-3	9.4E-3
^{97}Mo	1.2E-4	1.1E-3	9.7E-4
^{137}Cs	3.3E-6	4.9E-4	4.9E-4
^{238}U	1.8E-5	1.6E-4	1.4E-4
^{239}Pu	2.4E-5	2.0E-4	1.8E-4

The large fractional release after a short immersion in EJ-13 suggests that the fraction of fuel reacted is underrepresented by the ^{99}Tc release in the low-drip-rate tests because of minimal liquid for transport and because most of the reacted radionuclides are present on the fuel surface. If this hypothesis is true, then there is the potential for large radionuclide bursts if fracture flow occurs after a large portion of the spent fuel has reacted with low volumes of standing water or with water vapor for extended periods.

E. Conclusions

Our conclusions for the high-drip-rate tests are as follows. (1) The ^{99}Tc interval release fractions provide a lower limit for the spent fuel reaction. In the ATM-103 fuel, 3 wt% of the total inventory of ^{99}Tc is released in 3.7 years. (2) Oxidation of the ε-phase suggests that the oxidizing potential at the fuel surface may be as high as 0.6 V. The oxidant may be H_2O_2, a product of alpha radiolysis of water. (3) The constancy of the ^{99}Tc release fractions over 3.1 years of reaction indicates that a surface reaction is the rate-controlling mechanism for fuel reaction under unsaturated conditions and that the oxidant is possibly H_2O_2, a product of alpha radiolysis of water. (4) Two reaction pathways have been identified from SEM examination: a) through-grain dissolution with subsequent formation of uranyl alteration products and b) dissolution along grain boundaries. The latter results in the friability of a spent fuel fragment. (5) The major alteration product identified by XRD and SEM is Na-boltwoodite, $Na[(UO_2)(SiO_3OH)]\cdot H_2O$, which is formed from sodium and silicon in the water leachant. (6) Elements other than uranium, including Ru, Mo, Cs, and Ba, are incorporated into (U^{6+}) alteration products examined so far. (7) Pu appears to be concentrated on the spent fuel. It is not found in the leachate nor in the alteration products.

The high-drip-rate tests appeared to have sufficient liquid to transport dissolved material from the spent fuel to the test vessel. For the low-drip-rate tests, there is sufficient water for fuel reaction but, due to water evaporation from decay heat, water for radionuclide transport is reduced. Evaluation of the results from the vapor tests is ongoing.

F. Ongoing Studies

The unsaturated tests with ATM-103 and ATM-106 fuel samples are ongoing. Detailed analysis of the leachates will continue in the next year to determine if there is a diminution in the leach rate and a change in the concentration, form, and quantity of the radionuclides as determined from ICP-MS data. Identification of the alteration products on the spent fuel will continue using SEM, XRD, and TEM. The type and depth of reaction within a spent fuel fragment will be studied.

II. OPTICAL, SEM, AND XRD RESULTS FOR REACTED SPENT FUEL SAMPLES

This section describes results obtained during examination of reacted fuel by optical microscopy, scanning electron microscopy (SEM), and X-ray diffraction (XRD) analysis. We discuss the three types of tests, high-drip-rate, low-drip-rate, and vapor separately. We follow these sections with a summary of the results.

A. Results for High-Drip-Rate Tests

1. ATM-103 Fuel - 3.7 Years Reaction

The fragment removed from this test disaggregated upon manipulation during the initial sampling procedure, spreading particles of fuel grains and reaction products across the adhesive tape in the petri dish that contains the sample. Optical examination of the particles indicates fuel fragments range in size from approximately 10 to greater than 200 μm. The fuel particles range from single grains to aggregates made up of several tens of grains; many of these have yellow material adhering to them. Clusters (<10 to 200 μm) of light yellow acicular crystals are also abundant. In association with most of the yellow clusters is darker yellow material. Much of the dark yellow material is closely associated with adjacent fuel grains. This dark yellow material clings tenaciously to the fuel grains, where present.

We prepared several particles for SEM examination. Most are black fuel grains – essentially UO_2 (one cannot determine trace elements by SEM/EDS), most of which show some pitting, probably due to dissolution along the grain boundaries. The acicular crystals comprising the yellow clusters are an Na-U-silicate, shown from XRD analysis to be Na-boltwoodite, $Na[(UO_2)(SiO_3OH)](H_2O)$. We did not identify other phases during our SEM analyses.

One of the particles had a core of black fuel grains surrounded by a rind of yellow alteration products (Fig. 8). Optically, this rind appears to contain two layers, a densely crystalline, dark yellow material next to the fuel grains and light yellow, finely crystalline material. We mounted this sample in epoxy for examination in SEM. Figure 8 shows a cross-section through this fragment. The SEM image shows the fuel (brightest region) in which the grain boundaries are readily visible. Gaps of approximately 0.5 μm or less are visible between the fuel grains. We have not detected other alteration phases between the grain boundaries. Silicon is not evident from EDS analyses at the grain boundaries; however, strong absorption by the adjacent UO_2 matrix of the relatively low-energy Na-Ka and Si-Ka X-ray emissions emanating from alteration phases may preclude the detection of minor alteration phases within grain boundary regions.

Adjacent to the fuel is an alteration layer predominantly consisting of Na-boltwoodite. The thickness of the layer varies but is approximately 20-40 μm. This layer of Na-boltwoodite consists of the two regions with diverse appearances: a dense layer, approximately 10 μm thick, closest to the fuel surface, and a much less dense outer layer, 10–30 μm thick. No difference in composition is evident between the two layers using EDS. Near the outer edge of the denser (inner) layer is an interface (Fig. 8b) defined by a gap (dark band). This gap lies approximately 10 μm above the fuel surface and 2-3 μm below the outer edge of the dense layer. Just below this interface, crystals of Na-boltwoodite have formed approximately perpendicular to the fuel surface, whereas, above this interface, Na-boltwoodite forms the dense mat of crystals sub-parallel to the fuel surface. Above these flat-lying crystals is the low-density outer layer. The inner region of the dense layer shows several curvilinear features that may be pre-existing grain boundaries, although artifacts produced during sample grinding and polishing are also evident. The different densities of the two layers manifest themselves as different colors under optical examination: the inner layer is dark yellow and the outer layer is pale yellow to white. The inner

layer adheres quite tenaciously to the adjacent fuel grains, whereas the outer layer does not adhere strongly to the underlying denser layer. The consistency of the low-density outer layer might best be described as "fluffy."

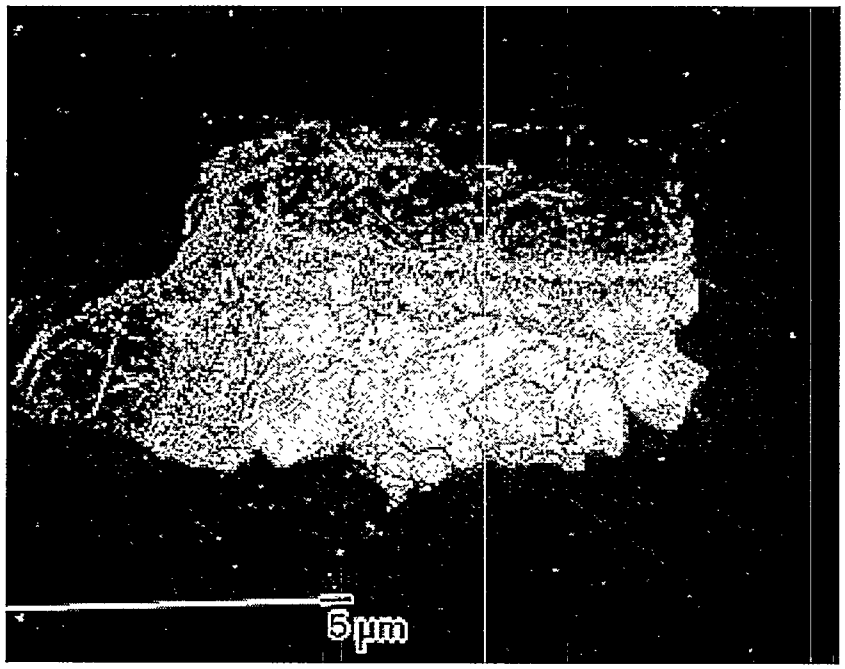

(a)

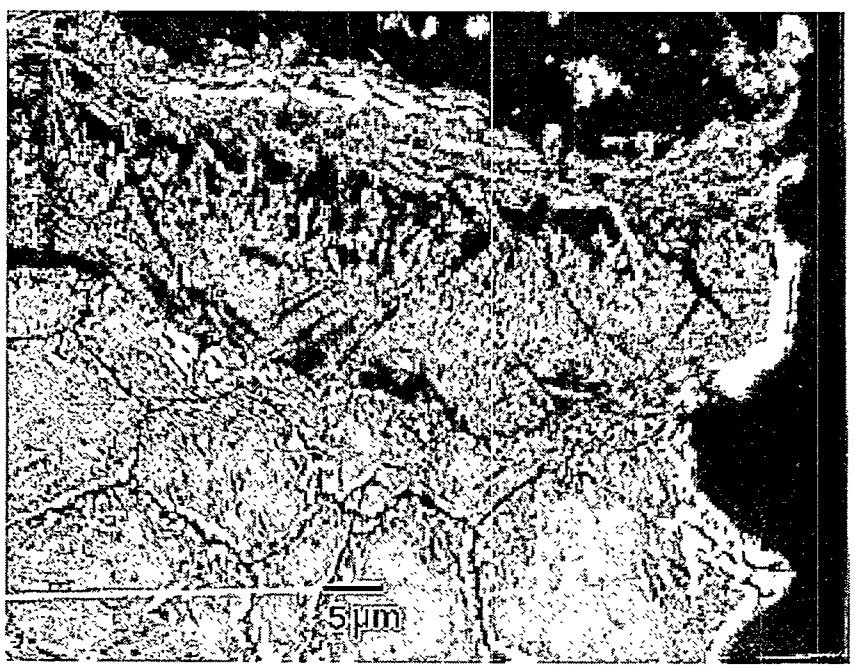

(b)

Fig. 8. ATM-103 Sample: SEM Micrographs of Polished Sections through the Contact between Fuel Grains and Corrosion Rind (a) Particle Showing both Corrosion Layers and the Adjacent Fuel Grains and (b) Magnified View of Particle Shown in Part a Illustrating Details of the Dense Inner Layer of Na-boltwoodite (high-drip-rate, 3.7 years reaction).

Table 7 contains the list of d-spacings and relative intensities (I values) obtained from scrapings from the surface of ATM-103 that had been reacted for 3.7 years. We measured these d-spacings from X-ray film following an eight-hour exposure (40 kV and 30 mA, Cu-Ka radiation, l = 0.154056 nm). The radiation from the sample is low and darkening of the X-ray film was slight. We identified 32 diffraction lines on the film, which are listed in bold type in Table 7. The X-ray powder patterns for natural β-uranophane, synthetic UO_2, and synthetic Na-boltwoodite are also listed in Table 7 for comparison to the experimental pattern. In addition, we show the d-spacings calculated for a least squares refinement of the unit cell parameters based on the experimental powder pattern for ATM-103 (*a* 1.401, *b* 1.578, *c* 0.660 nm, b 90.50°). The calculated cell parameters compare well with the unit-cell parameters reported by Gorman and Nuffield for the Na-boltwoodite (*a* 1.4010, *b* 1.5550, *c* 0.664 nm, b 91.0° [GORMAN and NUFFIELD, 1955]). Deviations in cell parameters from those shown in Table II-1 may reflect differences in the formation temperatures and/or trace-element substitutions.

The experimental XRD pattern is consistent with a mixture of Na-boltwoodite (approximately 80-90 vol%) and β-uranophane (approximately 10 vol%). Minor UO_2 (< 5 vol%) is also evident in the pattern, which is consistent with the presence of the black grains observed within the yellow masses.

2. XRD Results for ATM-106 Fuel Sample from the Zircaloy Retainer after 0.8 Years

We scraped the surface of the Zircaloy retainer from the base of the ATM-106 fuel test sample removing numerous particles for analysis by XRD. We mounted the resulting powdered material in a silica-glass capillary (0.2-mm inside diameter) without further grinding, then placed the capillary into a Debye-Scherrer X-ray camera (114-mm diameter).

Table 8 contains the list of d-spacings and relative intensities obtained from particles scraped from the Zircaloy retainer. We measured the d-spacings from X-ray film following a three-hour X-ray exposure (40 kV and 30 mA). The film was substantially darkened, presumably because of the high level of β and γ radiations caused by the large amount of Cs in the sample. We identified only ten diffraction lines on the film, and these are listed in bold-face type in Table 8. We also list five X-ray powder patterns from the Powder Diffraction File (PDF) for comparison.

The experimental XRD pattern for this sample is consistent with a mixture of predominantly two phases. One phase is probably a uranyl oxy-hydroxide, structurally related to billietite (PDF 29-208). The other phase is likely "dehydrated schoepite," $(UO_2)O_{0.25}(OH)_{1.5}$ [compositionally equivalent to $UO_3 \cdot 0.75H_2O$] (PDF 13-242). Table 8 also lists X-ray powder diffraction data for the minerals compreignacite and ianthinite (both structurally related to billietite) and for synthetic $UO_3 \cdot 0.8H_2O$ for purposes of comparison. These data support the interpretation of Buck et al. [BUCK-1997] that the Cs-Mo-U phase identified in this sample by analytical transmission electron microscopy (AEM) is structurally related to billietite, with a structural formula corresponding to $Cs_{0.9}Ba_{0.55}[(UO_2)_5(MoO_6)(OH)_6] \cdot nH_2O$ (n ~ 6).

The experimental pattern for our ATM-106 sample has one unidentified diffraction maximum, corresponding to 0.267 nm. The XRD data for billietite and compreignacite do not have this d-spacing, and the presence of a 0.267-nm diffraction maximum may indicate a third unidentified phase. However, this d-spacing may well correspond to the Cs-Mo-U phase. Although this d-spacing is not evident in the electron diffraction pattern obtained during AEM analysis, diffracted intensities can differ substantially between X-ray and electron diffraction.

Table 7. X-ray Diffraction d-Spacings for Sample from ATM-103 Reacted for 3.7 Years[a]

ATM-103		Na-boltwoodite[b] (1)		β-uranophane. 8-301		β-uranophane L-S cell fit	UO_2 5-550[c]	
I	d (nm)	I	d (nm)	I	d (nm)	d (nm)	I	d (nm)
20	0.790			100	0.783	0.790		
100	0.680	46	0.678					
60	0.660			40	0.666	0.660		
		57	0.6464					
60	0.600			40	0.616	0.600		
5	0.540	34	0.539					
5	0.500			40	0.507	0.506		
50	0.480	59	0.473	40	0.485	0.482		
1	0.420	22	0.426					
1	0.410			30	0.411	0.411		
60	0.393			90	0.39	0.394		
5	0.374			10	0.375	0.380		
2	0.360	17	0.358					
30	0.347	72	0.347	60	0.351			
30	0.338	9	0.338	10	0.341	0.338		
		7	0.336	20	0.335			
1	0.319			50	0.319	0.320	100	0.316
15	0.309	36	0.3089	40	0.304			
		14	0.3058					
15	0.299			30	0.299	0.301		
80	0.294	100	0.2942					
		94	0.293	20	0.291			
				40	0.283			
1	0.272			30	0.278		48	0.274
1	0.259			50	0.259			
5	0.250	5	0.2517					
		4	0.2493					
		4	0.2246					
		6	0.2272					
		17	0.2219					
5	0.219	23	0.2179					
		17	0.2154					
1	0.1923						49	0.193
10	0.1875							
1	0.1855							
1	0.1825							
1	0.1725							
5	0.1673							
1	0.1645							
1	0.1580							
10	0.1500							
1	0.1225							

I > 15% for all Powder Diffraction File patterns

[a]Cu-Ka radiation (l = 0.154056 nm); $I_{(rel)}$ > 10% for Powder Diffraction File PDF) patterns.
[b]Source: Ref. Vochten-1997.
[c]Numbers are PDF designations.
[d]Least-squares fit to unit cell dimensions: *a* 1.401, *b* 1.578, *c* 0.660 nm, b 90.50° [refer to reported unit-cell dimensions from Gorman-1955: *a* 1.4010, *b* 1.5550, *c* 0.664 nm, b 91.0°; (GORMAN & NUFFIELD-1955)].

Table 8. X-ray Diffraction d-Spacings in (nm) Measured for Specimen Scraped from Zircaloy Retainer from ATM-106 Reacted for 0.8 Years[a]

I	d (nm)	Billietite 29-208	Dehydrated schoepite 13-242	$UO_3 \cdot 0.8H_2$ 10-309	Compreignacit 33-1049	Ianthinite 12-272
100	**0.750**	0.753			0.746	0.763
38	**0.510**		0.509	0.511		
9	**0.380**	0.376			0.371	0.381
		0.356			0.358	0.359
47	**0.348**	0.350	0.345	0.345-0.343		
					0.353	
4	**0.340**		0.339			0.335
					0.323	0.324
1	**0.320**	0.321-18			0.320	
						0.2950
9	**0.2879**		0.2890	0.2857		
1	**0.2670**					0.2690
					0.2579	0.2610
		0.2557	0.2540	0.2557	0.2564	0.2530
5	**0.2500**		0.2480	0.2487	0.2475	
						0.2390
		0.2295/67				0.2150
		0.2295/67		0.2138		0.2070
		0.2049/39	0.2023	0.2053	0.2032	0.2030
1	**0.2000**					
		0.1996	0.1993	0.1986		0.1992

I > 15% for all PDF patterns

[a]The reported range in d-spacings is indicated by a -, while intensities for billietite ianthinite are indicated by /.

3. Analysis of Sample from ATM-106 Fuel after 3.7 Years Reaction

Optical examination shows that most of the particles removed from the alteration rind after 3.7 years of reaction consist of finely acicular (needle-shaped) crystals, approximately 1 μm in diameter and up to approximately 50 μm long. These crystals form pale-yellow clumps, 5-10 μm across. Many of the clumps also contain black grains, as well as some darker yellow material associated with the black grains. In many respects, this sample closely resembles the sample taken from ATM-103 fuel that had been reacted for 3.7 years (see Section II.A.1), although no disaggregation of the fuel fragments occurred when we manipulated them during initial sample

preparation in the hot cell, as occurred for one fuel fragment from the ATM-103 fuel after 3.7 years reaction.

We examined two specimens by SEM: one mounted fraction and one polished cross section (Fig. 9a = fragment; Fig. 9b = cross section). The SEM examinations show that the yellow clumps are a tangled mat of acicular crystals, approximately 5-10 μm long and less than 1 μm in the direction perpendicular to elongation. EDS analyses indicate that these crystals are a Na-U-silicate, either Na-boltwoodite or possibly the Na-analogue of weeksite, $(K,Na)_2(UO_2)_2(Si_5O_{13})(H_2O)_3$. While weeksite is a possible phase because some of the X-ray emission spectra display higher Si:U ratios than observed for boltwoodite and uranophane (Si:U ratios of 1:1), the assignment as Na-boltwoodite is consistent with that made for ATM-103, and with the assignment made in the 4.1 yr ATM-106 sample. We did not perform XRD analysis of this sample because of a lack of material.

The polished section examined does not display an interface between the ATM-106 fuel and alteration layer, as shown (Fig. 8) in a similarly prepared section from ATM-103 (3.7 yr reaction). Whether this sample from ATM-106 has experienced grain-boundary-enhanced dissolution similar to that observed for ATM-103 within the same reaction interval cannot be determined yet; additional samples need to be analyzed. The very small amount of sample obtained from the ATM-106 fuel after a 3.7-year reaction interval precluded preparation of additional SEM polished sections. Thus, the reacted layers formed on ATM-106 fuel could not be compared directly with those on ATM-103 fuel at this time. Solution analyses and visual examinations of the reacted fragments indicated that the reaction progress of the ATM-106 fuel has lagged behind reaction of the ATM-103 fuel by approximately six months. Continued examination of samples from both ATM-106 and ATM-103 fuels obtained after further reaction intervals have occurred, will provide needed insight into sample-dependent differences. We will describe additional SEM examinations in subsequent reports.

4. Analysis of Sample from ATM-106 Fuel after 4.1 Years Reaction

Optical examination of the particles removed from a fragment of ATM-106 reacted fuel after 4.1 years of reaction indicate that the alteration products consist primarily of light-yellow, finely acicular crystals. These crystals form small aggregates(10-200 mm across), many of which contain small black inclusions that are probably fuel grains. We also extracted similarly sized aggregates of fuel grains from the reacted fuel fragment, although in a much lesser amount. Along with the light-yellow clumps, and often included within them, is darker yellow material without visible crystals when viewed at this scale.

We mounted several particles for SEM examination. To date, we have investigated only those particles mounted on aluminum stubs. Our EDS analyses and the morphologies of the crystals indicate that the most abundant phase in the clumps of yellow crystals is Na-boltwoodite. The X-ray emission spectrum of the more dense-appearing material is similar to that of the larger acicular boltwoodite crystals, suggesting a similar paragenesis as described for the ATM-103 samples that had been reacted for 3.7 years. We have examined a few fuel grains, and these display loosely aggregated, or discrete grains with pitted grain boundaries, suggesting grain-boundary-enhanced dissolution of the fuel grains. We have not observed alteration phases within the gaps between fuel grains that were separated during SEM sample preparation.

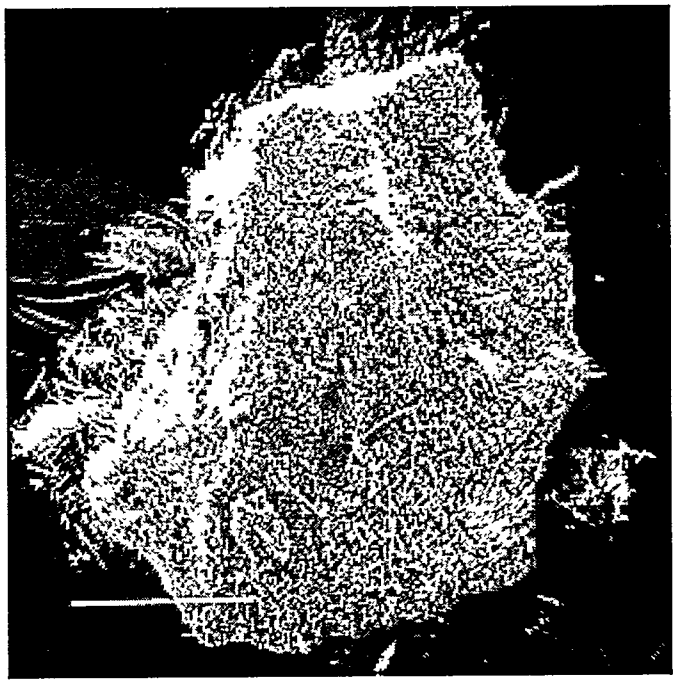

(a)

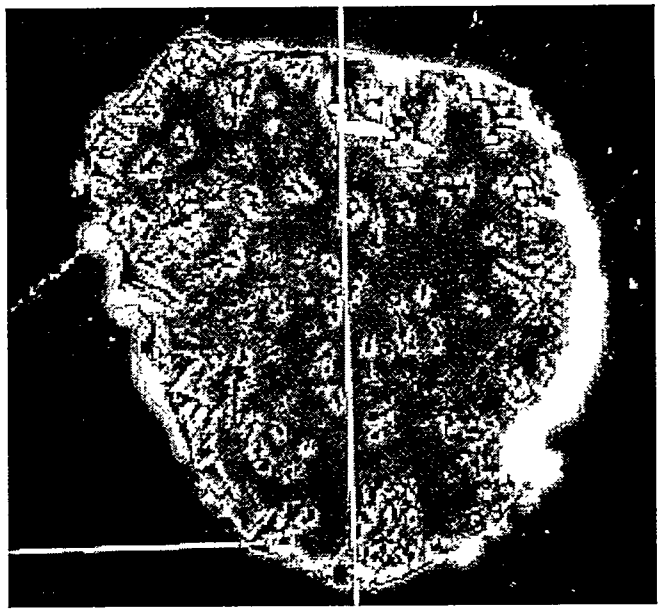

(b)

Fig. 9. ATM-106 Sample: SEM Micrographs of Na-boltwoodite (a) Cluster of Acicular Crystals, (b) Polished Cross Section through Cluster Similar to that Shown in Part a (Scale Bars ≅ 50 μm; high-drip-rate 3.7 years reaction, central stripe in (b) is an imaging artifact)

Table 9 lists the d-spacings and relative intensities obtained from the scrapings taken from this ATM-106 sample. We measured the d-spacings from X-ray film after a six-hour exposure (40 kV and 30 mA, Cu-Ka radiation, l = 0.154056 nm). The radiation due to the sample was moderate, darkening the X-ray film only slightly. We identified 18 diffraction lines on the film, and these are listed in bold type in Table 9 along with their relative intensities. We also list three X-ray powder patterns from the PDF for comparison: those of synthetic Na-boltwoodite, natural β-uranophane and synthetic soddyite.

The experimental XRD pattern (Table 9) is closely similar to that obtained from a sample from ATM-103 fuel that had been reacted for 3.7 years, so we have listed that pattern in Table 9 as well (compare with Table 7). The phase making up the bulk of this sample is Na-boltwoodite (~80-90 vol%). The phase (or phases) composing the remainder of the sample is unknown at this time, and we are planning additional analyses to identify it (them). Numerous black grains are apparent within the yellow mass, indicating that UO_2 fuel is present; however, UO_2 is not evident in the powder diffraction pattern. Thus the fuel grains probably make up less than 1-2 vol% of the sample examined.

A notable difference between this sample and the sample from ATM 103 fuel reacted for 3.7 years is the absence of a diffraction peak corresponding to ~0.79 nm in the ATM-106 fuel sample. The 0.79 nm d-spacing is the most intense reflection in the powder pattern of b-uranophane [FRONDEL et al., 1956]. We attributed this diffraction peak to β-uranophane in the sample from ATM-103 reacted for 3.7 years (see Table 7). We are uncertain whether the absence of a 0.79 nm diffraction maximum in the ATM-106 fuel sample pattern indicates a lack of β-uranophane in this sample or whether some unknown cause reduced the intensity of this peak (for example, sample preferred orientation or a change in space-group symmetry indicating a polymorphic transformation). Given the very close similarity of the pattern from the ATM-106 fuel to that of the sample from ATM-103 reacted for 3.7 years, we believe that the mineral phase identification is also similar (despite the differences noted above). This similarity leads us to believe that any as-yet unidentified phases present in the ATM-106 fuel sample are likely also present in the sample from ATM-103 fuel reacted for 3.7 years. Examination of this sample and the data derived from it are preliminary and are continuing.

5. Discussion of the High-Drip-Rate Tests

Crystal morphologies, chemical compositions (as determined by EDS), and the XRD analyses indicate that the most abundant alteration product formed in the high-drip-rate experiments is Na-boltwoodite, $Na[(UO_2)(SiO_3OH)](H_2O)$, with a lesser amount of β-uranophane, $Ca[(UO_2)_2(SiO_3OH)_2](H_2O)_5$. Additional phases present in amounts less than 5 vol% may also be present but have not been identified during SEM or XRD analyses. (Dehydrated schoepite and a Cs, Ba-U-Mo oxy-hydroxide were identified from the Zircaloy retainer after 0.8 years reaction (ATM-106), but these phases have not been identified in samples from later tests.) The β-uranophane apparently occurs primarily at the outermost surface of the alteration layers, whereas the bulk of the alteration layer is Na-boltwoodite The apparent lack of alteration products formed along fuel-grain boundaries in the high-drip-rate tests may reflect depletion of dissolved Si in fluids penetrating the grain boundaries, possibly due to the precipitation of uranyl silicates on the outer surface.

Table 9. X-ray Diffraction[a] d-Spacings (in nm) for Sample from ATM-106 Fuel Reacted for 4.1 Years

I	d (nm)	Na-boltwoodite[b]		β-uranophane 8-301		α-uranophane 39-1360		ATM-103 after 3.7 years	
				100	0.783	100	0.79	20	0.790
100	**0.686**	46	0.678					100	0.680
47	**0.669**			40	0.666	7	0.664	60	0.660
		57	0.646						
57	**0.602**			40	0.616			60	0.600
		34	0.539			14	0.543	5	0.540
				40	0.507			5	0.500
43	**0.482**	59	0.473	40	0.485			50	0.480
		22	0.426					1	0.420
				30	0.411			1	0.410
40	**0.395**			90	0.39	90	0.3950	60	0.393
9	**0.376**			10	0.375			5	0.374
11	**0.364**	17	0.358			20	0.3600	2	0.360
49	**0.347**	72	0.347	60	0.351	4	0.3508	30	0.347
20	**0.341**	9	0.338	10	0.341			30	0.338
		7	0.336	20	0.335				
		2	0.325						
				50	0.319	10	0.3210	1	0.319
27	**0.310**	36	0.3089	40	0.304			15	0.309
		14	0.3058						
20	**0.301**			30	0.299	16	0.2993	15	0.299
73	**0.294**	100	0.2942					80	0.294
		94	0.293	20	0.291	11	0.2915		
8	**0.281**			40	0.283				
				30	0.278	11	0.2698	1	0.272
5	**0.259**			50	0.259	40	0.2633	1	0.259
						12	0.2560		
4	**0.251**	5	0.2517					5	0.250
		4	0.2493						
		4	0.2246						
		6	0.2227						
		17	0.2219			10	0.2207		
4	**0.219**	23	0.2179					5	0.219
		17	0.2154			12	0.2106		
3	**0.209**					15	0.2100		
								1	0.1923
7	**0.188[illegible]**					10	0.1890	10	0.1875

[a]Cu-Ka radiation (l = 0.154056 nm); $I_{(rel)} > 10\%$ for all PDF patterns
[b]Source: Ref. Vochten-1997

There appears to have been extensive dissolution along grain boundaries, as was especially evident from the friable nature of the fragment removed from ATM-103 fuel after 3.7 years reaction. Wide gaps between grains also support this conclusion (Fig. 8). Although the oxidation of UO_2 to $UO_{2.25}$ may enhance the expansion of the gaps between grains, because of the smaller unit-cell size of $UO_{2.25}$, this sizes difference does not account fully for the observed widths of the gaps (~0.5 mm). Furthermore, no $UO_{2.25}$ was identified during TEM examinations of fuel grains.

The replacement of the fuel by the alteration products has progressed uniformly inward from the original outer surface without regard to grain boundaries. This "through-grain" dissolution of the fuel grains is evident from the lack of embayment at grain-boundaries (Fig. 8). The through-grain dissolution of the UO_2 fuel matrix accounts for a significant amount of fuel that has dissolved in the high-drip-rate tests and is greater than the amount of fuel that has dissolved by means of grain boundary-enhanced dissolution (see discussion below and in Section I).

We can write the (simplified) reaction for the oxidative dissolution of the UO_2 fuel:

$$UO_2 + 2H^+ + 1/2\ O_2 \Rightarrow (UO_2)^{2+} + H_2O. \qquad (2)$$

The precipitation of Na-boltwoodite is

$$(UO_2)^{2+} + H_4SiO_4^0 + Na^+ + H_2O \Rightarrow Na[(UO_2)(SiO_3OH)](H_2O) + 3H^+. \qquad (3)$$

Thus the *net* reaction for the replacement of the UO_2 fuel by Na-boltwoodite is

$$UO_2 + H_4SiO_4^0 + Na^+ + 1/2\ O_2 \Rightarrow Na[(UO_2)(SiO_3OH)](H_2O) + H^+. \qquad (4)$$

The reaction 4 (which is not an equilibrium expression) shows that the replacement reaction will continue as long as Na- and Si-rich EJ-13 water is added to the system and/or H^+ is removed (due to flowing water and/or reaction with fuel via reaction 2), provided that a sufficient supply of oxidants is available. We suspect that an abundant supply of oxidants is probably available due to the effects of radiolysis and from free O_2 in the reaction vessel atmosphere.

We have written reactions 2 through 4 with all U being conserved in the solid phases, which is consistent with the low quantities of U released to solution in the high-drip-rate tests. At the low-drip-rate, we expect similar U retention by the alteration phases.

To date, the only cross section of reacted fuel analyzed that clearly shows the contact between fuel grains and the alteration products on the fuel surface is the sample from ATM-103 fuel that had been reacted for 3.7 years (Fig. 8). The interface between the dense layer of Na-boltwoodite and the overlying "fluffy" layer may represent the position of the surface of the original fuel fragment, or it may be an artifact of the original surface that has been "pushed out" by Na-boltwoodite, which precipitated as the fuel was dissolving. The matted flat-lying crystals of Na-boltwoodite that lie above this interface either precipitated at the original surface of the fuel or may have precipitated after the formation of the dense inner layer. The formation of the dense inner layer is somewhat enigmatic. Clearly, the fuel grains were dissolved and replaced by the dense layer of Na-boltwoodite. What remains uncertain is whether this replacement has been isovolumetric, without inflation of the dense inner layer during replacement, or whether the replacement of the fuel by Na-boltwoodite has resulted in a volume increase. Therefore, the thickness of the dense inner layer represents the *maximum* thickness of fuel that was dissolved and replaced by Na-boltwoodite. If there has been some inflation of the reacted layer as Na-

boltwoodite replaced the fuel, then the thickness of the dense inner layer is *greater* than the thickness of the fuel that was dissolved.

One can infer physical evidence for both types of replacement from the cross section shown in Fig. 8. Isovolumetric replacement of the fuel grains may leave evidence of the pre-existing grain boundaries ("relict" grain boundaries). Indeed, several curvilinear features of the dense inner layer are indicative of relict grain boundaries. On the other hand, the dense inner layer next to the "corner" of the fragment shown in Fig. 8 appears less thick than the thickness on either side of the corner. This texture suggests that some inflation of the alteration layer may have occurred during replacement (this effect appears exaggerated farther out in the low-density outer layer). However, this cross section also displays several artifacts due to sample preparation, such as "holes" in the alteration layer caused by plucking of material during grinding and/or ultrasonic cleaning, and scratches caused by grinding and polishing. These artifacts may mask, or mimic, some features in Fig. 8. Such artifacts are difficult to avoid because the hardness of the UO_2 fuel is greater than that of the adjacent alteration layers (and the embedding epoxy resin). Nevertheless, these artifacts complicate the interpretation of Fig. 8. Only careful preparation of additional cross-sectioned samples will clarify our interpretation. At this time, we believe there is evidence to suggest the interface represents the original fuel surface and that little expansion has occurred.

The unit-cell volume of UO_2 is approximately 0.164 nm^3 (Z = 4), or 0.041 nm^3 per U atom; the ideal density of UO_2 is 10.9 $g{\cdot}cm^{-3}$. The unit-cell volume of Na-boltwoodite is 0.6286 nm^3 (Z = 4), or 0.157 nm^3 per U atom; the ideal density of Na-boltwoodite is 4.5 $g{\cdot}\ cm^{-3}$. An approximate four-fold volume increase would be needed between cubic UO_2 and monoclinic Na-boltwoodite if Na-boltwoodite is to incorporate all the U from the UO_2. Only approximately 25% of the U in the replaced outer fuel layer can be incorporated into an equal volume of Na-boltwoodite (if this layer is 100% of theoretical density). The remaining 75% (or more) of the U must be transported out of the replaced volume. The dense inner layer of Na-boltwoodite is 10-15 mm thick, indicating that the thickness of fuel that has dissolved by "through-grain" dissolution is probably no less than approximately 3 μm and no more than 10-15 μm.

The volume density of the outer, less-dense layer is only approximately 10 or 20% of the ideal density from a combination of through-grain and grain boundary dissolution. The source of U that formed this outer layer is uncertain. If all the U derived from through-grain dissolution at the surface remained within the inner dense layer, then the U in the outer layer must be from dissolution along grain boundaries. If the Na-boltwoodite in the inner layer did not incorporate all of the U from the dissolved surface, then some U in the outer layer must have come from the dissolving surface. In the case of isovolumetric replacement of the surface, a maximum amount of U must be derived from through-grain dissolution.

From our SEM observations, we can calculate the approximate volume of fuel replaced by Na-boltwoodite. The estimated original geometric surface area was 2.1 $x10^{-4}$ m^2/g, and the original mass of fuel was 8 g, giving an original total surface area of 0.00168 m^2. One may assume that the fragment of ATM-103 fuel shown in Fig. 8 is representative of the reacted fuel surface (that is, Na-boltwoodite replaced the outer 3-10 μm of the fuel surface). If this is true, the estimated volume of fuel that has reacted by through-grain dissolution is between 5.6 x 10^{-9} m^3 and 1.7 x 10^{-8} m^3. This range corresponds to the release of between 0.06 and 0.18 g of UO_2 ($D_{UO2} \cong 10.6$ g/cm^3) or a fractional release of between 0.7 and 2.2% of all the U in the fuel after 3.7 years *from the reacted layer only*. To this number, the additional mass of U released due to dissolution along grain boundaries must be added. Based on Tc release, approximately 0.25 g of UO_2 has reacted, so the mass of U corresponding to the replacement volume represents between 25 and 80% of the total fuel reacted. Approximately 20-75% of the total U released from the fuel is due to dissolution along the grain boundaries. No U^{6+} alteration phases have been observed along reacted grain boundaries within the fuel fragments. This is an unexpected result considering that

concentrations of dissolved U may be expected to reach quite high levels in solutions between fuel grains that are dissolving. We have no explanation for this result at this time.

Only about 1% of the U estimated to have reacted is in solution (based on Tc release), which means that approximately 99% of the reacted U is in alteration products and on the vessel and retainer walls. The alteration rind (both layers) observed by SEM may contain, at most, about 50% of the total reacted U. We believe that the retainer must have adsorbed some U, which will be taken into account when the tests are terminated.

B. Results for Low-Drip-Rate Tests

1. Analysis of Sample from ATM-103 Fuel after 4.1 Years Reaction

Optical examination of the particles removed from a sample taken from ATM-103 fuel after 4.1 years reaction show abundant crystals that are various shades of yellow. The yellow crystals are commonly bladed or blocky, rarely equant and prismatic. In addition, there are numerous clumps of black grains and several reddish-orange particles. The black grains are approximately 10-100 μm, and most of them are probably single fuel grains and aggregates of a few tens of fuel grains. The reddish particles are tabular, approximately 50 μm by 100 μm and 20-50 μm thick.

SEM examination indicates that several U-containing alteration products are present (Fig. 10). These products include metaschoepite and/or dehydrated schoepite, soddyite, $(UO_2)_2(SiO_4)(H_2O)_2$, Na-boltwoodite, and an unidentified uranyl oxide hydrate (UOH) that may be the Na-analogue of compreignacite. This Na-UOH may have the structural formula $(Na,K)[(UO_2)_3O_2(OH)_3](H_2O)_4$ (based on analogy with compreignacite) To date, we have not performed XRD analyses on this sample. Phase identifications are therefore tentative, and the relative abundances of the alteration products are uncertain. However, metaschoepite and "Na-compreignacite" are abundant in the particles examined by SEM, and these two phases probably constitute the major alteration phases formed in this test after 4.1 years. In contrast, Na-boltwoodite appears to be rare; we observed only a few small crystals associated with a single particle in the sample examined by SEM.

The reddish-orange particles do not contain uranium (Fig. 11), and they appear chemically complex and inhomogenous. Qualitative chemical analyses by EDS indicate that the major elements in these particles include Na, Se, Si, S, Cl, and Cr. An outer layer of what looks like a finely crystalline coating covers most of the particles (Fig. 11). Beneath this outer layer the particles are relatively featureless, with low electron reflectance. Sodium is consistently a major constituent in all spot analyses by EDS, but the relative amounts of Se, Si, S, Cr, and Cl vary substantially across the sample, from minor constituents to abundances comparable to that of Na. We have not completed XRD or AEM analyses on these particles, so identification is uncertain.

2. Discussion of Low-Drip-Rate Tests

To date we have examined only samples from the low-drip-rate test on ATM-103 fuel. The alteration-phase assemblage observed from the sample ATM-103 reacted for 4.1 years consists of at least four different uranyl phases: two oxy-hydroxides and two uranyl silicates. This is a somewhat more complex assemblage of alteration products than was observed in the samples form ATM-103 fuel reacted at the high-drip-rate for comparable time (3.7-4.1 years). In the samples from high-drip-tests, we identified only one or two uranyl silicates as major alteration products. Although we have not identified a clear paragenetic sequence of alteration products, analogy with the UO_2 drip tests suggests that the uranyl oxy-hydroxides (metaschoepite and Na-compreignacite) probably formed before the uranyl silicates, soddyite, and, later, Na-boltwoodite.

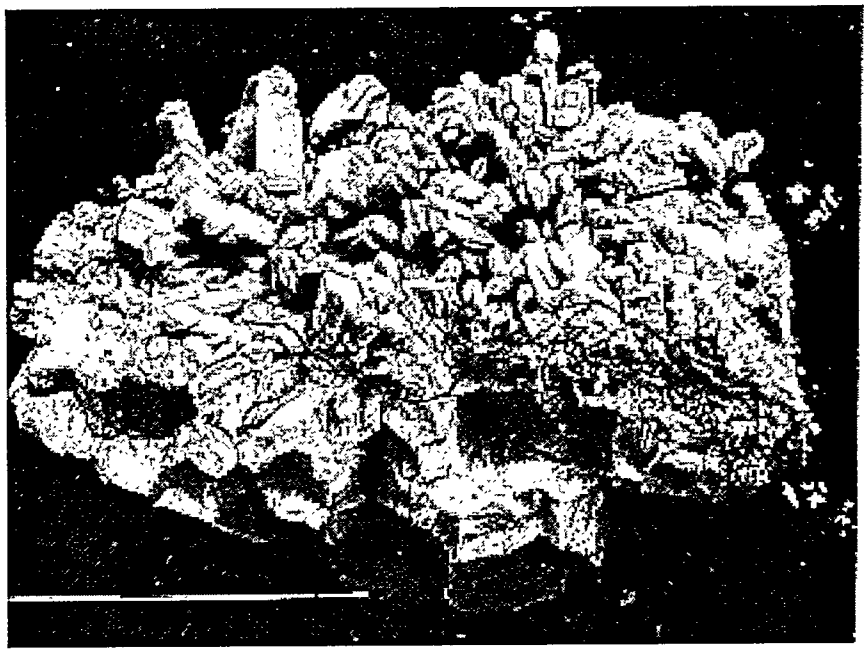

Fig. 10. ATM-103 Sample: Fuel Grains (bottom) Covered by Mixed U_{6+} Alteration Phases, Mounted on C-Tape. Alteration phases in this sample include metaschoepite, an unidentified Na-uranyl oxy-hydroxide (blocky crystals at top) and soddyite (fine-grained crystals at right). Scale bar ≅ 40 μm; low-drip-rate, 4.1 years reaction.

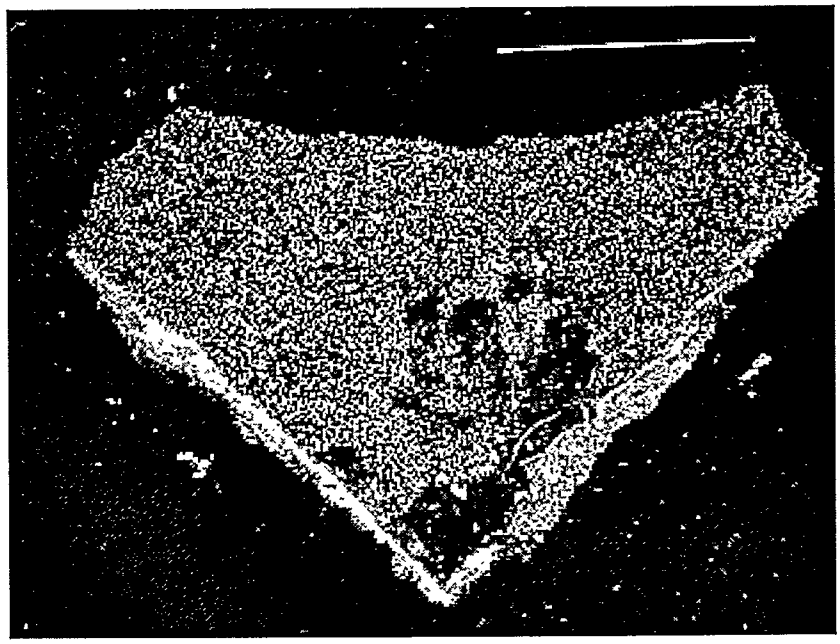

Fig. 11. ATM-103 Sample: Red-Orange Particle Mounted on C-Tape. Scale bar, top right ≅ 50 μm; low-drip-rate, 4.1 years reaction.

An interesting difference between this test and the tests on unirradiated UO_2 is the apparent absence of becquerelite in the test on spent fuel; becquerelite is at least rare in the samples from this test. This observation may reflect minor differences in the compositions of the leachants used; however, chemical and other disparities between UO_2 and spent fuel (for example, composition, radiation field, etc.) may explain observed differences in the alteration-phase assemblages of UO_2 and spent UO_2 fuel. Also, sample inhomogeneities across the fuel surface may exist. We need to analyze more samples before we can compile a comprehensive list of alteration products formed in these tests at this time.

Notably, the uranyl alteration products identified in the low-drip-rate test are chemically and structurally similar to the uranyl alteration minerals that occur at Nopal I uranium deposit at Peña Blanca, Mexico. Researchers have studied Nopal I as a natural analogue for the long-term behavior of spent UO_2 fuel at the proposed repository at Yucca Mountain [PEARCY-1994]. Such mineralogical similarities between laboratory tests and a natural U-ore deposit demonstrate the relevance of these tests for understanding long-term, unsaturated corrosion of spent fuel in a repository setting.

The fact that several diverse types of alteration phases coexist within the corrosion rind on ATM-103 fuel after 4.1 years reaction implies that the reactions controlling phase formation are incomplete. The physical state of the corrosion rind at this time is simply an interim state of the reaction as the fuel alters to an assemblage of phases more stable under the current test conditions. A simplified view of the alteration reaction, with the formation of a single phase being used to illustrate the overall reaction, is not possible given the complexity observed in this test sample. We strongly suspect that the uranyl oxide hydrates (such as metaschoepite and Na-compreignacite) are kinetic products that are replaced by such uranyl silicates as Na-boltwoodite and uranophane. The most likely reason that the uranyl oxy-hydroxides have not been replaced after 4.1 years exposure is that there is less water and dissolved cations supplied to the samples in these tests compared to the tests performed at the high-drip-rate. Nevertheless, an overview of the reactions that may be important for the precipitation and possible replacement of the alteration phases identified in this test sample is informative.

Again, we begin with the simplified reaction for the oxidative dissolution of the UO_2 fuel:

$$UO_2 + 2H^+ + 1/2\ O_2 \Rightarrow (UO_2)^{2+} + H_2O\ . \tag{5}$$

We identified four (or five) alteration phases (dehydrated schoepite is a tentative identification). Thus there are five precipitation reactions of interest. The precipitation of schoepite is

$$UO_2^{2+} + 3H_2O \Rightarrow UO_3{\cdot}2H_2O + 2H^+. \tag{6}$$

The precipitation of dehydrated schoepite is

$$UO_2^{2+} + 1.75H_2O \Rightarrow UO_3{\cdot}0.75H_2O + 2H^+. \tag{7}$$

The following reaction represents the precipitation of Na-compreignacite:

$$3(UO_2)^{2+} + Na^+ + 9H_2O \Rightarrow Na[(UO_2)_3O_2(OH)_3](H_2O)_3 + 7H^+\ . \tag{8}$$

The precipitation of soddyite is

$$2(UO_2)^{2+} + H_4SiO_4^0 + 2H_2O \Rightarrow [(UO_2)_2(SiO_4)](H_2O)_2 + 4H^+ . \quad (9)$$

The precipitation of Na-boltwoodite is

$$(UO_2)^{2+} + H_4SiO_4^0 + Na^+ + H_2O \Rightarrow Na[(UO_2)(SiO_3OH)](H_2O) + 3H^+ . \quad (10)$$

We believe that the replacement of the early formed uranyl oxide hydrates, metaschoepite, dehydrated schoepite, and Na-compreignacite, is probably important, based on the results of the UO_2 drip tests [WRONKIEWICZ et al.-1992; 1996]. For example, the replacement of metaschoepite by soddyite may be important

$$2UO_3{\cdot}2H_2O + H_4SiO_4^0 \Rightarrow [(UO_2)_2(SiO_4)](H_2O)_2 + 4H_2O . \quad (11)$$

The replacement of metaschoepite by "Na-compreignacite" may occur, although we did not observe evidence for this reaction:

$$3UO_3{\cdot}2H_2O + Na^+ \Rightarrow Na[(UO_2)_3O_2(OH)_3](H_2O)_3 + H_2O + H^+ . \quad (12)$$

Because both Si and Na are abundant in EJ-13 water, a reaction that is probably important is the replacement of "Na-compreignacite" by Na-boltwoodite:

$$Na[(UO_2)_3O_2(OH)_3](H_2O)_3 + 3H_4SiO_4^0 + 2Na^+ \Rightarrow 3Na[(UO_2)(SiO_3OH)](H_2O) + 5H_2O + 2H^+. \quad (13)$$

The replacement of soddyite by Na-boltwoodite may also be important:

$$[(UO_2)_2(SiO_4)](H_2O)_2 + H_4SiO_4^0 + 2Na^+ \Rightarrow 2Na[(UO_2)(SiO_3OH)](H_2O) + 2H^+. \quad (14)$$

All of these reactions are pH dependent. The precipitation and replacement of phases in the corrosion rind tend to decrease pH as these reactions remove Na from solution. A decrease in pH tends to enhance the dissolution of the spent fuel according to the reaction II-4. Other factors may moderate the pH; among the most important of these factors is carbonate equilibrium in the presence of atmospheric CO_2:

$$HCO_3^- + H^+ = H_2CO_3 \qquad K_{S1} = 6.33\ (25°C) . \quad (15)$$

We have written the foregoing reactions with all U being conserved in the solid phases. This is consistent with the low quantities of U released to solution in the high-drip-rate tests. We expect similar U retention by the alteration phases in the low-drip-rate tests.

C. Vapor-Hydration Tests

1. Analysis of Sample from ATM-103 Fuel after 4.1 Years Reaction

We removed only a small amount of material from the reacted spent fuel during sampling of this vapor-hydration test of ATM-103 fuel after 4.1 years reaction. Two morphologies are apparent among the solids examined optically: (a) finely fibrous tan-colored crystals and (b) tabular to bladed yellow crystals. We were readily able to extract the yellow crystals from the tape adhesive, whereas the tan crystals were not so easily extracted. Both

materials occur as scattered crystals, rather than as the tufts or clumps more common in the samples from the drip tests.

Scanning electron microscopy/energy dispersive spectroscopic (SEM/EDS) examination indicates that the tabular and blocky crystals are essentially pure U oxides. Most of these crystals are bladed to somewhat boat-shaped (Fig. 12), a morphology characteristic of dehydrated schoepite, $UO_3 \cdot 0.8H_2O$. However, the tabular morphologies of some crystals in this sample are characteristic of metaschoepite, $UO_3 \cdot 2H_2O$. Only pure H_2O reacts with the fuel (i.e., the condensed water vapor), and we expect U^{6+} oxy-hydroxides to be the most abundant alteration products formed in these tests. No transuranium- or fission-product-containing phases are apparent from SEM/EDS examinations of these samples. We did not conduct XRD analyses because of the extremely small amount of material obtained.

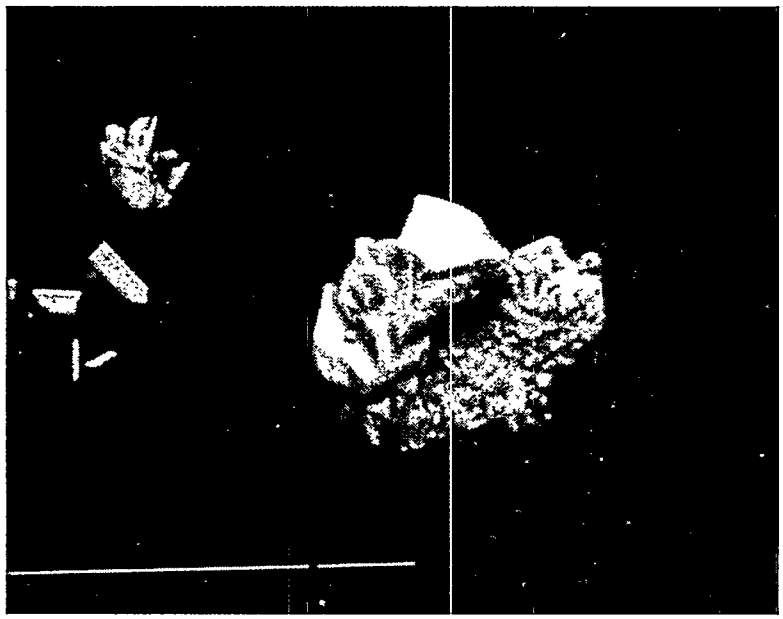

Fig. 12. ATM-103 Sample: Uranyl Oxy-Hydroxides from Surface of Sample, Mounted on C-Tape. Small crystals at left are probably dehydrated schoepite; central crystals may be metaschoepite; scale bar at bottom center ≅ 5 μm; vapor test, 4.1 years reaction.

The fuel fragments display discrete fuel grains, and the surfaces of individual fuel grains are commonly pitted, which is indicative of dissolution along grain boundaries. Examination of a polished cross section shows an interface between the U^{6+} alteration phases and reacted fuel grains, but no clear reaction boundary is evident. Instead, the fuel grains show open grain boundaries – probably caused by grain-boundary-enhanced corrosion near the surface of the reacted fuel fragment – as well as clusters of fuel grains surrounded by the alteration products. Most of the alteration products occur along the outer margins of the fuel fragments.

2. Analysis of Sample from ATM-106 Fuel after 4.1 Years Reaction

We obtained only a small amount of material from the alteration rind during sampling of the vapor-hydration test of the ATM-106 fuel after 4.1 years reaction. The overall appearance of particles from this test resembles that of particles from vapor-reacted ATM-103 described above in Section II.C.1. The fuel grains form loosely aggregated clumps that fall apart

when manipulated. Scattered within the tape are numerous isolated crystals and small clusters of crystals. Two morphologies are apparent, differing slightly in hue: (a) finely fibrous light tan-yellow crystals and (b) yellow, bladed to tabular crystals. Both morphologies are common, although the more equant yellow crystals are most abundant. We could not separate the fibrous crystals from the adhesive for examination by SEM/EDS. Under SEM examination, the fuel fragments display discrete fuel grains with pitted surfaces, indicating grain-boundary-enhanced dissolution. The yellow alteration products cling to the surfaces of the fuel grains, although not as tenaciously as observed for the drip-test samples. As noted for the sample from ATM-103 reacted in vapor, our SEM/EDS analyses indicate that the yellow crystals in this sample are essentially pure U oxides. Most are bladed or boat-shaped dehydrated schoepite, $(UO_2)O_{0.25+x}(OH)_{1.5-2x}$, although minor metaschoepite, $UO_3 \cdot 2H_2O$, may also be present (based on morphologies). We did not perform XRD analyses because of the small amount of material obtained.

3. Discussion of Vapor-Hydration Tests

The two samples of fuel examined from the vapor-hydration tests have similar appearance. Both show evidence for grain-boundary-enhanced dissolution. Pitted grain boundaries and loosely aggregated grains are common, and alteration products commonly surround the fuel grains nearest the surface. The extent of water penetration along the grain boundaries is uncertain at this time.

The alteration products identified include dehydrated schoepite and, possibly, metaschoepite. We detected no transuranic elements or fission-products as major constituents of any of the alteration products examined thus far with EDS (detection limit approximately 1-5 wt.%). See Section II-D for results of analyses of these samples using TEM.

The chemical reactions that occur in the water film on the fuel surfaces are important to understanding the evolution of the alteration products. Once again, we begin with the dissolution of the fuel. The (simplified) reaction for the oxidative dissolution of the UO_2 fuel is

$$UO_2 + 2H^+ + 1/2\ O_2 \Rightarrow (UO_2)^{2+} + H_2O\ . \tag{16}$$

The precipitation of dehydrated schoepite is

$$UO_2^{2+} + 1.8H_2O \Rightarrow UO_3 \cdot 0.8H_2O + 2H^+\ . \tag{17}$$

The replacement of the UO_2 fuel by dehydrated schoepite is

$$UO_2 + 1/2\ O_2 + 0.8H_2O \Rightarrow UO_3 \cdot 0.8H_2O\ . \tag{18}$$

There is no net effect on the pH from reaction (18) alone; however, we expect the pH to decrease somewhat due to hydrolysis of the uranyl ion:

$$UO_2^{2+} + yH_2O \Rightarrow UO_2(OH)_n^{(2-n)} + yH^+\ , \tag{19}$$

and in the presence of bicarbonate, uranyl dicarbonate may be significant at near-neutral pH:

$$UO_2^{2+} + 2HCO_3^- \Rightarrow UO_2(CO_3)_2^{2-} + 2H^+\ . \tag{20}$$

At high concentrations of dissolved U (greater than approximately 10^{-6} M), polynuclear uranyl species become important:

$$xUO_2^{2+} + yH_2O \Rightarrow (UO_2)_x(OH)_y^{(2x-y)} + yH^+ . \quad (21)$$

Atmospheric CO_2 will likely buffer the tendency towards lower pH values in the water film contacting the surface of the fuel. Furthermore, without additional cations available in solution, it is unlikely that pH values will decrease too sharply:

$$HCO_3^- + H^+ = H_2CO_3 \qquad K_{S1} = 6.33\ (25\ °C) . \quad (22)$$

We are uncertain at this time what roles that dissolved fission products and/or transuranic elements have on the pH. The concentration reached by such elements in the thin film of water that condenses on the surface of the fuel is probably small compared to total dissolved U, so the effect of dissolved U will dominate the chemistry of the water film. The abilities of the precipitated U^{6+} oxy-hydroxides, such as dehydrated schoepite, to incorporate additional elements may also influence the evolution of the water composition. Our early TEM results indicate that dehydrated schoepite and other U^{6+} oxy-hydroxides can incorporate some transuranic elements and fission products into their structures. Our simplifying assumption for the above equations, that the total U concentration effectively controls the chemistry of the film of water in the vapor-hydration tests, is probably valid.

D. Summary

Combined optical, SEM, EDS, and XRD examinations of samples taken from tests being performed on the two ATM fuels indicate that the rate at which groundwater contacts the fuel samples may be the most important single factor determining the alteration phases that form as spent UO_2 fuel corrodes in a humid oxidizing environment. Results from the three tests (high-drip-rate, low-drip-rate, and vapor) show several similarities, including corroded grain boundaries, dissolution of fuel grains, and precipitation of U^{6+}-phases (Table 10). The vapor tests display the simplest assemblage of alteration products; only U and the radionuclides in the fuel dissolve into the thin film of water in contact with the fuel surfaces. The most abundant phase identified in the vapor tests is probably dehydrated schoepite, $(UO_2)O_{0.25-x}(OH)_{1.5+2x}$ $(0 \leq x \leq 0.15)$.

The drip tests display more chemically complex alteration phases, because of the interaction of the fuel with EJ-13 water (rather than water vapor only). The most abundant elements in EJ-13 water are Na and Si, and, not surprisingly, the most abundant alteration products in the drip tests are Na- and Si-bearing U^{6+} phases. Other U^{6+} phases are also present, including metaschoepite and β-uranophane, indicating the importance of additional minor phases and elements to the overall corrosion process.

An important observation at this stage is that the time-dependent evolution of the alteration-phase assemblage appears to be strongly dependent on the rate at which the EJ-13 water contacts the spent fuel. Fuel samples exposed to the higher drip-rates (nominally 10 times higher than that of the low-drip-rate tests) display a comparatively simple phase assemblage, consisting of two uranophane-group silicates, β-uranophane and Na-boltwoodite (Table 10). In contrast, the sample from the low-drip-rate test displays a more complex alteration-phase assemblage, with four or five phases identified (Table 10). We believe that the simpler phase assemblage in the high-drip-rate tests reflects larger reaction rates for the spent fuel in these tests. Also, samples from the first sampling periods were not taken, and it is possible that the early phases formed but simply were not detected.

Table 10. Alteration Phases Identified by SEM or XRD from ATM Test Samples

Phase	Formula	Test
Metaschoepite (?)	$UO_3 \cdot 2H_2O$ (?)[a]	ATM-103 (LDR)[b] ATM-103 (vapor) ATM-106 (vapor)
Dehydrated schoepite	$(UO_2)O_{0.25-x}(OH)_{1.5+2x}$ $(0 \leq x \leq 0.15)$	ATM-103 (LDR) (?) ATM-103 (vapor) ATM-106 (vapor)
Unidentified Na-UOH	$(Na,K)[(UO_2)_3O_2(OH)_3](H_2O)$ (?)	ATM-103 (LDR)
Soddyite	$(UO_2)_2SiO_4(H_2O)_2$	ATM-103 (LDR)
β-uranophane	$Ca(UO_2)_2(SiO_3OH)_2(H_2O)_5$	ATM-103 (HDR)[b]
Na-boltwoodite	$(Na,K)(UO_2)(SiO_3OH)(H_2O)$	ATM-103 (LDR) ATM-103 (HDR) ATM-106 (HDR)

[a](?) indicates a tentative identification or an uncertain formula.
[b]LDR = low-drip-rate test; HDR = high-drip-rate test.

Another important observation concerns the identification of uranyl oxy-hydroxides in the vapor-hydration tests. The precipitation of dehydrated schoepite and metaschoepite in these tests indicates that the film of water that forms on the fuel surface is sufficiently corrosive to dissolve the fuel and form a thin corrosion rind of alteration products. Such a water film is likely present in the drip tests as well during those intervals that EJ-13 water is not being dripped onto the fuel. It seems likely that the corrosion processes important in the vapor tests remain important in the drip tests. Dehydrated schoepite and/or metaschoepite may continue to form in the drip tests between water injections. If these phases are present when contacted by EJ-13 water, they may be at least as susceptible to dissolution and/or replacement as the unoxidized fuel. The degree to which this may be important is unknown at this time.

The mechanism by which the fuel has reacted during these tests is important, although we have only limited information available at this time. Most striking is that the fuel in the high-drip-rate test on the sample from ATM-103 has dissolved along a uniform front that has penetrated from the outer surface into the spent fuel fragments. This through-grain dissolution has proceeded without regard to existing grain boundaries. The replacement of the fuel by Na-boltwoodite at the fuel surface may also be self-accelerating. Through-grain dissolution appears to be an important mechanism by which the fuel is reacting in the high-drip-rate tests. Of course, the dissolution of the fuel along grain boundaries is also important in the high-drip-rate tests. This type of dissolution is especially evident from the extent to which the grain boundaries in one fragment of the ATM-103 sample had been opened, resulting in a friable fragment that decomposed during sample handling.

These data are still preliminary. We must examine additional grains and fragments of reacted fuel to understand more fully the corrosion and alteration processes, including grain-boundary penetration by water, changes in the reactive surface area, and the distribution of radionuclides between the alteration phases and the EJ-13 water.

III. EXAMINATION OF SPENT NUCLEAR FUEL WITH ANALYTICAL TRANSMISSION ELECTRON MICROSCOPY

A. Introduction and Background

Analytical transmission electron microscopy is a versatile technique for examining the microstructure of corroded spent fuel. Thomas et al. [THOMAS-1989, -1990, -1992] demonstrated through their numerous studies characterizing spent nuclear fuels, that AEM was ideal for developing an understanding the microstructure of the low burnup fuels, especially ATM-103, ATM-104, and ATM-106. The features of interest in these fuels were not visible by any other technique. We have found that to determine the nature of oxidative corrosion in these materials, AEM has proven again to be an invaluable technique. The AEM samples extremely small regions so the representativeness of the data obtained must always be examined. The sample preparation methods employed, comparison with SEM and optical microscopy, and the number of AEM samples examined has helped to improve the representativeness of the analysis. Three important issues are addressed in this section: (a) the retention of Np in a secondary phase, (b) dissolution of the ε-particles, and (c) the segregation of Pu. Each of these issues is controversial and may be impossible to defend solely with the AEM data. Therefore, the comparison with the solution data (Section I) is critical in determining the total mass balance in the system.

B. Objectives

The objective of this task is to obtain information on the nature of the corrosion process in spent fuel, including compositional and structural information on the secondary phases and altered fuel. The behavior of the fission and neutron capture products during the anticipated corrosion of spent nuclear fuel in an oxidizing environment is important for determining the long-term release rates of radionuclides. With AEM, it has been possible to provide some information on the possible fates of some radionuclides present in spent fuel. In this section of the report, we describe the methods used for investigating the nature of the ε-phases within the fuel grains and in the grain boundaries. This evidence of corroded ε-phases is needed to support the use of the normalized loss of Tc as a measure of spent fuel corrosion.

C. Technical Approach

Representative particles of the corroded fuel were embedded in an epoxy resin and cut into thin sections with an ultramicrotome. The resultant 30-50 nm electron-transparent cross sections of corroded fuel grains were transferred to carbon-coated copper grids and examined in a JEOL 2000 FXII analytical transmission electron microscope operated at 200 kV with a LaB_6 filament. The AEM is equipped with a Gatan 666 parallel electron energy-loss spectrometer, which has an energy resolution of about 1.6-1.8 eV. The actinide M-edges were obtained by operating the spectrometer in the second-difference mode [BUCK-1997A]. This technique removes the channel-to-channel gain variation that occurs with parallel detectors. The method also acts as a frequency filter, enhancing such sharp features such as the "white-lines" on the absorption edges. Hence, peak shape will affect the ability to detect an element. A rounded or smooth edge, for instance, will be less visible than a sharp edge. Electron diffraction patterns were taken with a charged coupled device (CCD) camera, which permits very-low-intensity viewing and, therefore, is ideal for electron-beam-sensitive materials.

D. Results and Discussion

The results of AEM investigations with ATM-103 are discussed in three parts of this section. First, evidence for the incorporation of neptunium into an alteration product of spent fuel is presented. Second, we will describe the behavior of ε-particles in ATM-103 during vapor-phase

corrosion and under high-drip-rate conditions, which supports the use of Tc as a marker element for spent fuel corrosion. Third, we will show data indicating the enrichment of plutonium during the corrosion process.

1. Incorporation of Neptunium into Secondary Phases

Using a unique anion topology approach for comparing the structures of uranyl phases, Burns et al. [BURNS-1996] has predicted mechanisms by which transuranic species can be incorporated into the alteration products of corroded spent fuel. The U-O bond length (0.18 nm) in the linear species UO_2^{2+} is similar to that of Np-O in NpO_2^+ (0.165-0.181 nm), and when coordinated by O^{2-}, OH^-, or H_2O, the equatorial Np-O bond distances are only about 0.01 nm longer than those found in similarly coordinated uranyl polyhedra. Thus, it is reasonable to expect isomorphic substitution of the neptonyl ion in uranyl ion sites [BURNS-1996]. However, because of valence bonding considerations, the axial oxygens on the linear neptonyl species may require additional valence contributions from interlayer cations or protons in the uranyl phase.

a. Analysis of Dehydrated Schoepite from Vapor Tests with EELS

Analysis of the dehydrated schoepite phase with EELS indicated the presence of Np (Fig. 13). Since we examined cross sections of the corroded fuel grains and alteration products, it is unlikely that the occurrence of Np is due to sorption on the dehydrated schoepite; however, we cannot totally exclude this mechanism for retention of Np in an alteration phase. Neptunium was observed with EELS in three samples of dehydrated schoepite that were taken from different regions of the corroded fuel pellets. The U:Np ratio was estimated to be between 1:0.003 and 1:0.006, based on five analyses. In the dehydrated schoepite ($UO_3 \cdot 0.8H_2O$) where Np was detected, this ratio corresponds to one Np atom for every 250 unit cells of $UO_3 \cdot 0.8H_2O$ or about 550 ppm (Table 11). The U:Np ratio in the ATM-103 fuel is 1:0.0005, taken from calculated values reported by Guenther et al. [GUENTHER-1988] for ATM-103 at 35 MWd/kgM after 15 years. The estimated U:Np ratio in the alteration phase indicates that a large proportion of the Np has entered into the phase. Due to the scarcity of water on the fuel surface in the vapor tests, only a small amount of water was able to flow into the steel collection vessel positioned at the bottom of the test apparatus. Under these conditions, it might be expected that the highly soluble elements will become concentrated enough in the thin film of water to precipitate secondary phases. The absence of Pu and Am in the dehydrated schoepite supports the contention that mainly Np and U were mobilized during the corrosion process and incorporated into a secondary phase.

Under more dynamic conditions, where flowing water was present, the retention of the Np in alteration phases may not occur. The next section presents similar EELS analysis of uranium-bearing alteration phases formed under relatively high flow conditions.

b. Analysis of Uranium Silicate Alteration Phases from High-Drip-Rate Tests with EELS

In the related high-drip-rate tests, analysis of the corrosion products failed to indicate the presence of Np at the same level observed in the vapor tests. However, dehydrated schoepite was not one of the phases detected. In Fig. 14a and b, the EDS and electron diffraction analysis suggested that the corrosion product from this test was related to β-uranophane (ideally $Ca[(UO_2)(SiO_3OH)]_2 \cdot 5H_2O$). A trace amount of ruthenium is present in the phase, and it can also be seen in the energy-loss spectrum (see Fig. 14c). The form of the uranyl alteration phases is dependent on the composition of the fluid in contact with the fuel. In the high-drip-rate tests, the fuel is contacted by silica-saturated EJ-13; hence, uranyl silicates are the dominant alteration products.

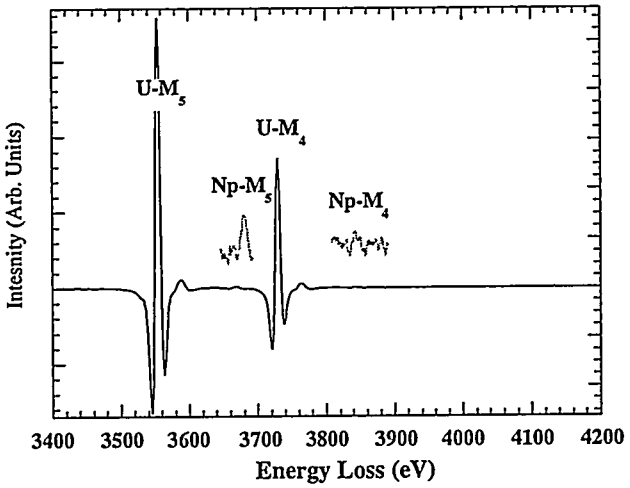

Fig. 13. Electron Energy-Loss Spectrum of Dehydrated Schoepite Showing the Presence of Np in the Phase. The two intense uranium edges (M_5 at 3552 eV and U-M_4 at 3728 eV) dominate the spectrum; however, the Np-M_5 edge at 3666 eV is clearly visible. The intensity of the Np edges has been increased 20x for easier viewing. The Np-M_4 edge at 3850 eV does not appear to be visible above the background.)

Table 11. Analyses of Dehydrated Shoepite

Analyses	U	Np	U:Np Ratio*
1	397912	3462	0.009
2	364624	3715	0.01
3	533660	3312	0.006
4	135517	300	0.002
5	576382	3482	0.006
6	16950	50	0.003
7	50300	206	0.004
8	471401	4769	0.01
9	336676	2081	0.006
	Average in dehyrated schoepite ~ 1000 ppm		**0.006**

*Assuming electron cross-sections between U and Np do not vary.

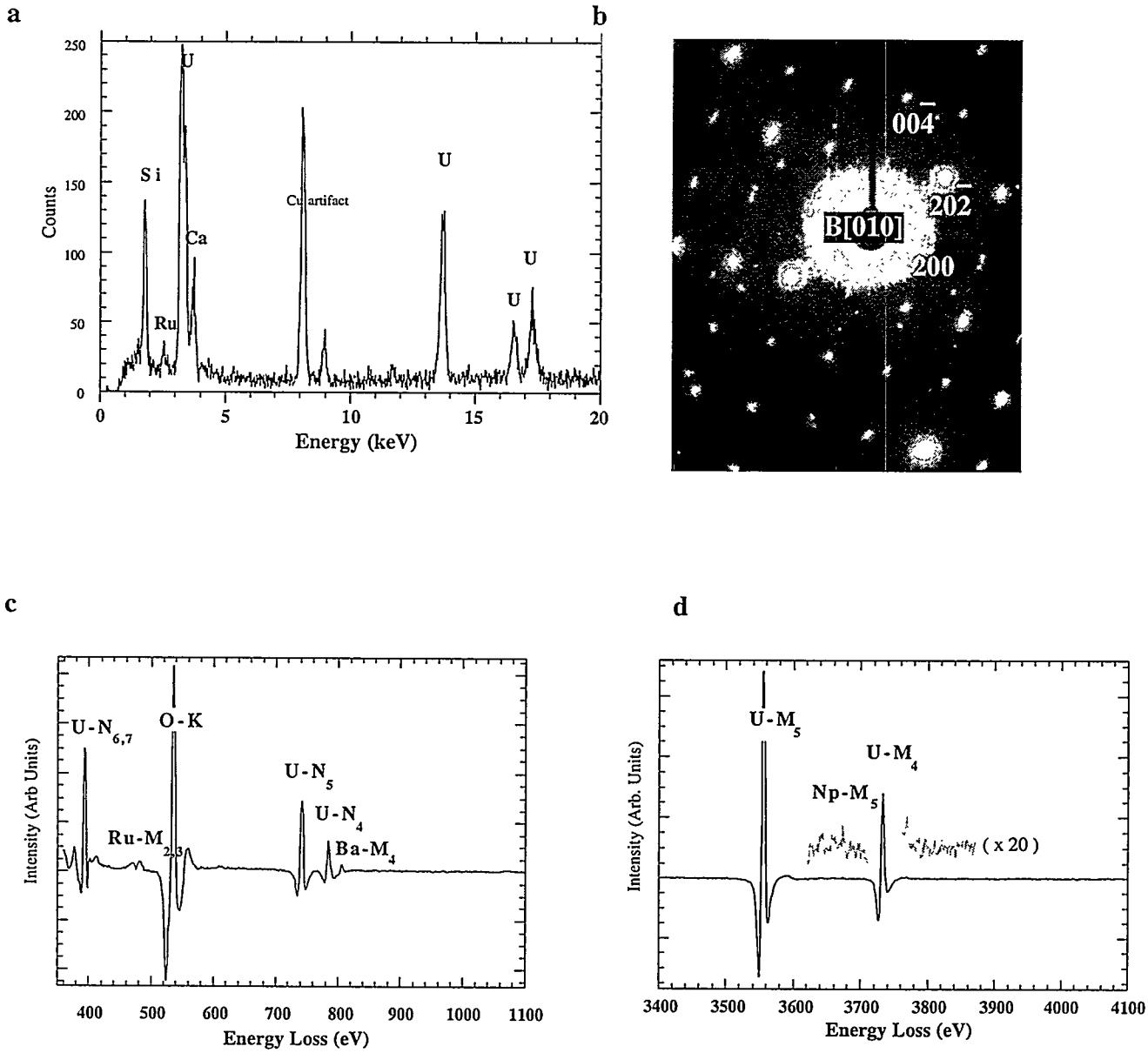

Fig. 14. (a) X-ray EDS of an Alteration Phase from a High-Drip-Rate Test Reacted for 44 Months; (b) Electron Diffraction Pattern Taken Along [010] from the Uranyl Silicate Phase is Shown. (A β-angle of about 93° was obtained from the analysis of the patterns.) (c) Electron Energy-Loss Spectrum of Uranyl Silicate Alteration Phase from the High-Drip-Rate Test Showing the U-N Edges and (d) Spectrum Showing the High Energy-Loss M-Edges of Uranium

Possibly some Np is in a uranyl silicate phase; if so, however, the levels are at or below the detection limits for the instrument. The estimated U:Np ratio is not more than 1:0.0005, which corresponds to <50 ppm Np in the phase; this level appears to be the detection limit. Substitutions of the type $Np^{5+} \leftrightarrow U^{6+}$ may occur in all uranyl structures [BURNS-1997]; however, evidence from the majority of solution analyses from waste-form testing suggests that

Np remains stable and complexes in solution under most common pH-Eh regimes. Nevertheless, within the thin film of water in contact with the spent nuclear fuel, significant alpha radiolysis will occur, leading to the possible formation of H_2O_2. The altered Eh conditions may result in changes in the Np chemistry that may favor incorporation into the uranyl sheets. These sheets may be easily charge balanced through substitutions of the type $O^{2-} \leftrightarrow OH^-$. The most common oxidation state for Np in oxygen-rich waters is Np(V). In the vapor tests, because the pH of the contacting solution is unknown, describing the form of the Np would be speculative. However, calculations suggest that in a J-13 Yucca Mountain groundwater above pH 7.5, the dominant species is $NpO_2(CO_3)^-$, and below this pH 7.5 NpO_2^+ would dominate[CLARK-1997]. The pH of the contacting solution in the high-drip-rate tests is known to be about 6 [FINN-1997], suggesting that NpO_2^+ will be the most prominent species.

The incorporation of transuranics into the alteration products of oxide spent fuel corrosion has been predicted on the basis of crystal chemical considerations [BURNS-1996], although it has seldom been observed. The lack of observation may be due, in part, to the limitations of instrumental techniques and the difficulty in working with transuranic-bearing samples; however, knowledge of the specific conditions required for substitution of particular radionuclides into alteration phases may lead to development of engineered systems that may retard the migration of these radionuclides.

The observation of Np incorporation into dehydrated schoepite was only possible by examining thin sections of the reacted material with EELS. This technique has excellent detection capabilities and spatial resolution to locate regions where transuranics have been concentrated. Although the limits of detection for EELS are essentially functions of analysis time and beam intensity, when using the second-difference method, peak shape is also important. Future improvements in detection limits should be possible with the use of an energy-loss imaging filter that, when operated as a two-dimensional array spectrometer, is much more efficient than the parallel detector used in this study.

2. Evidence for the Dissolution of ε-Particles in Vapor and High-Drip-Rate Tests with ATM-103

As the ATM-106 fuel was not heated sufficiently to cause significant redistribution of fission products, the volatile fission products were unable to reach grain boundaries. However, temperatures in the fuel pellet centers (700-1200°C) were high enough to coarsen the "4d" ε-metal particles, fission gas bubbles, and pressurized fission-gas solids [GUENTHER-1988]. The fission products that form during burnup of oxide fuels may aggregate in one of three types of precipitates: gaseous, metallic, or oxide, depending on the burnup . Low burnup fuels, such as ATM-103, have not been found to contain ceramic oxide molybdates, zirconates, uranates, or cesium-bearing phases. However, high pressure Kr and Xe gas bubbles have been observed, along with ε-"ruthenium" phases that contain Mo, Tc, Ru, Rh, and Pd. Based on AEM and EDS analyses of the samples of spent nuclear fuel, most fission products in the low-release ATM-103 are thought to remain dispersed within the UO_2 matrix. Views to the contrary are based primarily on the evidence from short-term leach tests. These tests have shown preferential release of Cs, I, Sr, and Tc, which, it is argued, originate from the grain boundary regions. However, the detection limits for fission products within spent nuclear fuel analyzed with TEM-EDS are perhaps not sufficient to exclude the presence of fission products within the grain boundaries. Therefore, significant quantities of these elements could be present in the boundary regions, which if released first during corrosion testing, will exaggerate the estimated corrosion rate (it is assumed that the fission products are uniformly distributed throughout the UO_2 matrix).

The fission product, Tc, due to its high solubility and general tendency not to become incorporated into alteration phases, is being used as a "marker element" for calculating the

corrosion rate of spent nuclear fuel in the ongoing drip tests. Based on the preceding discussion, the Tc marker may be appropriate, at least for low burnup fuels. However, previous studies have suggested that the ε-phase is highly insoluble, and therefore the observed leached Tc must originate from grain boundary regions in the fuel.

Fission product segregation and precipitation in low-burnup, light-water-reactor fuels can only be effectively studied with AEM, as the features that are characteristic of these types of spent nuclear fuel can only be probed with a high spatial resolution instrument. As only limited transport of fission products occurred in the fuel, the features observed in one series of spent nuclear fuel grains are most likely representative of the entire material.

a. Corrosion of the ε-Phase

Particles of corroded spent fuel from the ATM-103 test were selected for further analysis with electron microscopy. Several interesting features were observed in this sample. Mo-Tc-Ru (ε-phase) phases were found within the spent fuel grain. The particles were extremely small, around 20 - 50 nm in diameter (Fig. 15). Some appeared weathered, but on the whole, they appeared uniform. The composition of many of the particles did not match that reported by Thomas et al. [THOMAS-1989; -1990, -1992] during AEM characterization of the ATM-103. Quantitative analysis by Thomas et al. of the 4d metals in the ε-particles agreed with the fission product ratio for these elements in ATM-103. This result supports the contention that all the 4d metals partition to the ε-phases. In this study of the corroded fuel, Tc and Mo appeared suppressed relative to Ru and Pd, suggesting that the phases may have experienced preferential leaching of Te and Mo.

We found two types of ε-ruthenium phase in the fuel, which again is consistent with the work of Thomas et al. (see Table 12); however, the Pd-rich phase may be described as α-Pd(Ru,Rh) phase based on tertiary plots by [KLEYKAMP-1985]. The ε-ruthenium phase is the more acceptable 4d metal phase described by [THOMAS-1989]. Therefore, to describe the corrosion of the ε-phases, we have used the ratio of Mo/(Ru+Pd) to allow comparison of all particles observed. This ratio in uncorroded ATM-103 according to the ORIGEN2 code is one. Thomas et al. have also obtained this value in their analyses. In the particles found in the vapor test exposed to a corroding environment for 49 months, the Mo/(Ru+Pd) was found to be much lower for many of the analyzed particles. However, in comparison to the particles found in the ATM-103 high-drip-rate test, ε-ruthenium phases in the vapor tests retained more Mo (see Table 3). This indicates that the 4d-metal phases examined exhibited preferential removal of Mo during the corrosion tests. This partial corrosion of the ε-phases may provide some insight into the local oxidative conditions. The observed behavior is in agreement with the relative nobility of the 4d metals, but it goes against the egalitarian viewpoint of congruent alloy dissolution.

For comparison of quantification analysis results from Thomas and Charlot [THOMAS-1990] and from the ATM-103 high-drip-rate test fuel fragments are shown in Table 13. Thomas and Charlot [THOMAS-1990] were able to obtain very accurate EDS quantification of 4d metals in the ε-phases. We can quantify the ε-phases found in this vapor test, but for observing evidence of corrosion it may be better to use the spectra themselves. Table 12 also presents recent quantification of ε-phases with EELS and EDS. In the high-drip-rate sample, it was more difficult to prove evidence of corrosion of ε-ruthenium phases, as all appeared to be equally modified from the more typical composition. The Pu-rich region (Fig. 16) refers to a region in the ATM-103 fuel which had higher levels of Pu than most other portions of the fuel. This is discussed in more detail in the next section.

Evidence for the partial corrosion of the ε-phase supports the use of Tc as a marker element for spent fuel dissolution. However, there are still questions regarding the role of intra- and inter-granular ε-particles. Further analysis of thin sections of corroded fuel will be necessary to understand the possible differences.

3. Plutonium Enrichment During the Corrosion of Spent Nuclear Fuel

During the AEM examination of corroded ATM-103 fuel from both the vapor and high-drip-rate tests, regions were found that possessed anomalously high concentrations of plutonium (see Fig. 16). The enrichment levels in these regions far exceeded those reported in the uncorroded fuels [THOMAS-1989, -1992]. X-ray energy dispersive analysis indicated significant levels of Zr and Ru in this region. The origin of the Zr could be from either the cladding or the fuel. Although Zr is a fission product, the original fuel cladding was made of Zr and Zr is also the major component in the test apparatus as the retainer. It is possible that reaction might occur at the fuel's edge, where pellets are in contact with the Zr-bearing cladding. However, the levels of Pu in these regions are generally suppressed, due to the high burnup, and the regions exhibit high levels of fission products, such as rare earths. The EELS analysis indicated anomalously low concentrations of rare earths. Therefore, the enriched-Pu regions are most likely produced during oxidative corrosion. This may also suggest that Pu is not readily incorporated into uranyl phases. The possibility of $Pu^{6+} \leftrightarrow U^{6+}$ substitution or Pu^{4+} substitution into uranyl oxide hydrates and uranyl silicates has been speculated by Burns et al. [BURNS-1997]. In the high-drip tests, a possible pseudomorphic transformation of spent fuel (UO_2) to uranyl phases, might require isomorphic substitution of Pu for sites in the uranyl structures. To date, we have not found evidence for this occurrence; however, we do have supporting evidence for the accumulation of Pu into discrete areas in the corroded fuel. Regardless of their origin, the presence of enriched regions of Pu suggests that if these regions become friable, Pu-bearing colloids could be released.

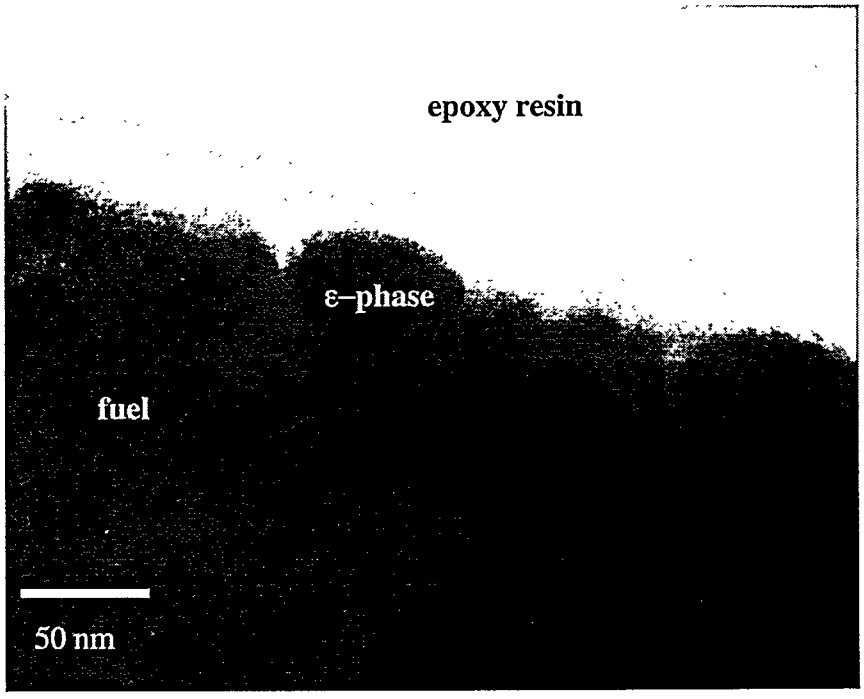

Fig. 15. Transmission Electron Microscopy Image of ε-Ruthenium Particle within a Spent Fuel Grain

Table 12. Composition of ε-Phase (elements in wt%) from the Results of the ATM-103 Vapor Hydration Tests

Element	Calculated[a]	Pd-Rich Particles			
Mo	*44*	29	30	30	
Tc	*11*	9	12	11	
Ru	*28*	40	30	30	
Rh	--	--	--	--	--
Pd	*17*	22	28	28	~100
Mo/(Ru+Pd)	0.98	0.47	0.51	0.52	--
		Ru-Rich Particles			
Mo		29	26	33	27
Tc		17	15	12	0
Ru		33	42	55	73
Rh[c]		--	--		--
Pd		22	17		--[b]
Mo/(Ru+Pd)		0.53	0.44	0.60	0.36

[a]Calculated from Guenther et al. [GUENTHER-1989] for ATM-103 and normalized without Rh.
[b]Pd not analyzed in this case.
[c]Rh not analyzed in any sample.

Table 13. Composition of ε-Phase (elements in wt%) from the Results of the ATM-103 High-Drip-Rate Tests

Element	Calculated[a]	Unreacted Phase[b]	Edge Region	Pit Region	Pu-Rich Region[c]
Mo	41.2	40	12.3	16.6	15.2
Tc	9.6	10	5.0	10.1	3.9
Ru	27.5	25	41.7	44.8	45.1
Rh	5.5	10	7.5	17.6	9.8
Pd	16.0	15	32.6	10.8	26.1
Mo/(Pd+Ru)	0.95	1.0	0.16	0.30	0.21

[a]Calculated from Guenther et al. [GUENTHER-1989] from ORIGEN2 code for 30 MWd/kgM at 15 years.
[b]Semiquantitative EDS analysis by Thomas and Charlot [THOMAS-1990].
[c]Quantification of EELS was performed using a 100-eV window and the oscillator strength values calculated from a Dirac-Foch model by Ahn et al. [AHN-1989].

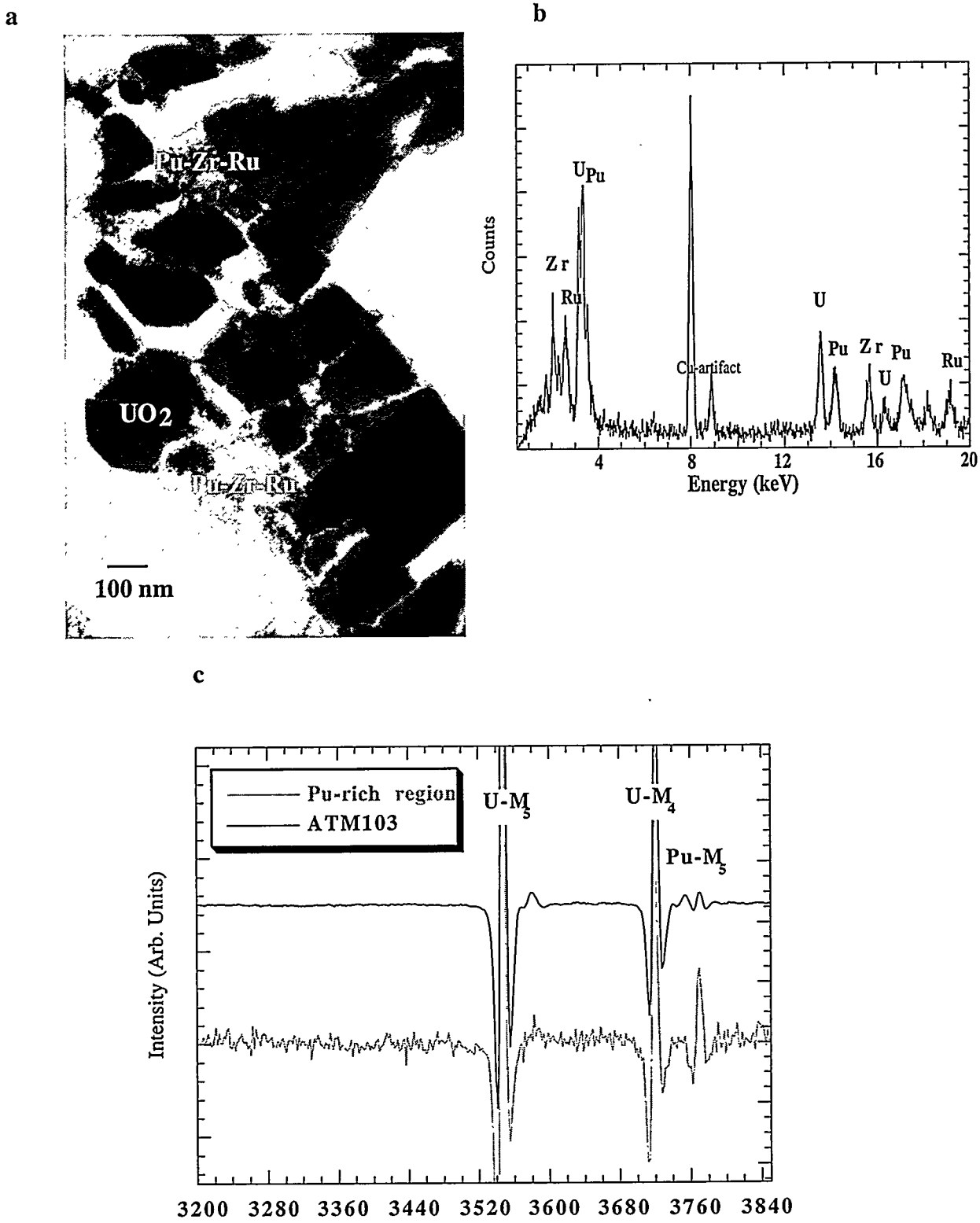

Fig. 16. Evidence of Pu-Rich Regions in a Vapor Test: (a) Transmission Electron Microscopy Image of Pu-Rich Regions within the Corroded ATM-103; (b) EDS of the Pu-Bearing Region Showing Enriched Levels of Ru and Zr; (c) Electron Energy-Loss Spectra from a High-Drip-Rate Test Comparing Enrichment of Pu in a Discrete Region against an Uncorroded Region of the Fuel.

E. Future Studies

We have demonstrated that the release of Np may be controlled by uranyl alteration phases formed during the corrosion of oxide spent nuclear fuel in an unsaturated environment. Although schoepite is only a transient phase in paragenesis of uraninite [WRONKIEWICZ-1997, FINCH-1992, PEARCY-1994], Finch et al. [FINCH-1989] have demonstrated that the schoepite at weathered uraninite deposit at Shinkolobwe has lasted over 250,000 years. Indeed, at the same site the uranyl carbonate, rutherfordine [$UO_2(CO_3)$], exhibited exceptional resistance to dissolution. This behavior may indicate that dehydrated schoepite may have the ability to retain neptunium for considerable periods.

The behavior of Pu during corrosion is extremely important, considering that even larger levels of Pu are being considered for placement in the proposed geologic repository. Accumulation of Pu as colloidal-sized aggregates imply for possible migration of Pu, whereas large accumulations of Pu may present criticality concerns. Further analysis of the nature of the Pu-rich regions is necessary to determine if the regions are amorphous sediments or well-defined structures.

IV. PETRI-DISH TESTS

A. Background

This section of the report describes several pilot tests that have been run to determine an experimental setup for batch tests on spent commercial fuel. These initial tests were not intended to be systematic experiments on the corrosion of UO_2; however, in addition to examining prospective test parameters, our results have provided some insights into UO_2 corrosion under the test conditions, and we describe our results here.

The "drip-tests" currently being performed on UO_2 and spent UO_2 fuel have demonstrated that these tests are effective methods of examining the alteration of UO_2 and spent fuel in an unsaturated environment, such as may be expected in the proposed repository at Yucca Mountain. Previous drip-test results demonstrated that UO_2 and spent fuel both react with a thin film of water to form a suite of U^{6+} alteration phases. Using current experimental designs, the suite of U^{6+} phases takes two to five years to fully develop. We have designed "petri-dish" batch tests that are intended to accelerate the alteration reactions observed in drip tests. We hope that relevant observations can be made in six months or less, allowing more rapid evaluation of test results.

In addition, the composition of the film of water in contact with UO_2 or fuel is not well-known for the drip tests. In the current drip test method, a solution of known composition (EJ-13) is injected into a test vessel, where the water reacts with UO_2 or fuel. This solution eventually drips down through the UO_2 or fuel and accumulates at the bottom of the reaction vessel, from where it is periodically sampled for analysis. This analysis gives an indication of the chemical changes that the solution undergoes between injection and sampling; however, a more detailed knowledge of the composition of the thin film of water that is actually reacting with the UO_2 or fuel remains elusive. By providing just enough water to maintain a constant film of water on a small quantity of fuel in the batch test, we hope to more closely monitor the compositional evolution of water as it reacts to form U^{6+} alteration phases. Note, however, that in drip tests, cations consumed during reaction can be replenished, whereas, in the petri-dish tests, cations are not replenished.

B. Experimental Setup

As noted above, the tests on UO_2 described here are pilot tests. Results from each experiment were used to evaluate current test equipment and procedures, with changes being made where deemed necessary. Consequently, the experimental setup was modified during the course of the seven tests described here (Table 14) Modifications were, for the most part, minor, and included modifying the screen hanger design, adding H_2O_2 to the EJ-13 water in some tests, and changing screen material. Although each change had some impact on experimental results, a systematic study of the effects of each change was not attempted.

We did not want consumption of O_2 during the corrosion process to be a limiting factor. The 45-mL reaction vessel chosen for these tests is large enough to oxidize 0.2 g of UO_2 completely. The amount of water was limited by total surface area of UO_2; a relatively high rate of the sample surface area to solution volume S/V ratio was desired, as this is thought to be a critical factor controlling compositional changes to the thin film of water present in drip tests.

The initial equipment used for tests PDT-1 through PDT-6 consisted of a 45-mL, 304L stainless steel (SS) Parr reaction vessel (Fig. 17) with a hanger made of ~1.6-mm diameter (1/16-inch) 304L-SS to which a 316-SS, 325-mesh screen was spot welded (Fig. 17). Each reaction vessel was sealed with a Cu gasket and a Ni-plated brass compression fitting; the compression

fitting was tightened to 160 ft-lb at the beginning of each test. Tests were conducted in a convection oven kept at 90 ± 1°C.

Table 14. Test Matrix

Test ID	Screen Stainless Steel	Water	UO_2 Prep.	UO_2 Mass (g)	EJ-13 Mass (g)	S/V[a] (m^{-1})	Run (days)	(S/V)[a]time ($days \cdot m^{-1}$)
PDT-1	316	EJ-13a	as sieved	0.1995	1.99	1200	42	50,400
PDT-3	316	EJ-13a	as sieved	0.2005	0.50	5000	28	140,000
PDT-4	316	EJ-13a (ox)	as sieved	0.2003	0.51	5000	35	175,000
PDT-5	316	EJ-13a	as sieved	0.1986	0.50	5000	114	570,000
PDT-6	316	EJ-13a (ox)	as sieved	0.2006	0.49	5000	70	350,000
PDT-7	304L	EJ-13b	EtOH rinsed	0.2004	0.50	5000	74	370,000
PDT-8	304L	EJ-13b (ox)	EtOH rinsed	1.9994	0.50	5000	70	350,000

[a]S/V is ratio of solid surface area to solution volume; UO_2-particle surface areas calculated for spherical particles, 45 μm in diameter.

Due to the corrosion of the 316-SS screens during the first six tests (the results are discussed in Section IV.C.2), a more corrosion-resistant screen material was used in the final two tests, PDT-7 and PDT-8. The new screen material chosen is a 304L-SS sintered and woven filter, manufactured by Pall (Rigimesh™). The new mesh was rated to remove 100% of particles greater than 45 μm in diameter and 98% of particles greater than 17 μm ("removal grade M").

The solid used in these tests was synthetic, unirradiated UO_2 with a natural isotopic abundance and an O:U ratio of 2.000 ± 0.002 (WRONKIEWICZ -1992). The UO_2, a pressed and sintered powder that had been formed into pellets (ANL special materials batch # 4-4-110), is the same material used in the unsaturated drip tests on UO_2 described by Wronkiewicz et al. [WRONKIEWICZ -1992, 1996]. X-ray diffraction analysis of the starting UO_2 powder demonstrated that storage had not oxidized the bulk of the UO_2.

Before use, pellets of UO_2 were crushed and ground by hand with an agate mortar and pestle. The resulting powder was sieved to between -200 and -325 mesh (particle sizes 75 - 45 μm). The first five tests (PDT-1 through PDT-6) were performed with as-sieved UO_2 powder. For the final two tests, PDT-7 and PDT-8, sieved UO_2 powder was rinsed with ethanol (E+OH) to remove fines before use. Prepared UO_2 powders were analyzed by SEM to check grain size distributions. SEM micrographs of polished cross sections made from UO_2 from both preparations are shown in Fig. 18.

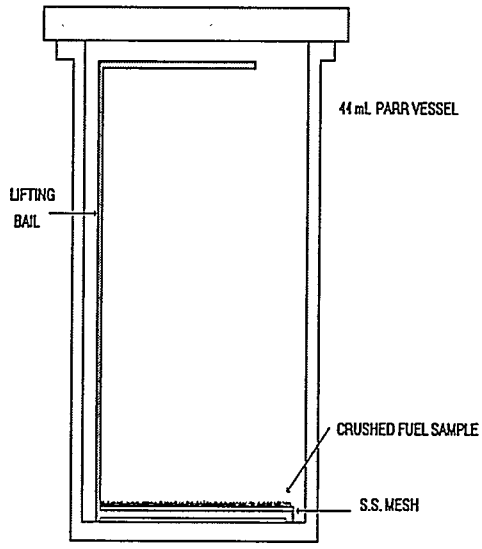

Fig. 17. Schematic Diagram of the Test Vessel and Hanger with Screen

At the start of each test, we placed 0.20 g of UO_2 powder onto the stainless steel screen. The total O_2 in each 45-mL reaction vessel was sufficient to oxidize 8 x 10^{-4} moles of U^{4+} to U^{6+}. The relevant reaction can be represented by reaction of the oxides: $UO_2 + 1/2\ O_2 \Rightarrow UO_3$. One mole of air with 20 vol% O_2 occupies 22.4 L at 25°C and 1 atm. Thus, approximately 0.0004 mole of O_2 are in each vessel (the hanger and other test components are assumed to occupy approximately 1 mL). This amount of O_2 will oxidize 0.216 g of UO_2 — hence our decision to use 0.2 g of UO_2 in these tests. Because of the small mass of UO_2 used, the total volume of water used was necessarily small.

SEM analyses of prepared UO_2 powder reveal a few solid impurities (Fig. 19). Qualitative chemical analyses of these impurities were performed by EDS during SEM examinations of polished sections. Material pictured in Fig. 19 is fine-grained and chemically inhomogeneous; it is probably a mixture of Fe-oxide(s) and an unidentified Fe-silicate. The number of known Fe-oxides and Fe-silicates that may occur as impurities in the UO_2 powder is extensive (Table 15), so more complete identification remains elusive at this time. Chemical impurities present in the initial UO_2 pellets at concentrations of greater than ~1 ppm include B, Si, Ca, Ni, Cu, Al, Cl, Th, and Fe [WRONKIEWICZ-1992]. Much of the Fe and Si are probably associated with Fe-silicate impurities, which are relatively common in the UO_2 starting material. EDS analyses of the Fe-silicate indicate Al, Ca, Mn, and U are also present. This material is very heterogeneous. The Fe-oxide has Al and minor Si.

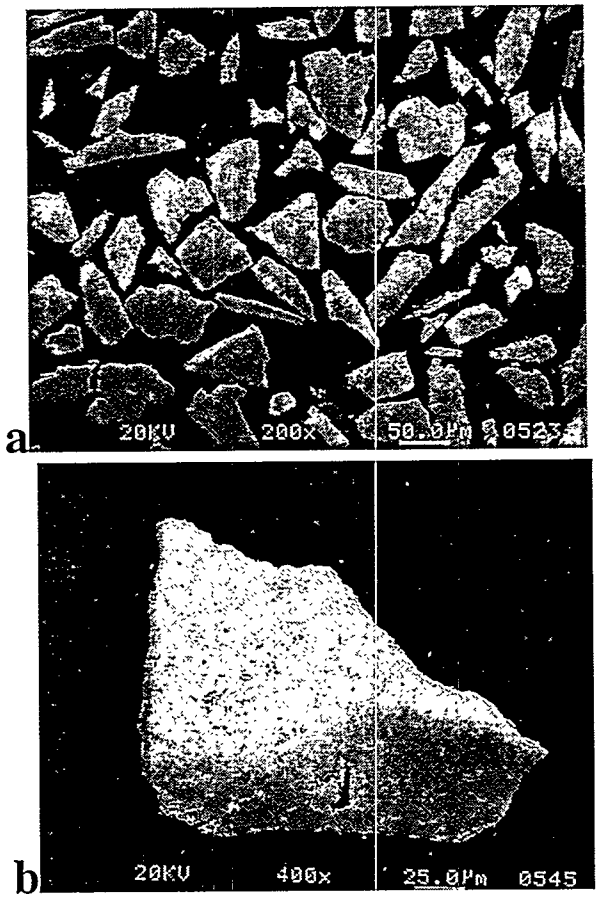

Fig. 18. SEM Micrographs of Polished Cross Sections through the UO_2 Starting Material: (a) Unwashed; (b) Washed

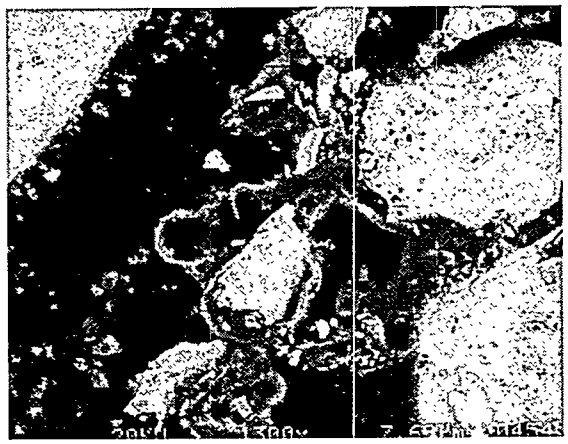

Fig. 19. SEM Micrograph of a Polished Cross Section through the UO_2 Starting Material Showing an Unidentified Fe-Silicate Impurity

Table 15. Listing of Several Ferric Oxides, Ferric Oxy-Hydroxides and Ferric Silicates

Mineral or Compound	Formula	Comments
Bernalite	$Fe(OH)_3$	"green rust," ←stottite grp.
Synthetic ferric hydroxide	$Fe(OH)_3$	several preparations
Goethite	a-FeO(OH)	
Akaganeite	b-FeO(OH,Cl)	
Lepidocrocite	g-FeO(OH)	
Feroxyhite	d-FeO(OH)	
Ferrihydrite	FeO(OH)	poorly crystalline
Hematite	a-Fe_2O_3	corundum group
Synthetic ferric oxide	b-Fe_2O_3	
Maghemite	g-Fe_2O_3	spinel group
Magnetite	Fe_3O_4	spinel group
Greenalite-1T	$(Fe^{2+},Fe^{3+})_{2-3}Si_2O_5(OH)_4$	kaolinite/serpentine grp.
Cronstedtite	$Fe^{2+}{}_2Fe^{3+}(SiFe^{3+})O_5(OH)_4$	kaolinite/serpentine grp.
Hisingerite	$Fe^{3+}{}_2Si_2O_5(OH)_4{\cdot}2H_2O$	kaolinite/serpentine grp. (?)
Erlianite	$(Fe^{2+},Mg)_4(Fe^{3+},V^{5+})_2Si_6O_{15}(O,OH)_8$	kaolinite/serpentine grp. (?)
Macaulayite	$(Fe^{3+},Al)_{24}Si_4O_{43}(OH)_2$	
Nontronite	$Na_{0.3}Fe^{3+}{}_2(Si,Al)_4O_{10}(OH)_2{\cdot}nH_2O$	smectite grp.
Synthetic Fe-silicate hydrate	$Fe_2Si_{90}O_{183}(H_2O)$	

Other impurities identified during analyses of starting material or during analyses of reacted materials were much less abundant than Fe-oxides and Fe-silicates. These other impurities include particles of a metal alloy (Fig. 20) with Fe, Cr, Zr, Mo, Mn, Na, and Ni. A few small shards of silica glass (Fig. 21) were found in micrographs from some tests. Polycrystalline ThO_2, possibly with minor $ThSiO_4$ is rare, but it was found in test PDT-7. X-ray diffraction analyses of starting UO_2 powder indicate only UO_2 in the powder-diffraction pattern, so crystalline impurities make up less than 1% of the UO_2 powder analyzed by XRD.

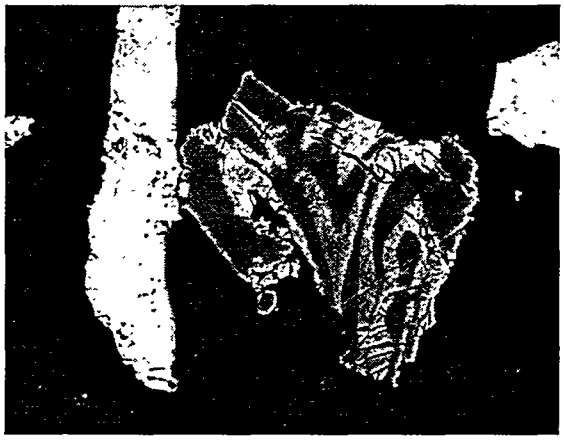

Fig. 20. SEM Micrograph of a Polished Cross Section through Reacted Solids from PDT-3 Showing Metal-Alloy Impurity from PDT-3 (EDS)

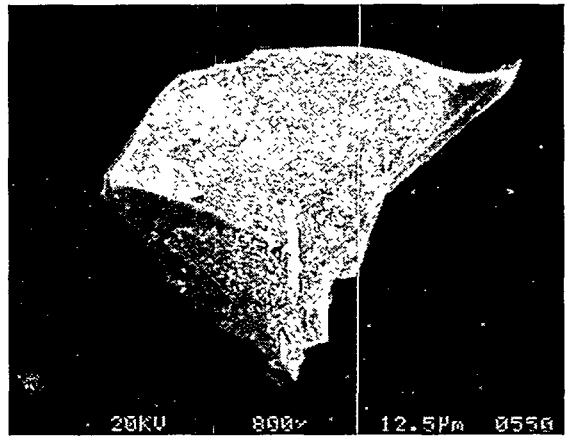

Fig. 21. SEM Micrograph of Glass Shard
Found in Reacted Solids from PDT-3

The leachant used in these experiments was EJ-13 water. This water is from well "J-13" and has been heated at 90°C for 80 days in contact with powdered Yucca Mountain tuff (ground to -200 to +100 mesh). Two batches of EJ-13 were used in tests reported here. They are referred to as EJ-13a and EJ-13b and have the compositions listed in Table 16. In addition, three tests were conducted using EJ-13 water to which sufficient H_2O_2 was added to attain a concentration of approximately 0.1 M H_2O_2 (tests PDT-4, PDT-6, PDT-8). Addition of H_2O_2 was intended to allow examination of possible effects of radiolysis products on the rate of UO_2 dissolution and formation of alteration products. This concentration of H_2O_2 was chosen because it is within a concentration range for which kinetics of oxidative dissolution of UO_2 show a simple linear dependence on H_2O_2 concentration [dePABLO-1996].

While the same procedure was used to prepare both batches of EJ-13 water, there was some variability. Yucca Mountain tuff is a fine-grained volcanic rock (a rhyolite) containing minerals such as plagioclase, sanidine, and quartz, as well as volcanic glass. These components represent a solidified magma (a complex mixture of liquids, gases, and crystals) that was quenched at temperatures on the order of 800°C. "Equilibration" of water with a volcanic tuff is not possible at 90°C, because no water composition is in equilibrium with the components of a volcanic tuff at this temperature. Equilibration of groundwater would require complete alteration of the tuff components to an assemblage of minerals stable in the presence of water at 90°C, such as quartz, zeolites, and clays. The intention behind preparing EJ-13 water is to try to mimic the composition of a groundwater that may evolve in contact with tuff at elevated temperatures at a proposed repository at Yucca Mountain. Thus, of EJ-13 represents a kind of steady state for groundwater in contact with tuff at 90°C. Because the concentration of EJ-13 does not reflect true equilibrium, concentrations of EJ-13 prepared according to a specific procedure can be expected to vary somewhat, both because reaction of J-13 well water may not reach the same "steady state" in all preparations and because the composition of both J-13 and EJ-13 waters may vary over time, even after preparation. The variability of several analyses of EJ-13 water is illustrated in Fig. 22. Error bars shown in Fig. 22 indicate a variance of 30% in measured Na and Si concentrations. The value of 30% is used because this value is required in order to make analyses of identical batches overlap (i.e., to make them statistically identical). Such variability can affect the interpretation of data when the interpretation requires an accurate knowledge of the starting composition of the test solution. Thus, the EJ-13 water should be analyzed prior to initiating tests.

Table 16. Compositions of the Two Batches of EJ-13 Water Used in PDTs (concentrations in ppm except pH) (25°C)

Element / Ion	EJ-13a	EJ-13b
Si	45.5	43.99
Na	53.6	58.19
Li	0.03	0.048
K	6.67	11.30
Ca	6.95	4.39
Mg	0.08	0.30
Fe	0	0.098
B	0.19	0.16
Al	0.68	1.02
U	0.001	0.001
F^-	2.4	3.4
Cl^-	7.5	21
NO_3^-	10	14.9
NO_2^-	0.12	0.71
SO_4^-	20	27.9
HCO_3^-	101.49	*nd*
pH	8.36	8.7

Approximately 0.5 mL of EJ-13 was added to each reaction vessel. This volume of water was chosen to maximize the S/V ratio, while providing sufficient liquid to wet the UO_2 powder completely (and provide enough liquid for chemical analyses). The first test (PDT-1) used a slightly different hanger construction that required a greater solution volume to wet the sample. Therefore, PDT-1 has a much lower S/V ratio than other tests (Table 14).

C. Analyses

1. Analytical Methodology

At the completion of each test, the vessel was cooled in an ice bath and opened. The hanger was removed and set aside to air dry. Sufficient solution was taken for determining pH. If enough solution was available (usually more than ~300 μL), 100 μL was placed into an anion vial for anion analysis by ion chromatography. The remaining liquid was put into a 3-mL syringe and passed through a 0.45 μm filter into a plastic (LPE) bottle where it was acidified to ~1% with high-purity nitric acid. The acidified, filtered solution was analyzed for cations by ICP-MS. The volume of water recovered at the end of each test varied, and anion analyses were not conducted for tests PDT-4 through PDT 8. Furthermore, due to loss of liquid to 0.45 μm filters (approximately 0.025 mL), solution aliquots from PDT-4 and PDT-6 were not filtered, as so little liquid was recovered from these two tests (Table 17).

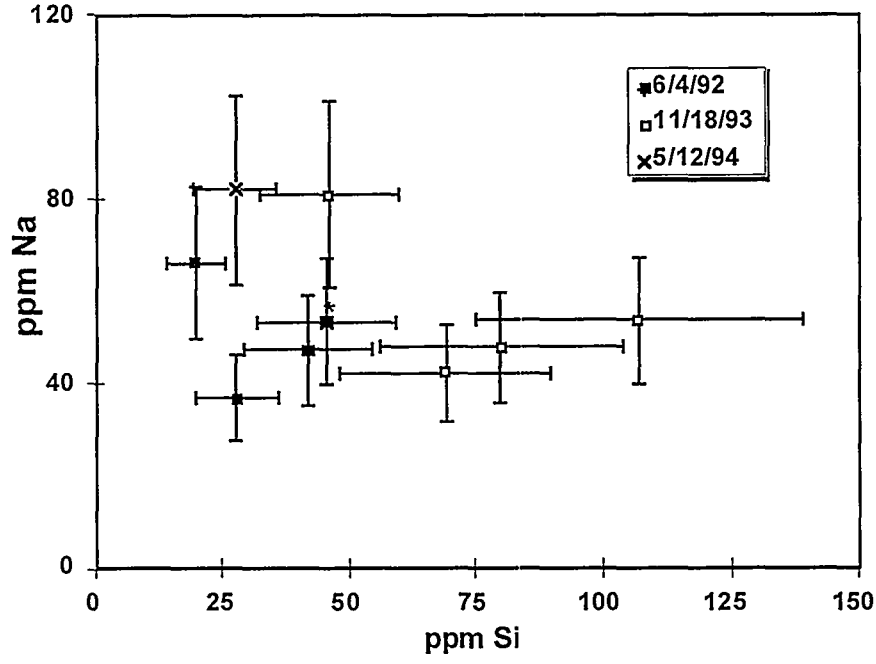

Fig 22. Reported Na and Si Concentrations in EJ-13 Waters Prepared by Reacting J-13 with Tuff at 90°C for 80 Days. Three preparations are shown, with analyses of each preparation indicated by the date of preparation. Error bars represent 30% sample variance. This is the variance necessary for different analyses from the same batch to be statistically identical. The analysis reported for EJ-13a in Table 16 is indicated by an asterisk.

Table 17. Mass and Recovery Rate of Solution Aliquots at Test Termination (all masses in grams)

Test ID	PDT-1C	PDT-3C	PDT-4C	PDT-5C	PDT-6C	PDT-7C	PDT-8C
Run loss[a]	0.08	0.09	0.04	0.14	0.19	0.13	0.24
Mass in vessel[b]	1.91	0.41	0.39	0.46	0.30	0.37	0.26
IC-PMS aliquot	1.40	0.195	0.125	0.183	0.175	0.189	0.046
pH & anion	0.15	~0.1	0.05	0.05	0.05	0.05	0.05
UO_2 & screen[d]	~0.335	~0.09	~0.215	~0.202	~0.075	~0.106	~0.164
total mass lost[e]	~0.44	~0.205	~0.335	~0.267	~0.265	~0.261	~0.429
% recovery	78%	59%	34%	47%	46%	48%	19%

[a]Difference between mass of vessel measured at test initiation and mass measured at test termination. This loss can be reduced by machining cut grooves into the vessel mating surface.
[b] At test termination.
[c]Mass of solution aliquot analyzed (after filtration, if filtered).
[d]Mass retained as estimated by assuming 0.025 g left in the 0.45 μm filter (except PDT-4 & PDT-6).
[e] Includes losses during run, loss to filter, and retention by UO_2 and screen.

Anion analysis was carried out for 0.1-mL aliquots taken from two tests (PDT-1 and PDT-3), although this analysis required too much solution; later test solutions have not been

analyzed for anions. Solutions for anion analysis were not filtered. The solution pH was measured after cooling the vessel to ~20°C by using a glass electrode and a Brinkman pH meter calibrated against approved NIST standard pH solutions.

After removing solid fragments of UO_2 and alteration products (if present) from each test vessel, they were dried in air while still on the screen. The dried powders were examined under an optical microscope. Particles were prepared for examination by SEM two ways: (1) several particles were selected during optical examination and mounted directly onto conductive carbon tape on an Al stub or (2) approximately one-half of the reacted powder (~0.1 g) was mounted in epoxy, which, when hardened, was ground and polished by hand using alumina polishing compound (0.3-μm final polish). All SEM samples were carbon-coated under vacuum. Analyses are performed with a TopCon SEM operated at an accelerating voltage of 15 kV and a beam current of 20 mA. Qualitative chemical analyses were performed by using EDS with a Li-drifted-Si solid-state detector and data-analysis software. Due to the small amount of reaction products generally present in these tests, the primary mode of phase identification was SEM/EDS. SEM provides information on phase morphologies and crystal habits, and EDS provides qualitative elemental analysis. When used in combination, these two methods usually permit positive identifications of most phases; however, anhedral or polycrystalline materials without distinct morphologies and chemically similar materials having similar habits cannot usually be distinguished without additional information.

Several U^{6+} phases known can be difficult to distinguish using SEM/EDS. These phases include, in particular, the U^{6+}-oxyhydroxides, schoepite, $(UO_2)_8O_2(OH)_{12}(H_2O)_{12}$; metaschoepite, $UO_3 \cdot 2H_2O$; dehydrated schoepite, $(UO_2)O_{0.25-x}(OH)_{1.5+2x}$ ($0 < x$ 0.15); and three synthetic hydroxide polymorphs of $UO_2(OH)_2$. Chemically, these phases appear virtually identical when examined by EDS. Morphologically, dehydrated schoepite tends to form small, thin, boat-shaped crystals, as does α-$UO_2(OH)_2$. Schoepite and metaschoepite tend to form blockier crystals but display morphologies that are similar to each other. Dehydrated schoepite, schoepite, and metaschoepite are difficult to distinguish. Schoepite is not likely to form in the PDTs, however, because it is not stable at 90°C; it dehydrates to metaschoepite or dehydrated schoepite above ~ 40°C [FINCH et al.-1996]. Dehydration of hydrous minerals in the vacuum of the SEM (and during C-coating of samples) is also common, as is dehydration due to sample heating while under an electron beam.

Some other U^{6+} phases that can be difficult (or impossible) to distinguish by SEM/EDS include U-silicates. Boltwoodite, $K(UO_2)(SiO_3OH)(H_2O)$, and weeksite, $K_2(UO_2)_2(Si_5O_{16})(H_2O)_4$, are similar, as are their Na analogues, $Na(UO_2)(SiO_3OH)(H_2O)$ and $Na_2(UO_2)_2(Si_5O_{16})(H_2O)_4$. The two uranophane polymorphs (α and β), $Ca(UO_2)_2(SiO_3OH)_2(H_2O)_4$, cannot be distinguished with SEM/EDS, and haiweeite, $Ca(UO_2)_2(Si_5O_{16})(H_2O)_4$, can be difficult to distinguish from the uranophane polymorphs. All these minerals share many structural elements and all have acicular habits. Weeksite, Na-weeksite, and haiweeite commonly form very small crystals, although this alone is rarely distinctive. Relatively high Si:U ratios in weeksite, Na-weeksite, and haiweeite can aid in distinguishing these phases from boltwoodite, Na-boltwoodite, and the uranophane polymorphs by EDS. Of course, the best way to distinguish these minerals is by diffraction methods, and diffraction is the only way to identify the uranophane polymorphs.

Finally, similarities in X-ray emission energies of U-M_β and U-M_λ lines to K-K_α and K-K_β lines make overlap of emission lines extreme. Potassium is exceedingly difficult to distinguish in the presence of uranium. Numerous K-bearing U^{6+} phases are known, and because of K in EJ-13 water, K-bearing phases might be expected to form. Only when K is present as a major constituent, however, can it be identified, but no semi-quantitative analysis of K is possible, even in that case.

The XRD powder diffraction is the most powerful technique for providing quantitative identification of materials present in sufficient quantities, usually ~1% or greater. TEM analysis can provide accurate phase identification, especially for very small crystals, provided that materials of interest can be isolated and adequately prepared. X-ray powder-diffraction data were collected from reacted solids from the PDT tests; however, we performed no TEM analyses on these samples.

In addition to phase identification, SEM provides information about replacement textures and phase paragenesis (sequence of phase formation). A paragenetic sequence can be inferred where late-stage minerals coat, replace, or surround earlier-formed phases.

2. Results

Solution compositions of leachates at test termination are reported in Tables 18 and 19. The mass of water recovered and recovery rate from each test are listed in Table 17. Solid U^{6+} alteration products identified are listed in Table 20.

Table 18. Concentrations of Components of EJ-13 Water and U at Test Termination (mg/L)

Test ID	PDT-1C	PDT-3C	PDT-4C	PDT-5C	PDT-6C	PDT-7C	PDT-8C
Filtration[a]	F	F	uF	F	uF	F	F
Si	35.9	41.5	69.0	40.3	51.3	32.7	37.4
Na	53.3	75.8	89.7	85.6	92.8	66.5	65.2
K	7.91	< 21.3	< 22.1	< 84.3	< 21.5	< 86.3	< 104
Li	0.385	< 5.33	< 5.52	< 6.33	< 5.37	< 6.48	< 7.83
Ca	1.99	< 21.3	< 22.1	< 21.1	< 21.5	< 21.6	< 26.1
Mg	0.208	1.34	3.16	4.00	1.94	0.543	1.40
B	0.793	1.88	5.56	1.32	3.75	2.98	3.96
Al	0.175	1.16	5.36	4.34	3.34	< 7.56	8.36
U	0.812	36.9	3920	> 5.93	717	15.4	71.3
F^-	12	15	nd	nd	nd	nd	nd
Cl^-	12	23	nd	nd	nd	nd	nd
NO_3^-	42	184	nd	nd	nd	nd	nd
NO_2^-	1.6	< 5	nd	nd	nd	nd	nd
SO_4^{2-}	57	105	nd	nd	nd	nd	nd
pH	7.52	5.75	4.5	4.35	4.59	6.07	5.04

* Filtration of solution aliquots: *F* = filtered (0.45 μm); *uF* = unfiltered. *nd* = not determined

Table 19. Concentrations of Stainless Steel Components in Leachant at Test Termination (mg/L)

Test ID	PDT-1C	PDT-3C	PDT-4C	PDT-5C	PDT-6C	PDT-7C	PDT-8C
Cr	0.060	0.043	< 0.724	0.160	0.025	< 0.076	< 0.091
Mn	0.160	30. 3	14. 6	3.75	8.24	3.06	3.04
Fe	1.42	< 6.40	< 38.2	10.5	< 10.5	< 10.8	< 13.0
Ni	0.139	9.89	81.5	230	41.1	1.08	2.51
Mo	0.134	< 0.012	0.541	0.012	0.220	0.011	0.013

Table 20. Solid Alteration Products Identified or Suggested in PDTs[a]

Solid Phase	Formula(s)	Test ID
dehydrated schoepite	$(UO_2)O_{0.25-x}(OH)_{0.15+2x}$ $(0 \leq x \leq 0.15)$	PDT-4, PDT-6, PDT-8 (?)[b]
metaschoepite	$UO_3 \cdot 2H_2O$	PDT-5
compreignacite (?)	$K_2(UO_2)_6O_4(OH)_6(H_2O)_8$	PDT-8
soddyite	$(UO_2)_2(SiO_4)(H_2O)_2$	PDT-6
uranophane (?)	$Ca(UO_2)_2(SiO_3OH)_2(H_2O)_5$	PDT-7
swamboite (?)	$U^{6+}(UO_2)_6(SiO_3OH)_6(H_2O)_{30}$	PDT-7

[a]All phase identifications are tentative, and are based on SEM and EDS only.
[b]"(?)" indicates a high degree of uncertainty in the phase indicated.

Results are presented separately for each test. Numbering of each test reflects the order in which each experiment was started; however, this does not necessarily reflect the order in which tests were completed. The discussion below is organized according to the order in which experiments were started. Some observations may therefore appear "out of order" in terms of reactions described. Results for those tests in which we used unmodified EJ-13 water (either from batch a or batch b) are presented first, followed by results for those tests in which EJ-13 water contained an added 0.1 M H_2O_2 ("EJ-13 ox"). H_2O_2 was added to three tests (PDT-4, PDT-6, and PDT-8) in order to enhance oxidative dissolution of UO_2; however, several other effects of adding the EJ-13 ox water to the starting test solution are apparent from the results. These effects include consistently lower pH values (Table 18), formation of dehydrated schoepite in only those tests with EJ-13 ox (Table 20), and a somewhat lower recovery rate of leachant at test termination (Table 17, Fig. 23).

Test PDT-1 was the first test conducted and served primarily as a preliminary test because we had little concrete information about potential reaction rates and what experimental conditions were necessary for a successful test run of minimal duration. Test PDT-1 had a much lower S/V ratio than other tests (Table 14). After terminating PDT-1, we decided to increase S/A in subsequent tests by decreasing the volume of water from approximately 2 g to approximately 0.5 g, resulting in a four-fold increase in the S/V (the mass of fuel is already near a maximum for the reaction vessel being used, and the grain sizes of UO_2 are as small as practicable). This decision required a slight redesign of the existing screen hanger, which was initially constructed with mesh screen welded to the top of a wire loop (Fig. 17). As discussed below, this change proved successful for enhancing dissolution of UO_2 and precipitation of alteration products. On the other hand, the smaller volume of water resulted in much less solution being available for chemical analyses at test termination (Table 17). However, it should be possible to do the major analysis with the amount of water recovered.